Analysing the Polarisation Sensitivity of the Near Infrared Spectrograph on board the James Webb Space Telescope

Jeffrey Huang

Delft University of Technology

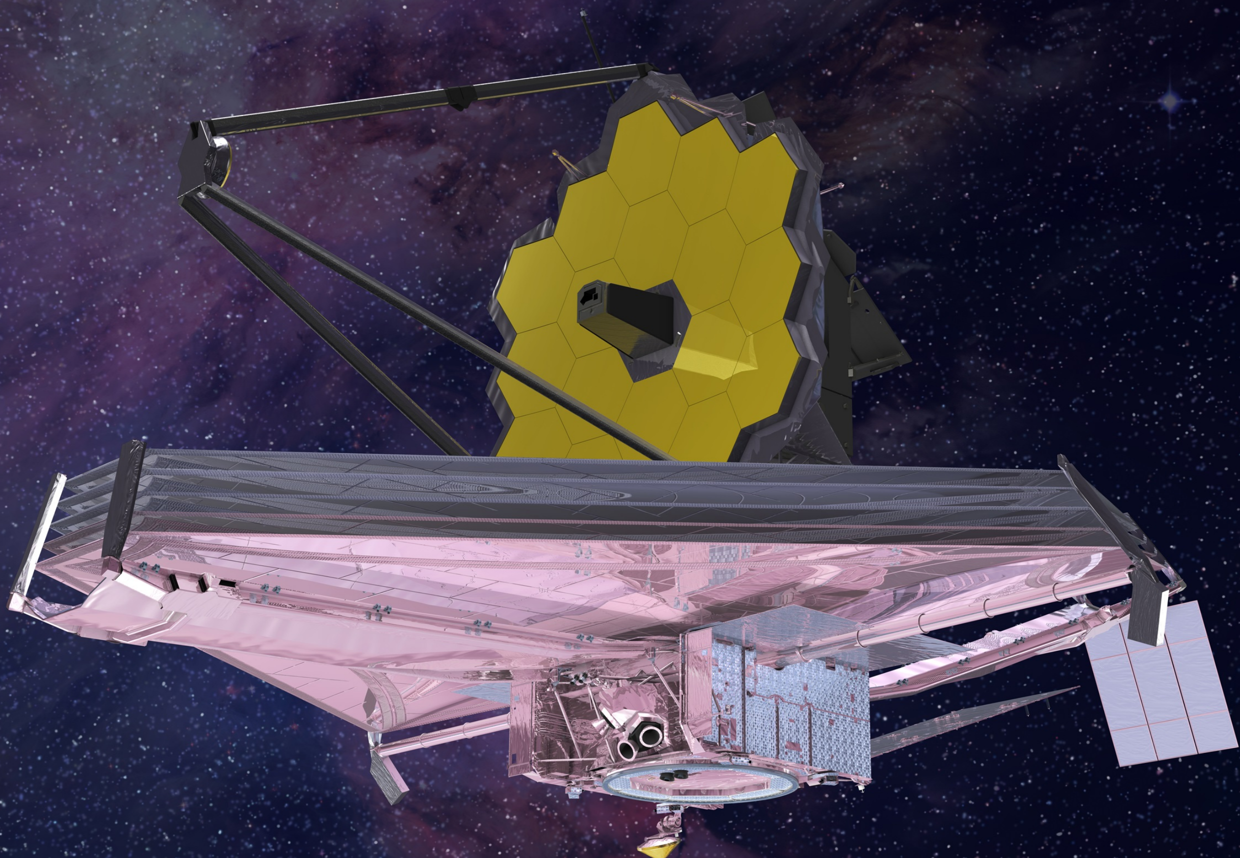

Challenge the future

Image credit: Northrop Grumman

Analysing the Polarisation Sensitivity of the Near Infrared Spectrograph on board the James Webb Space Telescope

by

Jeffrey Huang

to obtain the degree of Master of Science
at the Delft University of Technology.

Student number:	4234677	
Principal tutor:	Dr. D. M. Stam,	Delft University of Technology
Chair:	Dr. Ir. W. van der Wal,	Delft University of Technology
External Expert:	Dr. A. Endo	Delft University of Technology
External Expert:	Dr. G. Giardino	European Space Agency
External Expert:	Dr. P. Ferruit	European Space Agency
External Expert:	Ir. M. B. J. te Plate	European Space Agency

TU Delft

Executive Summary

The objective of this master thesis research project is to determine the overall polarisation sensitivity of the Near Infrared Spectograph (NIRSpec) on board the James Webb Space Telescope (JWST). Understanding the polarisation sensitivity is important to correctly interpret the output data and accurately calibrate the instrument during operational lifetime. As experimental research on this topic for NIRSpec was limited, a numerical code has been built to simulate the light following the optical path of NIRSpec. This numerical code is effectively a ray tracer with polarisation state analysis functions. They ray tracer is designed to be modular, making it straightforward to add new functions or optical elements, either for future work on NIRSpec or application to other instruments. The analyses regarding the polarisation sensitivity were performed in three main categories: the induced polarisation through reflections by mirrors, the grating efficiencies and overall throughput, and the effect on the calibration process.

The JWST is a large space telescope that aims to help better understand every time period of the universe from the Big Bang till the present. The launch is currently scheduled in March 2021. The JWST shall provide new data by observing thermal radiation from various celestial objects. It houses four main science instruments, one of which is NIRSpec developed by the European Space Agency.

The optical design of NIRSpec is based on three three-mirror anastigmats and six main opto-mechanical assemblies. Two of those assemblies are the grating wheel assembly which houses dispersive reflection gratings and the calibration assembly which is used to internally calibrate the instrument. These optical elements introduce a polarisation sensitivity, meaning that the instrument output data will depend on the polarisation state of the incoming radiation. Even though NIRSpec will mainly observe unpolarised light sources, a degree of polarisation will always be induced via reflections by the mirrors. The optical path of the calibration beam differs from the nominal science path, so a different degree of polarisation will be induced via the calibration path compared to the nominal science path. Application of the calibration measurements to the science measurements can thus lead to errors on the deduced signals.

The induced degree of polarisation for the nominal science path will likely remain below 2%. This degree of polarisation is slightly dependent on both wavelength and initial incidence angle, but not significantly.

The analysis of the grating efficiencies clearly indicates a polarisation sensitivity up to 20% for the medium resolution gratings and up to 40% for the high resolution gratings. Due to the low estimated induced polarisation below 2%, the maximum uncertainty in the output data for unpolarised incoming light would be lower than 1%. Observing celestial objects with an inherent degree of polarisation, however, could introduce a significant uncertainty in the measurements.

Finally, the calibration process has also been examined and it can be concluded that the induced degree of polarisation by the calibration mirrors before the light reaches the grating will be 1 to 2% higher compared the nominal science path. Whether or not this difference should be taken into account will depend on the application.

Recommendations for future work can be divided into four categories. First, the reflection grating efficiencies should be analysed in more details as the accuracy of the presented results is uncertain. Second, the filters and detector are modelled as single layer Fresnel surfaces, while in reality they consist of multiple layers of different materials. It should be researched how this assumption affects the presented results. Third, configurations using the long-slit spectroscopy and integral field spectroscopy have not been analysed while the microshutter assembly is modelled as ideal transmitter. Analysing these configurations would provide a more complete understanding of NIRSpec's polarisation sensitivity. Fourth, validation through measurement data would help determine the accuracy of the ray tracer presented in this master thesis research. This data could come from either measurements of NIRSpec during operational lifetime or comparable instruments of which measurement data is available.

Contents

List of Figures

List of Tables

Nomenclature

CAA	Calibration Assembly
CAM	Camera Optics
COL	Collimator Optics
COM	Coupling Optics
CSA	Canadian Space Agency
ESA	European Space Agency
FPA	Focal Plane Assembly
FOR	For Optics
FOV	Field of View
FSM	Fine Steering Mirror
FWA	Filter Wheel Assembly
GWA	Grating Wheel Assembly
IFU	Integral Field Unit
ISIM	Integrated Sciences Instrument Module
JWST	James Webb Space Telescope
MOS	Multi-Object Spectroscopy
MSA	Microshutter Assembly
NASA	National Aeronautics and Space Administration
NIRSpec	Near Infrared Spectrograph
OTE	Optical Telescope Element
RMA	Refocusing Mechanism Assembly
SLIT	Single Object Long-Slit Spectroscopy
TMA	Three-Mirror Anastigmat

LIST OF SYMBOLS

Symbol	Description	Unit
a	Grating slit spacing	m
a	Aspherical coefficient	-
a	Major axis of ellipse	m
B	Magnetic induction	T
b	Minor axis of ellipse	m
c	Velocity of light in vacuum	m/s
c	Curvature at the vertex	1/m
D_{eff}	Detector efficiency	-
DOP	Degree polarisation	-
E	Electric field	N/C
E_0	Electric field amplitude	-
G_{eff}	Grating efficiency	-
I	Irradiance	W/m^2
I	First Stokes parameter	
J	Jones matrix	-
k	Conic constant	-
L	Complex intensity of linear polarisation	-
M	Mueller matrix	-
M_{eff}	Overall Mirror efficiency	-
m	Order of diffraction	-
$\vec{N}$	Normal direction vector	-
n	Real refractive index	-
n	Normal direction vector	-
$\boldsymbol{n}$	Complex refractive index	-
NP	Non-polarised irradiance component	W/m^2
P	P-polarised irradiance component	W/m^2
r	Ray direction vector	-
R	Spectral resolution	-
R	Electric field of the reflected beam	N/C
R	Radial distance along horizontal axis	m
R	Rotation matrix	-
S	Stokes parameters vector	-
S	S-polarised irradiance component	W/m^2
T	Electric field of the transmitted beam	N/C
$\vec{T}$	Tangent direction vector	-
t	Time	s
Q	Second Stokes parameter	-
U	Third Stokes parameter	-
V	Fourth Stokes parameter	-
Z	Mirror height along vertical axis	m
ϵ	Phase difference	rad
ϵ_0	Vacuum permittivity	F/s
θ	Tilt angle	rad
κ	Extinction coefficient	-
λ	Wavelength	m
ϕ	Phase	rad
ϕ	Local polar angle	rad
ω	Angular frequency	rad/s

1 Introduction

The James Webb Space Telescope (JWST) is a large space telescope that aims to help better understand every time period of the universe from the Big Bang till the present [11]. The launch is currently scheduled in March 2021 [25]. The JWST shall provide new data by observing radiation from various celestial objects. It houses four main science instruments, one of which is NIRSpec developed by the European Space Agency [6] [3].

The optical design of NIRSpec is based on three three-mirror anastigmats and six main opto-mechanical assemblies. Two of those assemblies are the grating wheel assembly which houses dispersive reflection gratings and the calibration assembly which is used to internally calibrate the instrument. The optical elements in NIRSpec introduce a polarisation sensitivity, meaning that the instrument output data will polarisation state dependent of the incident light. Even though NIRSpec will mainly observe unpolarised light sources, a degree of polarisation will always be induced via reflections by the mirrors. Furthermore, the optical path of the calibration beam differs from the nominal science path, so a different degree of polarisation might be induced via the calibration path compared to the nominal science path. Calibration of NIRSpec's nominal science path through the calibration assembly can thus lead to errors on the deduced signals.

Within this master thesis research, a numerical model has been developed to simulate the optical path through NIRSpec which takes into account both the induced polarisation by the mirrors as well as the polarisation efficiencies of the reflection gratings. This can then be combined to determine the overall polarisation sensitivity and utilised to improve the calibration process.

The overall sensitivity can be described by the measured irradiance at the detector I which follows Equation (1.1) where I_{COL3} is the irradiance after COL3, the last mirror in the optical path before reaching the grating, G_{eff} is the effective grating efficiency, M_{eff} is the combined mirrors efficiency and D_{eff} is the detector efficiency which varies with incidence angle. G_{eff} is dependent on I_{COL3} described by Equation (1.2) in which NP, P, and S are the non-polarised, P-polarised, and S-polarised parts of I_{COL3}.

$$I = I_{COL3}\, G_{eff}\, M_{eff}\, D_{eff} \tag{1.1}$$

$$G_{eff} = \frac{NP}{I_{COL3}} \frac{P_{eff} + S_{eff}}{2} + \frac{P}{I_{COL3}} P_{eff} + \frac{S}{I_{COL3}} S_{eff} \tag{1.2}$$

The report structure is as follows: Chapter 2 provides some context on the Near Infrared Spectrograph. Essential optics literature used for the analyses is discussed in Chapter 3. In Chapter 4, a detailed description is given of the used ray tracer that is used for all the analyses. The induced polarisation and sensitivity analysis are shown in Chapter 5 and Chapter 6, respectively. The last analysis on the calibration assembly is given in Chapter 7. Finally, a conclusion is drawn and presented in Chapter 8 while recommendations for future work are given in Chapter 9.

2

The Near Infrared Spectrograph

The Near Infrared Spectrograph (NIRSpec) is one of the four main instruments onboard the James Webb Space Telescope (JWST), a large space telescope scheduled to launch in March 2021 [1]. The JWST has an aperture of 25 m^2, Figure 2.1 and a payload that covers the near and mid-infrared wavelength range at an operational temperature below 50 K [6]. This payload is is housed within the integrated science instrument module (ISIM) as shown in Figure 2.2. To passively aid the cooling, the JWST shall orbit the Sun-Earth second Lagrange point such that it stays in line with the Earth while its sunshield protects the telescope from the light and heat of the Sun [14]. As the second Lagrange point is unstable, it requires propellant to maintain its orbit, limiting the maximum operational lifetime. The nominal scientific lifetime of the JWST is five years and the propellant is budgeted such that it can remain operational for ten years. The JWST is a result of an international collaboration between the National Aeronautics and Space Administration (NASA), the European Space Agency (ESA), and the Canadian Space Agency (CSA). The primary scientific objectives can be divided into four themes: first light and reionisation, the assembly of galaxies, the birth of stars and protoplanetary systems, and formation of planetary systems and the origin of life. The emphasis of the science goals of NIRSpec is on the assembly of galaxies [8]

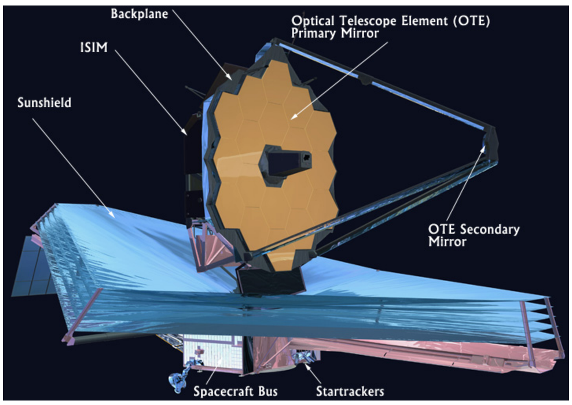

Figure 2.1: The 25m^2 aperture of JWST consisting of multiple hexagons fitted together [25]

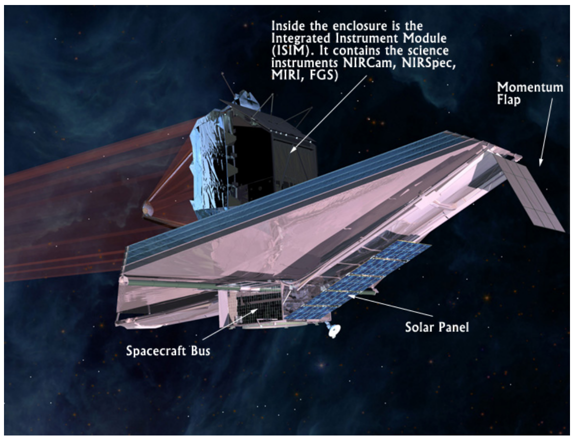

Figure 2.2: The back of the aperture of JWST with the ISIM housing all four main science instruments [25]

2.1. CAPABILITIES

NIRSpec has been developed by ESA with Airbus Defence and Space Germany as prime contractor [3] and has the capacity over three primary science features: multi-object spectroscopy (MOS), single-object long-slit spectroscopy (SLIT), and integral field spectroscopy via an integral field unit (IFU). Furthermore, NIRSpec provides three additional functions: target acquisition, on-board calibration, and re-focusing.

Large spectroscopic surveys are performed in MOS mode in which individually addressable shutters are used to select objects within the field of view (FOV) of approximately 9 square arcmin, while high-contrast, high resolution spectroscopy is enabled through SLIT mode. The IFU combines spectrographic and imaging capabilities to obtain spectra as a function of position. SLIT mode can be used independently of and simultaneously with MOS mode as they utilise different areas on the detector plane, whereas the IFU uses the same area as MOS mode.

The target acquisition is performed by imaging the whole FOV on the detector plane by replacing the dispersive elements in the instrument with a mirror and opening the slits. The image is then used for the attitude determination and control of the space telescope. On-board calibration can be achieved through various methods; so-called dark calibration, flat-field calibration, spectral calibration, and absolute spectral calibration. Finally, NIRSpec is able to change its focus independently from the JWST telescope focus for optimisation activities.

NIRSpec covers the wavelength range of 0.6 to 5.3 μm which is mainly divided into three main bands I, II, and III as shown in Table 2.1 [8]. A specific band is selected by moving the matching long-pass filter into the optical beam. In each band, two spectral resolutions of R ≈ 1000 and R ≈ 2700 are provided by two dedicated gratings. The complete spectral range can also be observed in a lower spectral resolution of R ≈ 100 by using a prism instead of a grating.

Band	**Spectral Range** [μm]	**R** [$\lambda/\Delta\lambda$]	**GWA element**	**FWA element**
I	1.0 - 1.8	1000, 2700	GRT1000-I, GRT2700-I	F100LP
II	1.7 - 3.1	1000, 2700	GRT1000-II, GRT2700-II	F170LP
III	2.9 - 5.2	1000, 2700	GRT1000-III, GRT2700-III	F290LP
0.7	0.7 - 1.2	1000, 2700	GRT1000-I, GRT2700-I	F070LP
n/a	0.6 - 5.3	100	Prism	Clear
IMA	1.0 - 1.2, 0.8 - 2.0	n/a	Mirror	F110W, F140X

Table 2.1: Available bands and their respective nominal operation configurations [8]. Note that the 'band' that covers the complete spectral range does not have a dedicated name. Furthermore, the IMA band is an image at a single wavelength, thus there is no spectral resolution.

2.2. OPTICAL ELEMENTS

Light enters NIRSpec via the optical telescope element (OTE) of JWST and a fine steering mirror (FSM), schematically shown in Figure 2.3. The optical design of NIRSpec, schematically shown in Figure 2.4 excluding the calibration assembly, is based on three three-mirror anastigmats (TMAs) (excluding the TMA of the optical telescope element of JWST) and six main opto-mechanical assemblies. TMAs are three sequentially placed aspherical mirrors to minimize the main optical aberrations: spherical aberration, coma, and astigmatism. The three TMAs are the fore optics (FOR), collimator optics (COL), and camera optics (CAM). The six opto-mechanical assemblies consist of the microshutter assembly (MSA), focal plane assembly (FPA), filter wheel assembly (FWA), refocusing mechanism assembly (RMA), grating wheel assembly (GWA), and calibration assembly (CAA). The layout, excluding the CAA, is shown in Figure 2.4 [3] and the individual elements are given in Table 2.2 in order of how the light travels through the instrument, with the exception of the CAA elements. Note that the optical path starts at the OTE of JWST, which consists of a TMA and FSM, before it reaches NIRSpec. All mirrors (excluding OTE) are made of Silicon Carbide (SiC) for their low coefficient of thermal expansion and are coated with enhanced silver [12].

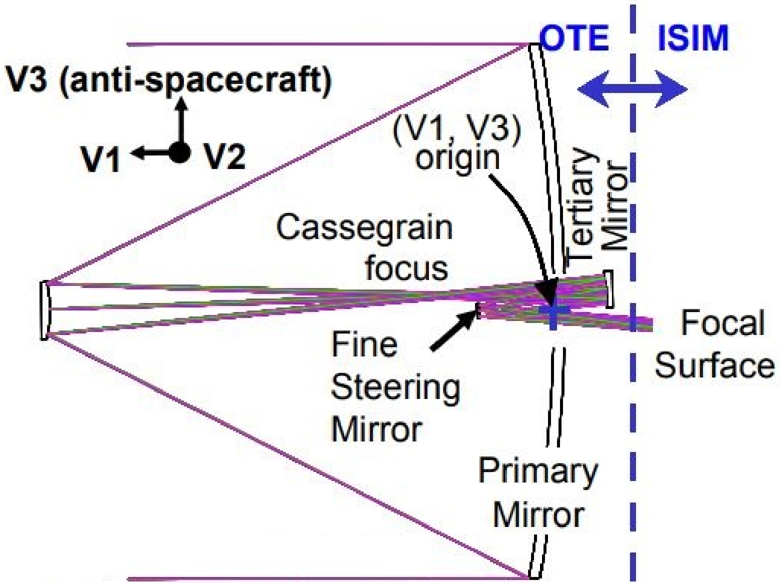

Figure 2.3: Schematic of the OTE TMA and FSM light focusing towards NIRSpec [33]. This is a textbook example of a TMA where three aspherical mirrors are used to eliminate the main optical aberrations. The FSM finally directs the light into the ISIM where all the instruments are located.

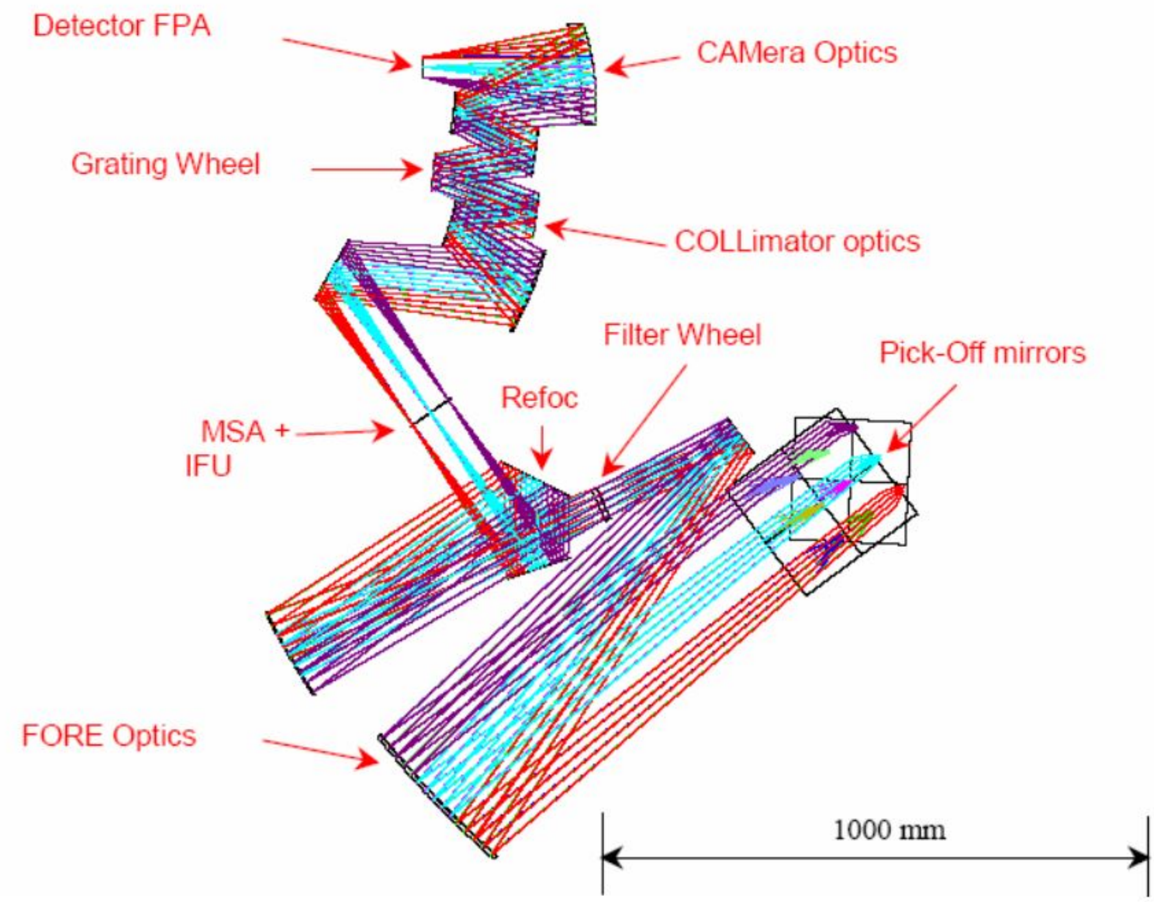

Figure 2.4: Optical layout of NIRSpec after the after the light traversed the optical telescope element. The different colours represent rays from different area in the FOV [3]. Note that the pick-off mirrors are the coupling optics and the two flat mirrors directly underneath 'Refoc' represent the refocusing mechanism assembly.

Description	Element	Description
Optical Telescope Element	OTE1	Aspherical mirror
	OTE2	Aspherical mirror
	OTE3	Aspherical mirror
Fine Steering Mirror	FSM	Flat mirror
Pick-Off Mirrors (Coupling Optics)	COM1	Flat mirror
	COM2	Flat mirror
Fore Optics	FORE1	Aspherical mirror
	FORE2	Aspherical mirror
Filter Wheel Assembly	FWA	Long-pass filters
	FORE3	Aspherical mirror
Refocusing Mechanism Assembly	RMA1	Flat mirror
	RMA2	Flat mirror
Microshutter Assembly	MSA	Transmission
Folding Mirror	FOM	Flat mirror
Collimator Optics	COL1	Aspherical mirror
	COL2	Aspherical mirror
	COL3	Aspherical mirror
Grating Wheel Assembly	GWA	Reflection gratings
Camera Optics	CAM1	Aspherical mirror
	CAM2	Aspherical mirror
	CAM3	Aspherical mirror
Focal Plane Assembly	FPA	Detector
Calibration Assembly	CAL1	Aspherical mirror
	CAL2	Aspherical mirror
	CAL3	Aspherical mirror

Table 2.2: The optical path of the incoming light towards the detector in order of occurrence for incoming light with the exception of the CAA elements which are only utilised in during the calibration process.

OPTICAL TELESCOPE ELEMENT

Light enters NIRSpec via the OTE TMA and the FSM as schematically depicted in Figure 2.3 [33]. The primary mirror of JWST consists of 18 hexagonal mirror segments which will fold out and fit together to form a single mirror after launch. All mirrors are made of beryllium and coated with protected gold [20].

COUPLING AND FORE OPTICS

The coupling optics (COM) consist of two flat pick-off mirrors [31]. Together, the two flat mirrors pick-off the NIRSpec FOV from the OTE of JWST and direct the diverging beam to FOR. There, the light is telecentrically re-imaged from the OTE onto the aperture plane of the MSA through the FWA via the RMA as shown in Figure 2.4.

FILTER WHEEL ASSEMBLY

The FWA consists of a total of six filters and a clear element used for imaging, see Table 2.1, and one additional element used for calibration purposes excluded from this table [9]. The four filters ending with 'LP' in their name are CaF_2 substrate long-pass filters. The long-pass filters block all shorter wavelengths and are matched with a specific diffraction grating to define the wavelength band. The spectral band passes of the long-pass filters are shown in Figure 2.5. The clear element lets through all incoming light and the filters for the IMA band are radiation-hardened B7-G18 broadband filters. Broadband filters pass an inherent wavelength band, cutting off all wavelengths outside of this band as shown specifically for the IMA broadband passes in Figure 2.6.

The long-pass and broadband filters have a special coating to reach the required transmission specifications during the operational lifetime. The dielectric coatings are based on optical interference filters which basically consist of a stack of transparent layers of alternating high and low refractive index materials, namely TiO_2 and SiO_2. The refractive indices, layer thicknesses, and number of layers determine the coating's spectral properties.

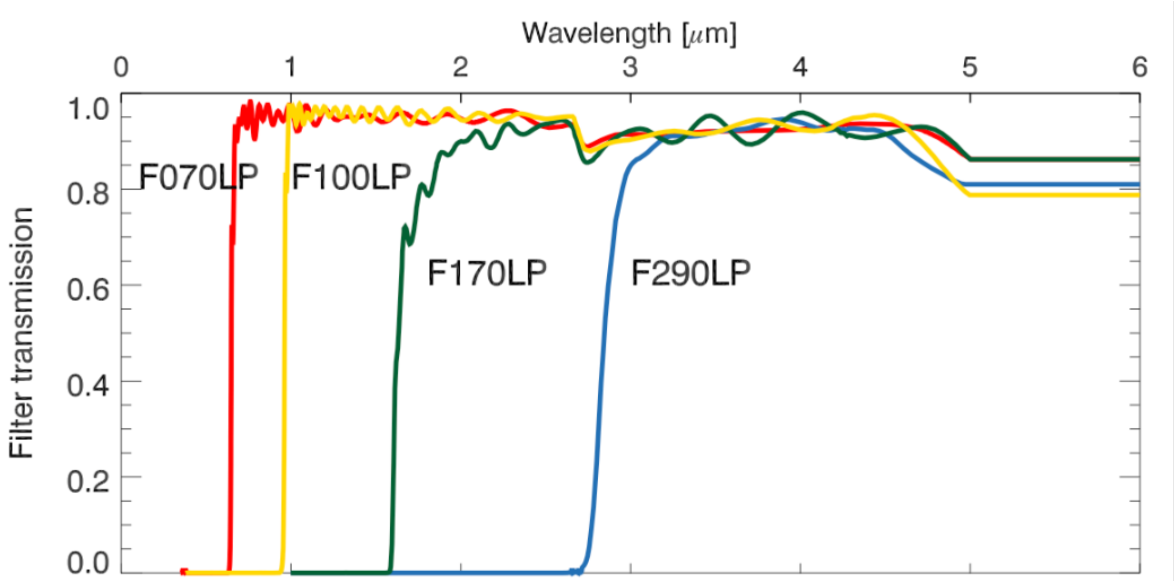

Figure 2.5: The band passes of all four long-pass filters over wavelength [18]. They show how wavelengths over their respective limits are transmitted through the filter.

REFOCUSING MECHANISM AND MICROSHUTTER ASSEMBLY

During launch or operational lifetime, the OTE focus position might shift inadvertly, affecting NIRSpec's performance. The refocusing mechanism assembly is a set of two flat mirrors that can be used to effectively change the optical beam path length to refocus the beam onto the microshutter aperture plane if necessary. The RMA is made of Zerodur and coated with protected silver [26].

The microshutter assembly transmits specific areas of the light while blocking others as shown in Figure 2.7. Through this method, the spectral information of more than 100 targets can be acquired simultaneously. The individual shutters are controlled by magnetic actuation and electrostatic latching.

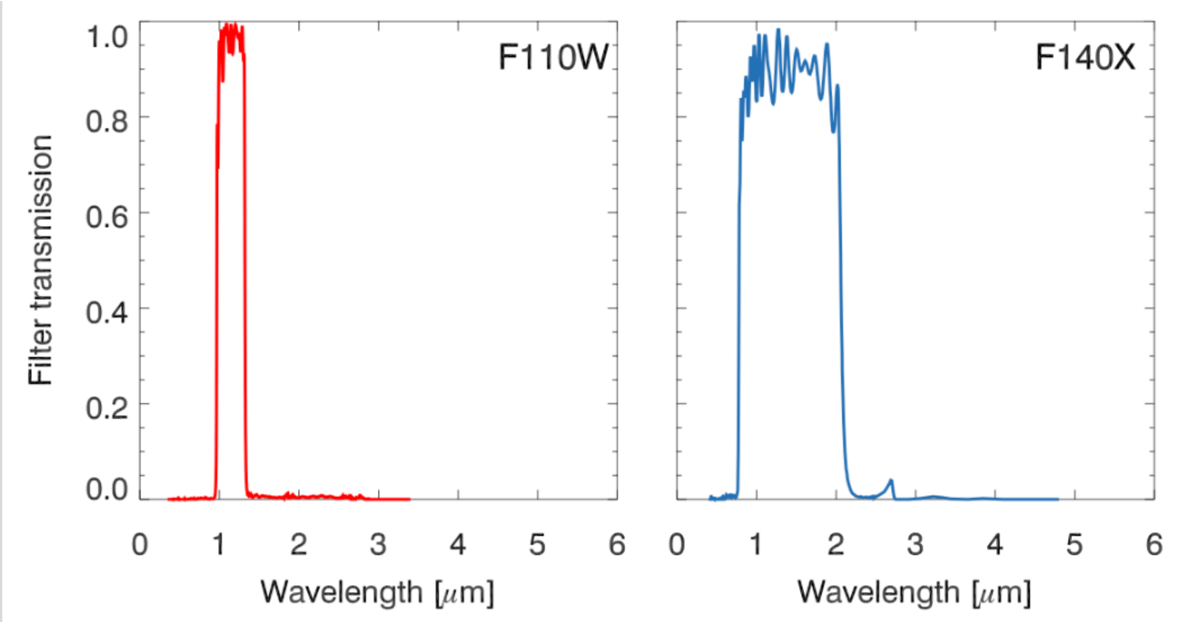

Figure 2.6: The band passes the two broadband filters [18]. Only wavelengths within a specific band are transmitted.

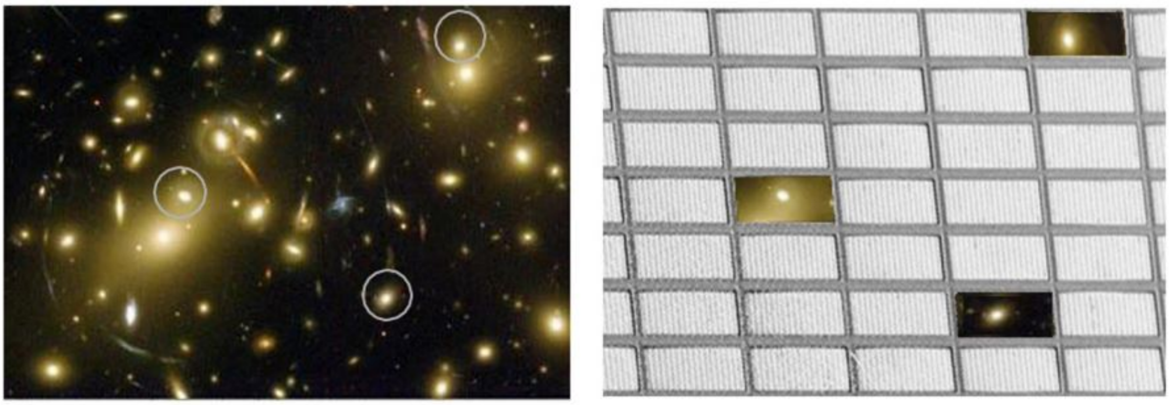

Figure 2.7: Example of object selection via the MSA [22]. It can be seen how several objects within the field of view can be observed simultaneously while blocking other objects by shutting the arrays in the MSA on the right.

COLLIMATOR OPTICS, GRATING WHEEL ASSEMBLY, AND CAMERA OPTICS

Behind the MSA, a flat folding mirror is used to direct the light towards COL. The diverging beam is then transformed to a collimated beam for the GWA. The blazed reflection gratings are used to disperse the beam as a function of wavelength. The grating wheel assembly houses six diffraction gratings, Table 2.3, a prism, and a target acquisition mirror [9]. The gratings diffract in multiple orders of diffraction, as will be elaborated on in Chapter 3, and their peak efficiency is reached in the negative first order (-1). The grating substrate is made of Zerodur and has a reflective gold mirror coating. The specifications of the gratings are given in Table 2.3. Finally, at CAM the beam is focussed and de-magnified for the focal plane assembly via the last TMA system.

CALIBRATION ASSEMBLY

As previously stated, NIRSpec houses a CAA for which the initial light path will slightly differ from the nominal science path. The CAA is used to calibrate the response of all detector pixels for all wavelengths. An internal light source is used and is reflected via two additional mirrors, CAL1 and CAL2, via REM2 to a mirror on the back of the FWA, CAL3, towards FOR3 as shown in Figure 2.8. This simulates the light coming through the FWA and from there on the optical path is identical to the nominal science path. The light source is an integrating sphere with cylindrical light sources as depicted in Figure 2.9. The light first bounces around within the sphere before exiting which ensures that the calibration beam consists of unpolarised light with homogeneous irradiance across the wavelength range.

To further analyse how these optical elements influence the polarisation sensitivity of NIRSpec, first a theoretical background in optics must be established. This is done in Chapter 3.

Grating	**Groove density [mm^{-1}]**	**Blaze angle [deg]**	**Tilt angle [deg]**	**Wavelength range [μm]**
GRT1000-I	95.3971	3.72	4.2	1.0 - 1.8
GRT1000-II	56.8756	3.86	4.2	1.7 - 3.1
GRT1000-III	33.8217	3.64	4.1	2.9 - 5.2
GRT2700-I	252.2858	10.41	8.8	1.0 - 1.8
GRT2700-II	150.2927	10.41	8.75	1.7 - 3.1
GRT2700-III	89.4087	10.36	8.8	2.9 - 5.2

Table 2.3: The blazed gratings specifications [9] [30]. Note that the tilt angle is the angle that the grating is tilted with respect to the GWA.

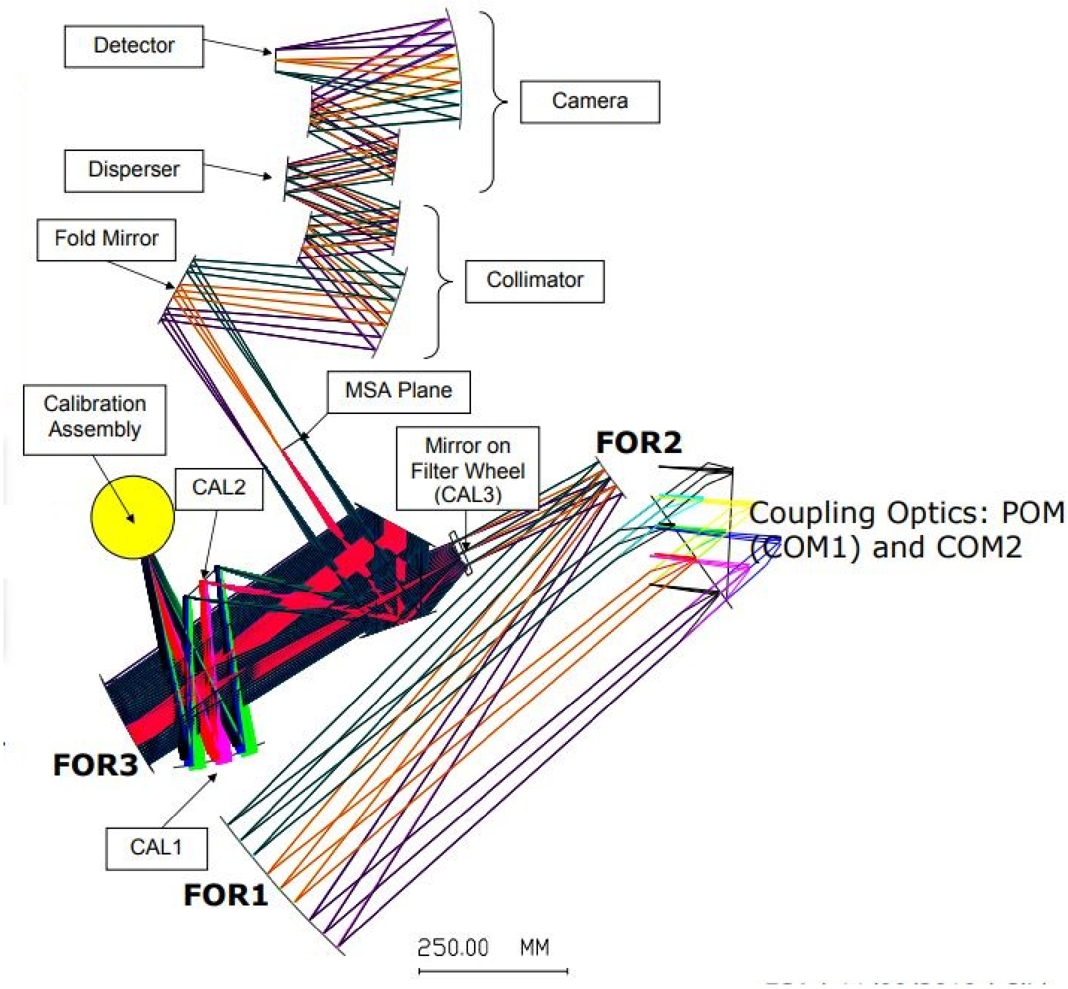

Figure 2.8: A schematic of the calibration path from the integrating sphere (yellow circle) towards the nominal science path (from CAL3 onwards to FOR3) [30].

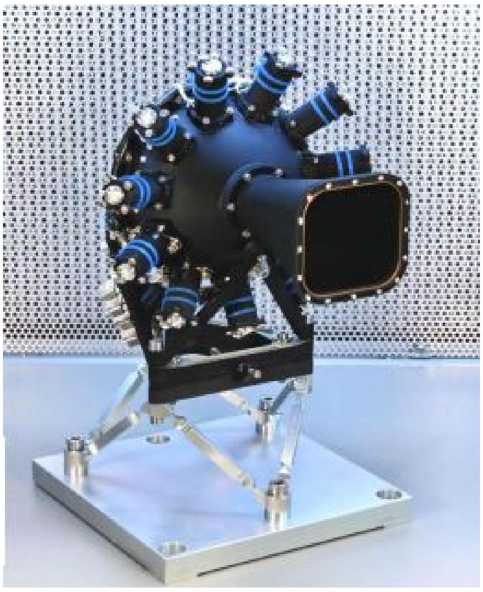

Figure 2.9: The gold-plated integrating sphere with eleven distinct illumination sources to produce an unpolarised and homogeneous diffuse light beam for onboard calibration purposes [4]. This is represented by the yellow circle in Figure 2.8

3

Optics Literature

This chapter contains relevant background literature on four topics: the fundamentals of polarisation, Fresnel equations for reflection and transmission, an introduction to Mueller calculus, and theory of reflection gratings. This theoretical background is necessary to model the polarisation state of the light throughout the instruments where it is reflected by the mirrors.

3.1. Fundamentals of Polarisation

This section serves as an introduction to light polarisation and discusses its theoretic fundamentals based on Optics by Hecht [17]. It will give a better understanding of the physics behind polarisation and how specifically reflections can introduce polarisation.

Definitions

Light can be described as a transverse electromagnetic wave, which means it consists of a coupled electric and magnetic force field [19], this is illustrated in Figure 3.1. The two fields are at right angles to each other and are transverse to the direction of propagation. Polarisation is the variability over time of amplitude and phase of the electromagnetic wave. One identifies light for which the orientation of the electric field is constant as linearly polarised light. The direction of the electric field is called the plane-of-vibration containing both the electric field vector $\vec{\boldsymbol{E}}$ and the propagation vector $\vec{\boldsymbol{k}}$ in the z-direction of motion.

Suppose two orthogonal electromagnetic waves propagate in z-direction over time with their electric field directions in x- and y-direction, described by Equation (3.1) and Equation (3.2), respectively. n these equations, E_0 is the electric field amplitude and ϵ is the phase difference, while $(kz-\omega t)$ describes the phase depending on, the propagation vector, the location in z-direction, the angular frequency, and time. Furthermore, $\hat{\imath}$, $\hat{\jmath}$, $\hat{k}$ are the unit direction vectors in x-, y-, and z-direction. Note that in this formulation of the phase, E_y lags E_x by positive ϵ. Two electromagnetic waves with the same frequency and direction of propagation superimpose into a resultant wave of which $\vec{\boldsymbol{E}}$ is equal to the sum of the two component electric field vectors as shown in Equation (3.3). I

$$\vec{\boldsymbol{E}}_{\boldsymbol{x}}(z,t) = E_{0,x}\cos(kz-\omega t)\,\hat{\boldsymbol{\imath}} \tag{3.1}$$

$$\vec{\boldsymbol{E}}_{\boldsymbol{y}}(z,t) = E_{0,y}\cos(kz-\omega t+\epsilon)\,\hat{\boldsymbol{\jmath}} \tag{3.2}$$

$$\vec{\boldsymbol{E}}(z,t) = \vec{\boldsymbol{E}}_{\boldsymbol{x}}(z,t) + \vec{\boldsymbol{E}}_{\boldsymbol{y}}(z,t) \tag{3.3}$$

The resultant light will be linearly polarised (the so-called $\mathscr{P}$-state) when $\epsilon = \pm 2n\pi$, in which n is any integer, because of the fixed amplitude direction as shown in Equation (3.4).

$$\vec{\boldsymbol{E}}(z,t) = (E_{0,x}\,\hat{\boldsymbol{\imath}} + E_{0,y}\,\hat{\boldsymbol{\jmath}})\cos(kz-\omega t) \tag{3.4}$$

Furthermore, if the amplitudes are equal, $\epsilon = 2n\pi \pm \frac{1}{2}\pi$ results in circular polarised light, more specifically when the $\pm$ sign is negative, the resultant light is in right-circular polarised state ($\mathscr{R}$-state), and when the $\pm$ sign is positive the light is in a left-circular polarised state ($\mathscr{L}$-state). As an example, this is shown in the

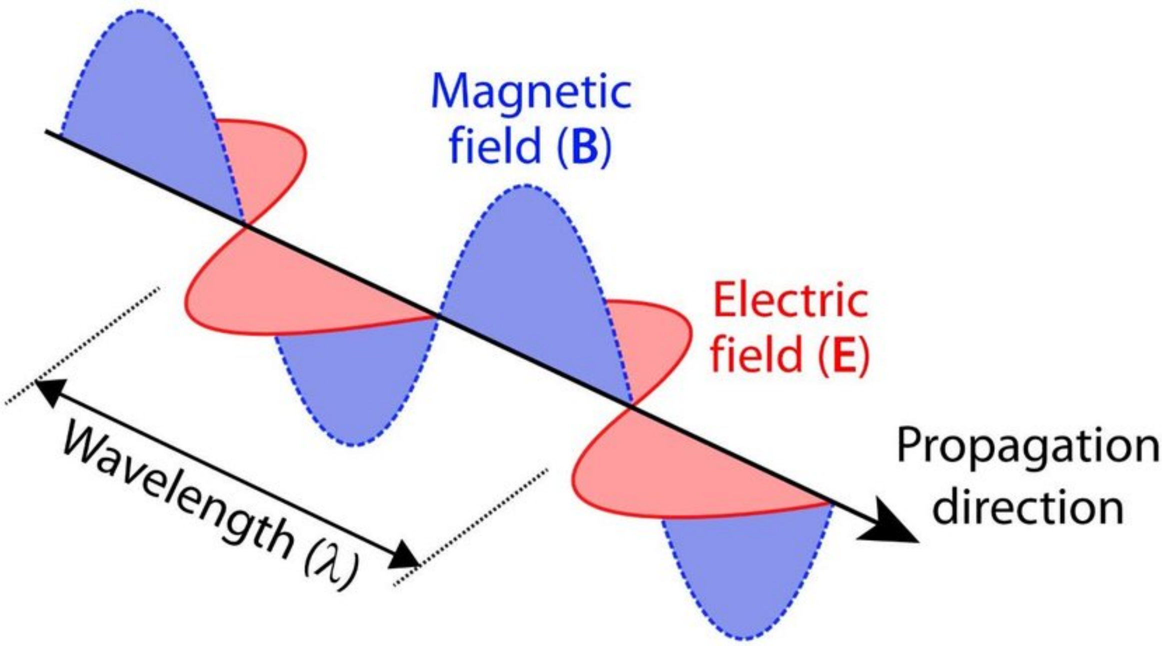

Figure 3.1: Schematic of a ray of light propagating through space with an electric and magnetic field component [32]

specific case where $\epsilon = -\frac{1}{2}\pi$ in Equation (3.5) and Equation (3.6). One can deduct that this is an $\mathscr{R}$-state by checking $\vec{\boldsymbol{E}}$ at $t_0 = 0$ and $t_1 = kz/\omega$. Filling in those values for an arbitrary kz_0 and kz, respectively, the result is shown in Figure 3.2 in which $\vec{\boldsymbol{E}}_{\mathbf{0}}$ aligns with the reference axis and $\vec{\boldsymbol{E}}_{\mathbf{1}}$ aligns with the x-axis. It can thus be concluded that the wave function describes an $\mathscr{R}$-state. Linear and circular polarisation can be considered special cases of elliptically polarised light ($\mathscr{E}$-state), in which generally both the direction and magnitude of the electrical field vary over time.

$$\vec{\boldsymbol{E}}_{\boldsymbol{y}}(z,t) = E_0 \cos(kz - \omega t - \frac{1}{2}\pi)\,\hat{\boldsymbol{j}} = E_0 \sin(kz - \omega t)\,\hat{\boldsymbol{j}} \tag{3.5}$$

$$\vec{\boldsymbol{E}} = E_0[\cos(kz - \omega t)\,\hat{\boldsymbol{\imath}} + \sin(kz - \omega t)\,\hat{\boldsymbol{j}}] \tag{3.6}$$

Starlight is emitted by a very large number of randomly oriented atomic emitters and each excited atom radiates a monochromatic, thus fully linearly polarised, wavetrain for roughly 10^{-8} s. The emissions with the same frequency combine together and new wavetrains are constantly added to this. The end product is then light of which the overall polarisation is effectively random, this is defined as unpolarised light or natural light. In practice, light in general is usually neither completely polarised nor completely unpolarised, but rather a superposition of specific amounts of both, it is thus partially polarised.

POLARISATION INDUCED BY REFLECTIONS

The polarisation state of light can be altered in various ways, but they are all based on one of four physical mechanisms: dichroism, birefringence, scattering, and reflection. The underlying principle for all four mechanisms is that there must be some form of asymmetry associated with the process. In other words, not all polarisation states will be affected in the same way. Only polarisation through reflection will be elaborated on in this report as it is of interest for the induced polarisation in NIRSpec.

According to [17], the electron-oscillator model can be used to depict the polarisation of light through reflection by a dielectric surface. Consider a $\mathscr{P}$-state beam of which the electric field is perpendicular to the plane of incidence as shown in Figure 3.3, this is later referred to as S-polarised light. The plane of incidence is defined as the plane that contains both the incident light as well as the normal on the reflection surface. When this beam hits a dielectric surface, the electrons of that surface are excited by the electric field and the beam is partially refracted through the medium and partially reflected due to reradiation. The electric field of both the refracted and reflected light have the same direction as that of the incident beam.

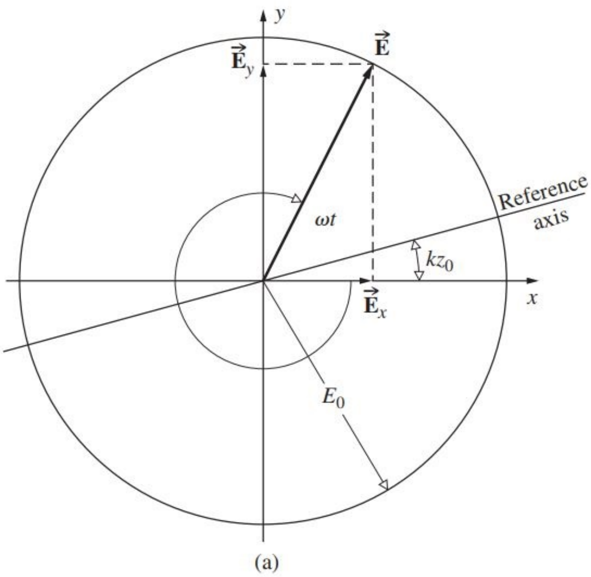

Figure 3.2: Visualization of the electric field direction for an $\mathscr{R}$-state wave function with direction of propagation into the paper and arbitrary reference axis as starting direction [17].

Now consider a $\mathscr{P}$-state beam light with its electric field in the same plane as the plane of incidence as shown in Figure 3.4, this is later referred to as P-polarised light. The amplitude of the reflected beam's electric field is now smaller because the direction of the beam makes a small angle, θ, with the axes of the dipoles. When the angle of incidence, θ_i, such that $\theta = 0°$ holds, the direction of the dipoles is perpendicular to the direction of reflection, and as a result, there will be no reflected beam. For that value of θ_i, $\theta_r + \theta_t = 90°$, as can be seen in Figure 3.4.

This means that if an unpolarised wave, that can be described as two incoherent orthogonal $\mathscr{P}$-states, would intersect with a surface with θ_i for which $\theta_r + \theta_t = 90°$ holds, only the component normal to the plane of incidence would be reflected, creating a $\mathscr{P}$-state beam of which the electric field vector is perpendicular to the plane of incidence, so-called S-polarisation used in further sections of this report. The angle of incidence at which this occurs is called the polarisation angle or Brewster's angle and is indicated by θ_p, .

3.2. Fresnel Equations for Reflection and Transmission

Mirrors used in space telescopes require a high spectral reflectivity to minimize the loss of photons [13]. Conducting materials such as metals and semiconductors posses this characteristic because Joule heating occurs due to their molecular structure. Joule heating is a thermodynamic process in which electromagnetic energy is irreversibly transformed into heat. This phenomenon attenuates the optical field within the absorbing media and makes the material practically opaque. This effect can be described by defining the complex refractive index as Equation (3.7) with a real refractive index n and an extinction coefficient κ.

$$\boldsymbol{n} = n + i\kappa \tag{3.7}$$

The Fresnel equations describe the interaction of light beams with surfaces and their subsequent reflection and transmission and they can be derived from Maxwell's equations. The Fresnel equations describe the change in amplitude and phase of the components of light so they are intimately tied to the polarisation.

Consider the same situation as described before in which a $\mathscr{P}$-polarised incident light beam is incident on a surface. Two separate cases are studied again; in the first case the light is S-polarised, with the electric field vector perpendicular to the plane of incidence (Figure 3.5) and in the second case it is P-polarised, with the electric field vector parallel to the plane of incidence (Figure 3.6). For the first case, the subscript s will be used from the German word for perpendicular, 'senkrecht', and for the second case the subscript p will be used for parallel. Furthermore, the magnetic field is represented by $\vec{\boldsymbol{B}}$ while the reflected and transmitted electric fields are shown as $\vec{\boldsymbol{R}}$ and $\vec{\boldsymbol{T}}$, respectively. Finally, the real parts n_1 and n_2 indicate the two different refractive indices of the media.

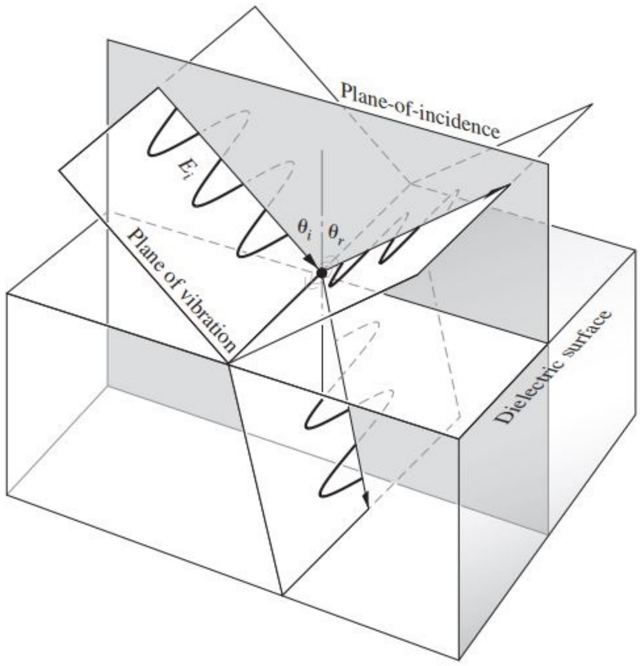

Figure 3.3: The refraction and reflection of an incident beam of light with an electric field perpendicular to the plane of incidence [17]

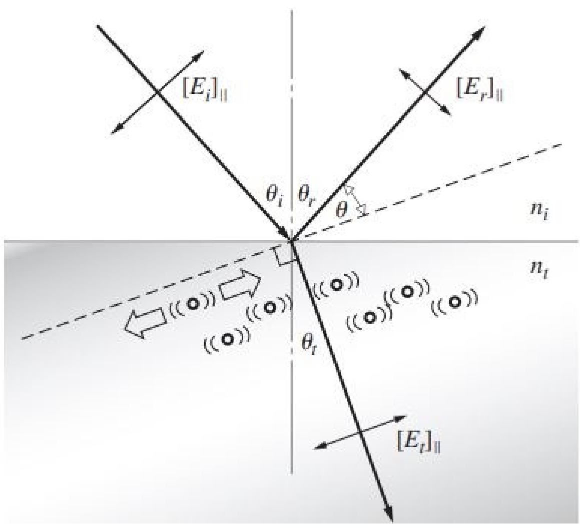

Figure 3.4: The refraction and reflection of an incident beam of light with an electric field in the plane of incidence [17]

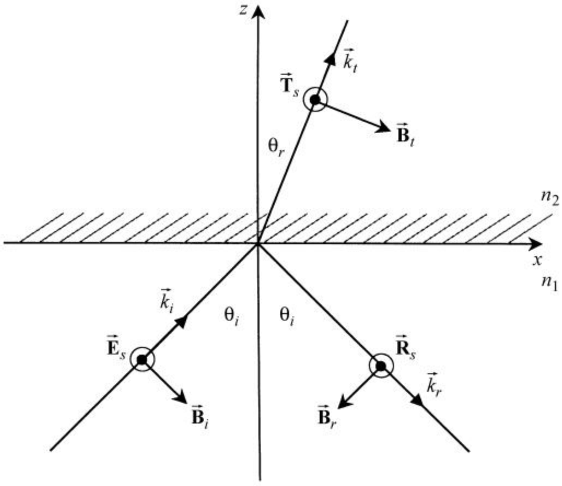

Figure 3.5: First case in which the electric field vector is perpendicular to the plane of incidence (coming out of the paper), thus S-polarised [13]. The incident beam (with subscript i) is partially reflected (subscript r) and transmitted (subscript t) at the intersection with the surface. The electric field of the reflected and transmitted beam are denoted by R and T, respectively, instead of E as for the incident beam. The medium in which the incident light travels has a real refractive index n_1, while the material of the surface has real refractive index n_2.

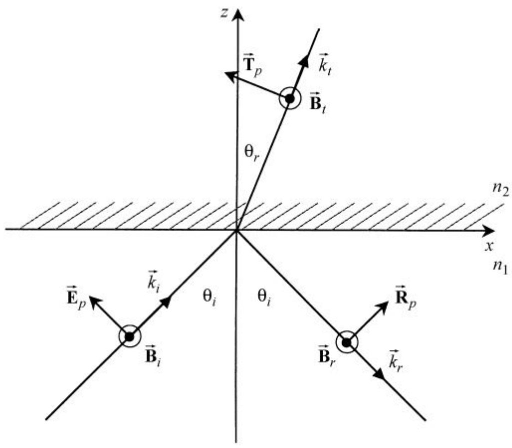

Figure 3.6: Similar to Figure 3.5, but now the electric field vector of the incident beam is parallel to the plane of incidence and thus P-polarised [13]

From Maxwell's equations for homogeneous isotropic media and using Snell's law, the Fresnel equations that describe the amplitudes of the reflected and transmitted beams for Figure 3.5 are given in Equation (3.8) and Equation (3.9), respectfully [13] [section 8.2.3]. Similarly, the Fresnel equations for the reflection amplitude and transmission amplitude are given in Equation (3.10) and Equation (3.11), respectively. Note that for the derivation of these equations, the assumption is made that the permeability of the media is approximately equal to that of vacuum, i.e. $\mu \approx 1$ (non-magnetic). These Fresnel equations will be used to compute reflections by mirrors and transmission through filters for light rays.

$$R_s = \frac{\boldsymbol{n}_1 \cos(\theta_i) - \boldsymbol{n}_2 \cos(\theta_r)}{\boldsymbol{n}_1 \cos(\theta_i) + \boldsymbol{n}_2 \cos(\theta_r)} E_s \tag{3.8}$$

$$T_s = \frac{2\boldsymbol{n}_1 \cos(\theta_i)}{\boldsymbol{n}_1 \cos(\theta_i) + \boldsymbol{n}_2 \cos(\theta_r)} E_s \tag{3.9}$$

$$R_p = \frac{\boldsymbol{n}_2 \cos(\theta_i) - \boldsymbol{n}_1 \cos(\theta_r)}{\boldsymbol{n}_2 \cos(\theta_i) + \boldsymbol{n}_1 \cos(\theta_r)} E_p = \frac{\tan(\theta_i - \theta_r)}{\tan(\theta_i + \theta_r)} E_p \tag{3.10}$$

$$T_p = \frac{2\boldsymbol{n}_1 \cos(\theta_i)}{\boldsymbol{n}_2 \cos(\theta_i) + \boldsymbol{n}_1 \cos(\theta_r)} E_p = \frac{2\sin(\theta_r)\cos(\theta_i)}{\sin(\theta_i + \theta_r)\cos(\theta_i - \theta_r)} E_p \tag{3.11}$$

3.3. INTRODUCTION TO JONES AND MUELLER CALCULUS

To fully understand polarisation, it is important to be able to experimentally and theoretically analyse, describe, and predict the state of polarisation. In this section, an introduction is given on Jones and Mueller calculus.

MALUS'S LAW

To define the Stokes parameters, first Malus' law is explained through a demonstration in which a setup is used as shown in Figure 3.7, consisting of a light source, the linear polariser, an analyser, and a detector. Unpolarised light is to be used as a source with an arbitrary irradiance. The expected output of the polariser is $\mathscr{P}$-state light parallel to the transmission axis at an angle θ, and half the irradiance, I_1, assuming an ideal polariser. The general equation to compute this irradiance is shown in Equation (3.12) in which ϵ_0 is the vacuum permittivity. By using a vertical polariser as analyser, the amplitude of the wave and irradiance of the light at the detector can then be described as a function of θ as shown in Equation (3.13), this is known as Malus's law. These equations give a better understanding of how irradiance can change over polarisation orientation with a linear polariser and help with the explanation of the Stokes parameters.

$$I_1 = \frac{c\epsilon_0}{2} {E_{0,1}}^2 \tag{3.12}$$

$$E_{0,2} = E_{0,1}\cos(\theta) \rightarrow I(\theta) = I_1\cos^2(\theta) \tag{3.13}$$

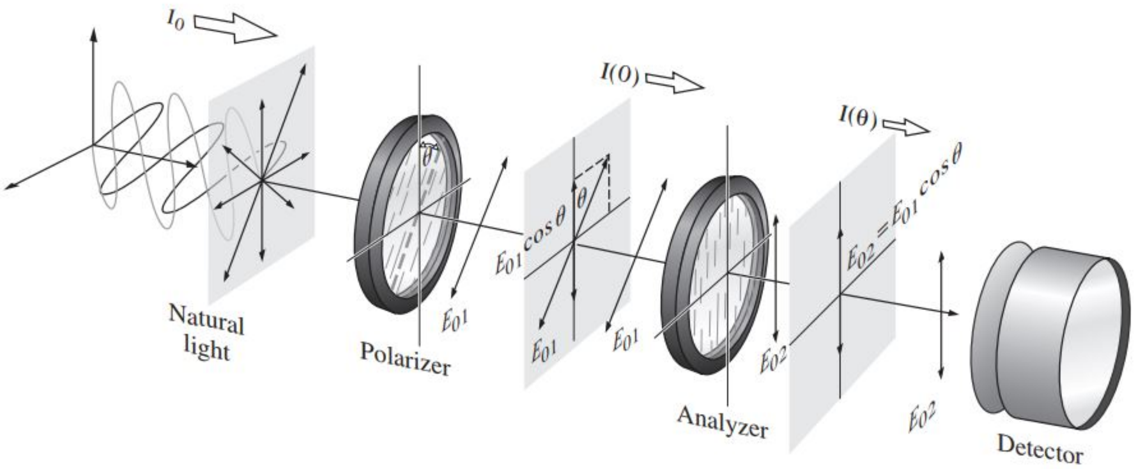

Figure 3.7: Demonstration of Malus's law using a polariser and analyser [17]

STOKES PARAMETERS

Imagine using four filters that each transmit half of the incident light under natural light illumination. The first filter is isotropic and transmits light regardless of polarisation state. The second is a linear polariser with horizontal transmission axis. The third is also a linear polariser but with a +45° transmission axis. The fourth is a circular polariser that transmits right circular polarised light. When the polariser and analyser in Figure 3.7 are both replaced by a single filter, the respective transmitted irradiances of the four filters mentioned above are then defined as I_0, I_1, I_2, and I_3. The Stokes parameters are then defined as in Equation (3.14) [17] in which S_0 represents the total irradiance, S_1 represents horizontal $\mathscr{P}$-state, S_2 represents 45° $\mathscr{P}$-state, and S_3 represents $\mathscr{R}$-state. The Stokes parameters are also defined as I, Q, U, and V, respectively.

$$\boldsymbol{S} = \begin{bmatrix} S_0 \\ S_1 \\ S_2 \\ S_3 \end{bmatrix} = \begin{bmatrix} I \\ Q \\ U \\ V \end{bmatrix} \rightarrow \begin{matrix} S_0 = 2I_0 \\ S_1 = 2I_1 - 2I_0 \\ S_2 = 2I_2 - 2I_0 \\ S_3 = 2I_3 - 2I_0 \end{matrix} \tag{3.14}$$

This means that for a horizontal $\mathscr{P}$-state beam $S_1 > 0$ and for a vertical $\mathscr{P}$-state beam $S_1 < 0$. Furthermore, in the case where the beam does not display a preferential orientation w.r.t. these axes, e.g. 45° $\mathscr{P}$-state or right-circularly polarised $\mathscr{R}$-state, $S_1 = 0$. Similarly, the sign convention of S_2 and S_3 is determined by the tendency of 45° $\mathscr{P}$-state and $\mathscr{R}$-state or $\mathscr{L}$-state, respectively.

S_1, S_2, and S_3 are often normalized w.r.t. S_0 which means that e.g. natural light would be [1; 0; 0; 0] and horizontal $\mathscr{P}$-state results in [1; 1; 0; 0]. For completely polarised light, Equation (3.15) holds, while the degree of polarisation (DOP) for partially polarised light can be computed using Equation (3.16).

$$S_0^2 = S_1^2 + S_2^2 + S_3^2 \tag{3.15}$$

$$DOP = \frac{\sqrt{S_1^2 + S_2^2 + S_3^2}}{S_0} \tag{3.16}$$

In the case of two incoherent quasimonochromatic waves, the Stokes parameters of the resultant beam will be the sum of the corresponding parameters of the constituents. An example is shown in Equation (3.17) in which a vertical $\mathscr{P}$-state is added to an incoherent $\mathscr{R}$-state beam with twice the flux density. The resultant is an elliptically polarised $\mathscr{E}$-state beam with three times the unit flux density, more vertical than horizontal and moves right circularly.

$$\begin{bmatrix} 1 \\ -1 \\ 0 \\ 0 \end{bmatrix} + \begin{bmatrix} 2 \\ 0 \\ 0 \\ 2 \end{bmatrix} = \begin{bmatrix} 3 \\ -1 \\ 0 \\ 2 \end{bmatrix} \tag{3.17}$$

JONES VECTORS

Jones vectors are another method of representing polarised light, shown in Equation (3.18), which is applicable to coherent, thus fully polarised, beams. To be able to handle coherent waves, the phase information must be preserved, therefore the Jones vector can be rewritten in complex form $\tilde{\boldsymbol{E}}$, also shown in Equation (3.18), in which ϕ represents the respective phases. Note that Equation (3.19) is used to create the complex form.

$$\vec{\boldsymbol{E}} = \begin{bmatrix} E_x(t) \\ E_y(t) \end{bmatrix} \rightarrow \tilde{\boldsymbol{E}} = \begin{bmatrix} E_{0,x}e^{i\phi_x} \\ E_{0,y}e^{i\phi_y} \end{bmatrix} \tag{3.18}$$

$$e^{i\phi} = \cos(\phi) + i\sin(\phi) \tag{3.19}$$

The sum of two coherent beams is formed by a sum of the corresponding components. So the summation of a horizontal $\mathscr{P}$-state with a vertical $\mathscr{P}$-state of which the amplitude and phase are equal is shown in Equation (3.20) which results in a $\mathscr{P}$-state at 45° as one would expect. As exact amplitude and phase are not usually necessary, the irradiance can be normalized by dividing both elements by a scalar, such that the sum of the squares of the components is 1, as is also shown.

$$\tilde{\boldsymbol{E}} = \begin{bmatrix} E_{0,x}e^{i\phi_x} \\ 0 \end{bmatrix} + \begin{bmatrix} 0 \\ E_{0,y}e^{i\phi_y} \end{bmatrix} = E_0 e^{i\phi} \begin{bmatrix} 1 \\ 1 \end{bmatrix} \rightarrow \tilde{\boldsymbol{E}}_{\boldsymbol{45^\circ}} = \frac{1}{\sqrt{2}} \begin{bmatrix} 1 \\ 1 \end{bmatrix} \tag{3.20}$$

Similarly, the normalized form of horizontal and vertical $\mathscr{P}$-state light is shown in Equation (3.21). For $\mathscr{R}$-state light, again $E_{0,x} = E_{0,y}$ and the y-component leads the x-component by 90°. This means that, due to the used notation, a $\frac{1}{2}\pi$ is subtracted from ϕ_y resulting in Equation (3.22). The final result after some modification is then shown in Equation (3.23) for both $\mathscr{R}$-state and left circularly polarised $\mathscr{L}$-state.

$$\tilde{\boldsymbol{E}}_{\boldsymbol{h}} = \begin{bmatrix} 1 \\ 0 \end{bmatrix}, \tilde{\boldsymbol{E}}_{\boldsymbol{v}} = \begin{bmatrix} 0 \\ 1 \end{bmatrix} \tag{3.21}$$

$$\tilde{\boldsymbol{E}}_{\mathscr{R}} = \begin{bmatrix} E_{0,x}e^{i\phi_x} \\ E_{0,x}e^{i(\phi_x - \frac{1}{2}\pi)} \end{bmatrix} \rightarrow \begin{bmatrix} 1 \\ e^{i(-\frac{1}{2}\pi)} \end{bmatrix} = \begin{bmatrix} 1 \\ -i \end{bmatrix} \tag{3.22}$$

$$\tilde{\boldsymbol{E}}_{\mathscr{R}} = \frac{1}{\sqrt{2}} \begin{bmatrix} 1 \\ -i \end{bmatrix}, \tilde{\boldsymbol{E}}_{\mathscr{L}} = \frac{1}{\sqrt{2}} \begin{bmatrix} 1 \\ i \end{bmatrix} \tag{3.23}$$

JONES AND MUELLER MATRICES

Suppose an incident beam described by $\tilde{\boldsymbol{E}}_{\boldsymbol{i}}$ passes through an optical element and the transmitted wave is described by $\tilde{\boldsymbol{E}}_{\boldsymbol{t}}$. The transformation of the Jones vector can be described by a matrix $\boldsymbol{J}$ as shown in Equation (3.24). This matrix is called the Jones matrix and shares the same characteristics as Jones vectors; that is the Jones matrix is applies to coherent waves only. Similarly, this principle can be applied to Stokes parameters using a Mueller matrix $\boldsymbol{M}$ as shown in Equation (3.25). As an example, consider unpolarised light going through an ideal linear horizontal polariser. The resultant can be computed using a Mueller matrix for the linear horizontal polariser as shown in Equation (3.26). It can be seen that the resultant is a horizontal $\mathscr{P}$-state with half the irradiance, as is expected. A beam passing though n optical elements can be described by n matrices as shown in Equation (3.27). Similarly, Mueller matrices can also be used to describe the polarisation state change by reflections, e.g. via mirrors. Note that the matrices do not commute and must be applied in the proper order.

$$\tilde{\boldsymbol{E}}_{\boldsymbol{t}} = \boldsymbol{J}\tilde{\boldsymbol{E}}_{\boldsymbol{i}}, \quad \boldsymbol{J} = \begin{bmatrix} j_{11}, j_{12} \\ j_{21}, j_{22} \end{bmatrix} \tag{3.24}$$

$$S_t = \boldsymbol{M}S_i, \quad \boldsymbol{M} = \begin{bmatrix} m_{11}, m_{12}, m_{13}, m_{14} \\ m_{21}, m_{22}, m_{23}, m_{24} \\ m_{31}, m_{32}, m_{33}, m_{34} \\ m_{41}, m_{42}, m_{43}, m_{44} \end{bmatrix} \tag{3.25}$$

$$\mathscr{S}_t = \frac{1}{2}\begin{bmatrix} 1,1,0,0 \\ 1,1,0,0 \\ 0,0,0,0 \\ 0,0,0,0 \end{bmatrix}\begin{bmatrix} 1 \\ 0 \\ 0 \\ 0 \end{bmatrix} = \frac{1}{2}\begin{bmatrix} 1 \\ 1 \\ 0 \\ 0 \end{bmatrix} \tag{3.26}$$

$$S_t = \boldsymbol{M_n}\ldots\boldsymbol{M_2}\boldsymbol{M_1}S_i \tag{3.27}$$

This is relevant for this master thesis research because this means that the polarisation state change throughout NIRSpec can be described by the individual Mueller matrices of the optical elements. If all Mueller matrices would be known, they could also be combined to a single Mueller matrix as shown in Equation (3.27) to describe the polarisation state change over the complete instrument at once.

3.4. THEORY OF REFLECTION GRATINGS

Diffraction is the deviation of light from rectilinear propagation; a region of the wavefront is altered in amplitude and/or phase [17]. When this happens due to encountering an object, the propagating wavefront segments interfere with each other afterwards, creating a diffraction pattern. Physics-wise, there is no distinction between interference and diffraction, but it has become customary to use diffraction when considering a large number of waves.

The phenomenon of diffraction can be described by the Huygens-Fresnel principle; "every unobstructed point of a wavefront, at a given instant, serves as as source of spherical secondary wavelets (with the same frequency as that of the primary wave). The amplitude of the optical field at any point beyond is the superposition of all these wavelets (considering their amplitudes and relative phases)" [17].

A repetitive array of diffracting elements that causes periodic alterations in the phase, amplitude, or both of an emergent wave is called a diffraction grating. Diffraction gratings can be divided into transmission amplitude gratings, transmission phase gratings, and reflection phase gratings. An example of a reflection grating is shown in Figure 3.8. The reflection grating diffracts the light such that the interference of the reflected light beams results in local maxima and minima. The local maxima are indicated by the order of diffraction or principal maxima m. The minima are, angle-wise, located in between the maxima.

The effect of diffraction gratings can be described by the general grating equation Equation (3.28) in which a is the distance between two centers of adjacent slits, and θ_m is the angle between the mth order maximum of the diffracted ray and the grating's normal vector. As the directions of the maxima are dependent on the wavelength, gratings can be used to disperse light by wavelength. The grating equation can be expanded by including an incidence angle θ_i as shown in Equation (3.29). From this equation, it is clear the the zeroth order of m represents specular reflection as $\theta_0 = \theta_i$.

In Figure 3.8, most of the light undergoes specular reflection as if encountering a plane mirror, in the direction of the zeroth order. The reflection angle of this order is hereafter referred to as θ_0. As θ_0 is independent of wavelength, the light that follows this path is undispersed. To shift energy out of the zeroth order, that is useless for dispersion by wavelength, to a different order, the specular reflection angle, θ_r should be independently changed from θ_m. This can be done by using a blazed reflection phase grating (also called echelette grating) as shown in Figure 3.9 with blaze angle γ. As the specular reflection angle, θ_r, is purely dependent on the incidence angle w.r.t. the individual groove surface and θ_m is dependent on the incidence angle w.r.t. the grating normal, the specular reflection can be independently varied from θ_0, thus changing the diffraction peak to a different order.

The energy distribution of reflected light by blazed gratings tends to be polarisation dependent according to Handbook of optics by Bennett [5]. The exact theory behind the polarisation dependent efficiencies appeared hard to find, unfortunately. This means that there does not appear to be a theory to describe reflection gratings as a Mueller matrix as discussed before. Instead, PCGrate, a software that specialises in reflection grating analysis, is commonly used in practice and has had good to excellent results compared to real life measurements. Therefore, the gratings of NIRSpec will be defined by empirical data from PCGrate instead of a theoretically defined Mueller matrix.

$$a\sin(\theta_m) = m\lambda \tag{3.28}$$

$$a\left[\sin(\theta_m) - \sin(\theta_i)\right] = m\lambda \tag{3.29}$$

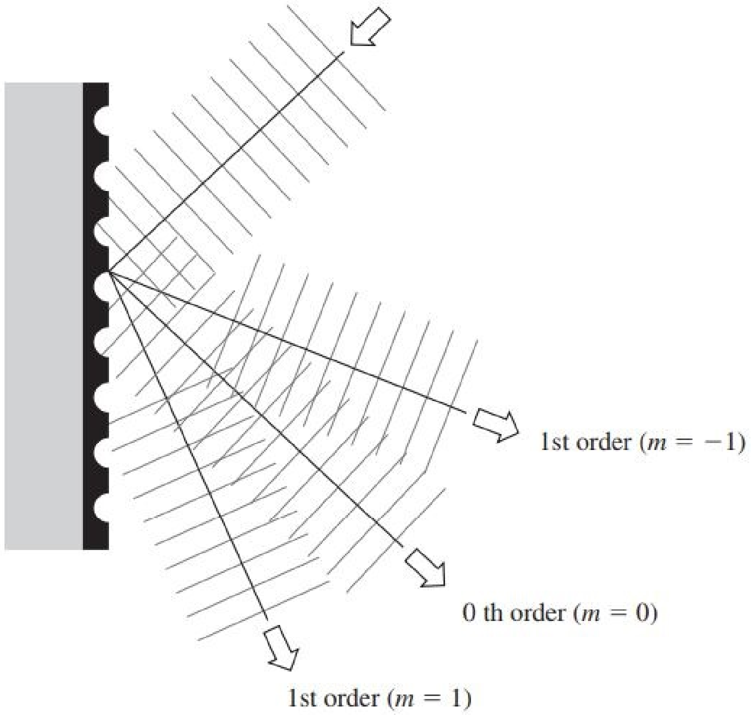

Figure 3.8: An example of a generic reflection phase grating [17]

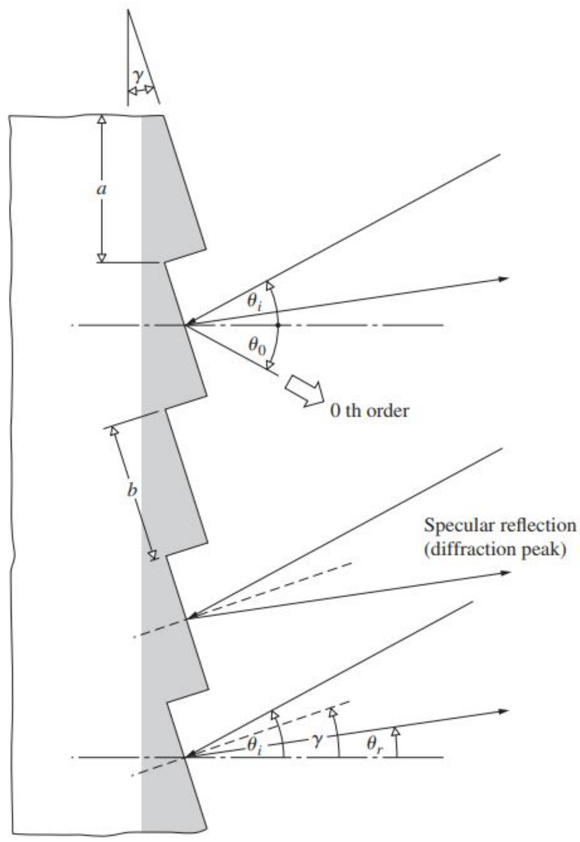

Figure 3.9: A blazed reflection phase grating with blaze angle γ, groove spacing a, and incidence and reflection angle θ_i and θ_r, respectively [17]

4

Ray Tracer

To accurately determine the polarisation state of the light throughout NIRSpec, a numerical code is written in Python [29] equivalent to a ray tracer. The main objective of the ray tracer is to determine the polarisation state of light observed by JWST throughout NIRSpec and specifically just before it reaches the grating wheel assembly. This polarisation state is computed in between all optical elements because it changes throughout the optical path, mainly through reflections by the mirrors. The reason it is important to know this polarisation state specifically before they reach the grating wheel assembly, is because these gratings are the main elements that introduce the polarisation sensitivity; differently polarised light can be reflected in different irradiances resulting in a mismatch between light that enters the telescope and light that reaches the detector. Unfortunately there appeared to be no information available to determine the polarisation state change by reflections with blazed reflection gratings, therefore an uncertainty is introduced to the polarisation state after the grating wheel assembly.

To determine the polarisation state throughout NIRSpec, a numerical code must describe several aspects: defining a beam of light, creating mirrors, pass filters, and gratings, and visualising Stokes parameters as polarisation ellipses. Every part will be described in detail on how it is defined, what the capabilities are, and the verification process. The built ray tracer is only used to model used for band I, II, and III, the main science bands of NIRSpec, in MOS mode and the calibration path with their respective filter and grating elements. This means that the slits and IFU in the microshutter array are not modelled in this research. Furthermore, the prism in the grating wheel assembly has also not been modelled. The ray tracer is designed to be modular, making addition of other configurations, optical elements, or analyses in follow-up work possible. Note that this ray tracer is built in a global x-, y-, z-, coordinate system instead of changing the z-axis with light propagation direction.

4.1. Light Beam

Individual rays of light enter JWST through the primary mirror, OTE1. The rays across the complete field of view together represent a beam of light. Because these individual rays have slightly different starting locations, they will be reflected by different areas of the mirrors in NIRSpec. Because most mirrors are non-flat, the rays will therefore undergo reflection by different angles which effectively changes their optical path and thus the polarisation state changes. By modelling a beam instead of a single ray, these differences can easily be compared. For this report a grid of 3x3 rays is used to define the light beam, such that both the center as well as the edges of a square field of view can be analysed. This provides information on the outer boundaries of expected polarisation state as the centre ray is expected to have the lowest induced degree of polarisation, while the edges will gain the highest induced degree of polarisation. If one were interested in a detailed analysis on how the polarisation state change over the field of view, more rays could be added. For this report, however, the outer boundaries are of more interest and increasing the ray density over the field of would not be worth the increase in computation time. The numbering of rays and positive direction of Stokes parameters Q and U are shown in Figure 4.1 with respect to the first mirror OTE1, the primary mirror of JWST, and looking into the direction of propagation.

The individual rays that that are modelled must be described in three main parameters; the starting position, the propagation direction, and Stokes parameters. Both the position and direction of each individual ray

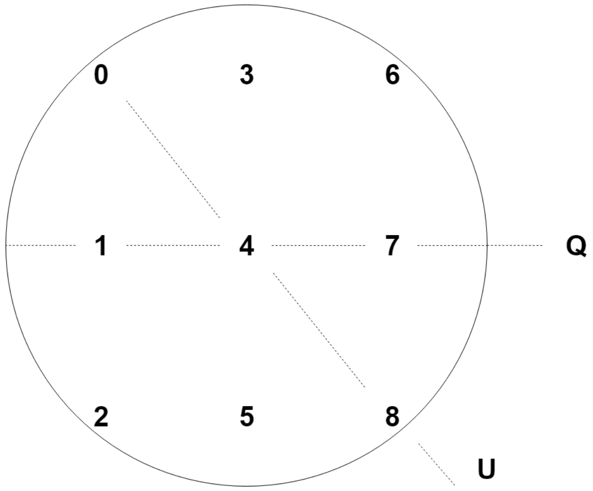

Figure 4.1: The position of the rays 0 to 8 with respect to the primary mirror of JWST, OTE1, looking into the direction of propagation into NIRSpec and the definitions of the positive Q and U Stokes parameters directions.

are described as a vector with an x-, y-, and z-component. For the analyses in this report, the start positions are fixed spots on OTE1.

The direction vector can be rotated to simulate different areas in the field of view. For a rotation around an axis with unit direction vector $\boldsymbol{u}$ and rotation angle θ, the rotation matrix is described as Equation (4.1). This rotation matrix is then used such that Equation (4.2) holds. In this equation, the accents represent the rotated values. The direction vectors of all rays are set equal because the rays that are observed by JWST are virtually parallel due to the large distance of the observed objects. Finally, every ray is given a set of Stokes parameters defined by 4 values in vector form as shown in Equation (4.3).

$$R = \begin{bmatrix} \cos(\theta) + u_x^2\big(1-\cos(\theta)\big) & u_x u_y\big(1-\cos(\theta)\big) - u_z\sin(\theta) & u_x u_z\big(1-\cos(\theta)\big) + u_y\sin(\theta) \\ u_y u_x\big(1-\cos(\theta)\big) + u_z\sin(\theta) & \cos(\theta) + u_y^2\big(1-\cos(\theta)\big) & u_y u_z\big(1-\cos(\theta)\big) - u_x\sin(\theta) \\ u_z u_x\big(1-\cos(\theta)\big) - u_y\sin(\theta) & u_z u_y\big(1-\cos(\theta)\big) + u_x\sin(\theta) & \cos(\theta) + u_z^2\big(1-\cos(\theta)\big) \end{bmatrix} \tag{4.1}$$

$$\begin{bmatrix} x' \\ y' \\ z' \end{bmatrix} = R \begin{bmatrix} x \\ y \\ z \end{bmatrix} \tag{4.2}$$

$$S = \begin{bmatrix} I \\ Q \\ U \\ V \end{bmatrix} \tag{4.3}$$

The performed verification process is given below. These steps were taking throughout and at the end of the development of the light beam. The code can be found in Appendix A.

1. Plot single ray in two-dimensional space
2. Apply rotations to single ray
3. Add multiple rays parallel to central ray
4. Rotate all rays together
5. Implement possibility of converging and diverging beams of light
6. Repeat all of the above for three-dimensional space

4.2. MIRRORS

The optical design of NIRSpec, including its mirrors, was done in OpticStudio by Zemax [34], an optics design software. The optical design was therefore also only accessible as Zemax files. Because the software was not easily accessible, it was decided to create an own code that is also more flexible in a way that new functions, such as specific for this master thesis research, can added more easily. The shape and position of the mirrors is imported from the Zemax files into the built ray tracer. The mirrors consisted of either flat or (off-centre) aspheric mirrors.

Implementing mirrors in the ray tracer consists of four parts. First, the mirror shape has to be defined and put in the correct position and orientation in the global reference system. Second, the intersection points with the incident beam must be computed. Third, the incidence angle and reflected rays must be computed. Last, Mueller calculus is applied to compute the Stokes parameters of the reflected rays. An overview of the complete process is given below.

1. Create rough meshgrid in x- and y-space based on the mirror's diameter
2. Decentre in relevant direction for off-centre mirrors
3. Apply Equation (4.4) to create mirrors in three-dimensional space and local reference frame
4. Rotate and translate mirror to global reference frame
5. Compute intersection points with incident light beam
6. Repeat the steps above for the relevant area with smaller meshgrid steps
7. Compute the normal of the mirror at intersection points
8. Compute the incidence angles
9. Compute the direction vector of reflected rays
10. Compute Fresnel reflection coefficients
11. Transform to correct orientation
12. Compute Jones matrices
13. Compute Mueller matrices
14. Compute Stokes parameters of reflected rays

MIRROR SHAPE AND POSITION

There are two types of mirrors used in the optical path of NIRSpec: flat and (off-centre) aspherical mirrors. The aspherical mirrors can be described in two-dimensional space by the general asphere equation Equation (4.4), where Z is the height along the axis normal to the mirror centre, R is the radial distance along any axis in the plane of the mirror centre, c is the curvature at vertex, k is the conic constant, a_x are aspherical coefficients that describe the asphericity of the mirror. It should be noted that in general the number of aspheric parameters used can differ, but these specific aspheric parameters are shown because specifically these have been used in the design of NIRSpec's mirrors. For the flat mirrors, Z(R) is set to 0, while for spherical mirrors, k and a_x are set to 0.

$$Z(R) = \frac{cR^2}{1+\sqrt{1-(1+k)c^2R^2}} + a_4R^4 + a_6R^6 + a_8R^8 + a_{10}R^{10} \tag{4.4}$$

The mirrors are then created in a three-dimensional space where R is created from x- and y-coordinates while Z(R) is represented in the z-axis. A domain is appointed in the x- and y-direction separately, based on the mirror's diameter, from which a meshgrid is produced. This will create squared mirrors without thickness. The lack of thickness does not have any effect on the optical path because the reflection surfaces of the mirrors are modelled, but possible future extensions could include the thicknesses to compute and optimise for e.g. mass properties. To account for off-centre mirrors, the mirrors are decentred in the direction of the specific axis domain. Now, the optically correct mirror can be computed from Equation (4.4) in a local reference frame. The points of this mirror are saved such that the indices of the intersection points that are found later on can be used to determine where the rays hit the mirror locally and from where the normal vector needs to be computed.

The last step is to rotate and transpose the mirror into the right location and orientation in the global reference system. This is done by a tilt around x-, y-, and z-axis as well as translation along those axes. This means that a maximum of three rotations and three translation are performed. For every rotation, a rotation matrix is computed, Equation (4.1), and applied to both the points on the mirror as well as the x-, y-, and z-axes for sequential rotations due to the definition of tilt angles of the mirrors. Finally, the translations are added along the globally defined axes and the mirror is defined in the ray tracer global reference frame.

The verification process of creating and positioning of the mirrors is given below.

1. Create and plot a flat mirror in two-dimensional space
2. Apply Equation (4.4) to create a spherical and parabolic mirror
3. Decentre to create off-centre spherical mirror
4. Create off-centre aspherical mirror
5. Apply rotations
6. Apply translations
7. Repeat all of the above for three-dimensional space
8. Additional validation was done by comparison with Zemax data

INTERSECTION POINTS

The following task is to compute the intersection points of the incoming rays with the mirrors. This is done for each ray separately in main two steps:

1. Compute a set of direction vectors from the ray origin to every point of the mirror.
2. Determine which direction vector from step 1 is matches the actual ray direction vector.

First, a set of direction vector is computed from the ray origin to every point of the mirror. Mathematically, the ray origin vector is subtracted from all mirror point vectors. The point for which the computed vector is closest to the actual actual propagation direction vector of the ray, the so-called ray direction vector, is seen as the intersection point.

Second, it has to be determined which of the computed direction vectors matches the ray direction vector. This is done by normalising the computed vectors and projecting them on the (normalised) ray direction vector; mathematically this means using the dot product. The computed vector of which the dot product is closest to 1 is the computed vector most parallel to the ray direction vector. Now by relating that computed vector to its corresponding point of the mirror, the intersection point with the mirror is found.

When more points are used for the mirror, a more accurate intersection point can be computed at the cost of computation time. As rays only hit a small section of each mirror, an optimisation algorithm is applied.

First, a rough intersection point is computed by defining the mirror in an 10x10 grid. Then based on that rough estimate, only the relevant area of the mirror is computed in smaller step sizes. Determination of the used step sizes and their resultant accuracy are discussed in Section 4.6.

The verification process performed during the development of and of finding the intersection points is given below.

1. Find intersection point between straight line and flat mirror
2. Translate line
3. Rotate line
4. Translate flat mirror
5. Rotate flat mirror
6. Repeat all of the above for a spherical mirror
7. Additional validation was done by comparison with Zemax data

INCIDENCE ANGLES AND REFLECTION RAYS

Both the incidence angles as well as the reflected rays can be computed from the incident direction vector and the normal vector on the mirror at each intersection point. As the incident direction vector is already known, only the normal vector needs to be determined.

The normal vector is computed by taking the derivative of Equation (4.4) over R, computing the local tangent and rotating and transforming it to the correct three-dimensional local normal vector. The derivative of Equation (4.4) was found through SymPy: Symbolic computing in Python [24]. From the derivative, R can be computed from the local x- and y-coordinates stored before and filled in to find the local tangent in two dimensions. The normal is taken as the perpendicular vector of the tangent and is then transformed to three-dimensional form using ϕ, the local polar angle of the ray. This sequence is shown in Equation (4.5) where $\vec{T}$ is the tangent vector, consisting of a radial component R_T and depth component Z_T, and a normal vector $\vec{N}$. R_T consists of an x- and y- component in three-dimensional space, while Z_T is equivalent to the z-component in three-dimensional space.

After the normal is constructed in the local reference frame, the same 3 rotations are applied as for the mirrors to transform the normal vector to the global reference frame.

$$\vec{T}_{2D} = \begin{bmatrix} R_T \\ Z_T \end{bmatrix} \rightarrow \vec{N}_{2D} = \begin{bmatrix} Z_T \\ -R_T \end{bmatrix} \rightarrow \vec{N}_{3D} = \begin{bmatrix} Z_T\cos(\phi) \\ Z_T\sin(\phi) \\ -R_T \end{bmatrix} \tag{4.5}$$

With the normal known, the incidence angle and reflection direction vector can be computed. The incidence angle is given by Equation (4.6) where $\vec{r}_{in}$ is the direction vector of the incoming ray and $\vec{n}$ is the normal vector. Using the same input parameters, Equation (4.7) shows how the direction vector of the reflected ray is computed.

$$\theta_i = \arccos\left(\frac{\vec{r}_{in}\cdot\vec{n}}{||\vec{r}_{in}|| \quad ||\vec{n}||}\right) \tag{4.6}$$

$$\vec{r}_{out} = \vec{r}_{in} - \frac{2\vec{r}_{in}\cdot\vec{n}}{||\vec{n}||^2}\vec{n} \tag{4.7}$$

Verification steps for the incidence angle and reflection direction vector are given below.

1. Test ray perpendicular to flat mirror surface in two-dimensional space
2. Rotate and translate ray
3. Rotate and translate mirror mirror
4. Compute collimated beam of rays on flat mirror
5. Compute collimated beam of rays on parabolic mirror
6. Repeat in three-dimensional space
7. Additional validation was done by comparison with Zemax data

CHANGE IN POLARISATION STATE

The final step is to determine the polarisation state change by the reflection though Mueller calculus on the incoming Stokes parameters. Using the complex refractive index of the mediums through which the light travels, Equation (3.7), and the outgoing angle from Snell's law, Equation (4.8), the Fresnel reflection coefficients can be computed as shown in Equation (4.9) and Equation (4.10) for perpendicular and parallel polarisation with respect to the plane of reflection, respectively.

$$\boldsymbol{n} = n + i\kappa \tag{3.7}$$

$$\theta_r = \arcsin\left(\frac{\boldsymbol{n}_i}{\boldsymbol{n}_t}\sin(\theta_i)\right) \tag{4.8}$$

$$r_s = \frac{\boldsymbol{n}_i \cos(\theta_i) - \boldsymbol{n}_t \cos(\theta_r)}{\boldsymbol{n}_i \cos(\theta_i) + \boldsymbol{n}_t \cos(\theta_r)} \quad (4.9) \qquad r_p = \frac{\boldsymbol{n}_t \cos(\theta_i) - \boldsymbol{n}_i \cos(\theta_r)}{\boldsymbol{n}_t \cos(\theta_i) + \boldsymbol{n}_i \cos(\theta_r)} \quad (4.10)$$

The Fresnel coefficients can be used to compute the Jones matrix using Equation (4.11) to Equation (4.15) detailed in [16] which yields Equation (4.15).

$$\vec{e}_s = \frac{\vec{n} \times \vec{r}_{in}}{||\vec{n} \times \vec{r}_{in}||} \quad (4.11) \qquad \vec{e}_p = \vec{e}_s \times \vec{n} \quad (4.12)$$

$$\boldsymbol{P}_s = \vec{e}_s \otimes \vec{e}_s \quad (4.13) \qquad \boldsymbol{P}_p = \vec{e}_p \otimes \vec{e}_p \quad (4.14) \qquad \boldsymbol{J} = r_s \boldsymbol{P}_s - r_p \boldsymbol{P}_p \quad (4.15)$$

The final step to the Mueller matrix and reflected Stokes parameters are then determined from the Jones matrix as shown in Equation (4.16) to Equation (4.18) [10].

$$\boldsymbol{A} = \frac{1}{\sqrt{2}} \begin{bmatrix} 1 & 0 & 0 & 1 \\ 1 & 0 & 0 & -1 \\ 0 & 1 & 1 & 0 \\ 0 & -i & i & 0 \end{bmatrix} \quad (4.16) \qquad \boldsymbol{M} = \boldsymbol{A}(\boldsymbol{J} \otimes \boldsymbol{J}^*)\boldsymbol{A}^{-1} \quad (4.17) \qquad S_t = \boldsymbol{M} S_i \quad (4.18)$$

The verification process is given below. These steps were performed both during the design as well as afterwards as validation. The code can be found in Appendix B.

1. Unpolarised ray perpendicular to a flat mirror
2. Polarised ray perpendicular to a flat mirror
3. Unpolarised ray with an incidence angle towards a flat mirror
4. A collimated beam with incidence angle towards a flat mirror
5. Rotate the beam w.r.t. the flat mirror
6. Rotate the beam w.r.t. a spherical mirror

4.3. PASS FILTERS

Pass filters largely follow the same description as the mirrors described above. They are computed in a local reference frame, but are flat such that Z(R) = 0. Then they are rotated and translated to the global reference frame and the intersection points are calculated in the same manner. The computation of the normal vector is also simplified, as it starts at $[0, 0, -1]^T$ locally and is rotated as before. The differences lie in the fact that pass filters transmit rays instead of reflecting them, therefore the Fresnel transmission coefficients are used to determine the direction vector of transmitted rays.

To compute the direction vectors of transmitted rays, one can combine the incidence angle, Equation (4.6), and Snell's law, Equation (4.8) and determine the outgoing angle. If one were to do this in vector notation, it looks like Equation (4.19) for which a detailed derivation can be found in [7].

Furthermore, the Fresnel transmission coefficients can be described by Equation (4.20) and Equation (4.21). These are then used to compute the Jones matrix as shown in Equation (4.22). Note that the sign of the parallel polarisation direction is positive now because the orientation upon transmission does not rotate unlike with a reflection.

$$\vec{r}_{out} = \frac{n_i}{n_t}\vec{r}_{in} + \left(\frac{n_i}{n_t}(-\vec{n} \cdot \vec{r}_{in}) - \sqrt{1 - \left(\frac{n_i}{n_t}\right)^2 \left(1 - (-\vec{n} \cdot \vec{r}_{in})^2\right)}\right)\vec{n} \quad (4.19)$$

$$t_s = \frac{2n_i \cos(\theta_i)}{n_i \cos(\theta_i) + n_t \cos(\theta_r)} \quad (4.20) \qquad t_p = \frac{2n_i \cos(\theta_i)}{n_t \cos(\theta_i) + n_i \cos(\theta_r)} \quad (4.21)$$

$$\boldsymbol{J} = t_s \boldsymbol{P}_s + t_p \boldsymbol{P}_p \quad (4.22)$$

The medium in which the light travels within the instrument is vacuum, so a refractive index of 1 is assumed. The modelled long-pass filters are made of CaF_2 and simplified as a single layer of that material. The refractive index was taken from [21]. For the filters, this function is applied twice, one time entering the filter from vacuum, and then another time exiting the filter into vacuum after travelling through the medium.

The detector of NIRSpec can also be modelled as a filter where light only enters and does not exit at the other end. The detector is made of HgCdTe, but it is not clear what the exact refractive index for this detector is. It has been reported that the detector reaches an efficiency of over 80% [28] and to achieve this efficiency with a simplified Fresnel transmission, a refractive index of 1.2 is used.

The code can be found in Appendix C. The performed verification steps are detailed below:

1. Simulate transmission of ray without incidence angle and filter refractive index as 1

2. Add incidence angle
3. Remove incidence angle and change refractive index of filter above 1
4. Add incidence angle
5. Add second filter with reversed refractive indices to see whether final ray has the same direction as initial ray

4.4. REFLECTION GRATINGS

Similarly to the pass filters, the gratings are initially modelled as a flat surface and positioned in the global reference frame in the correct orientation. The reflections are all computed along the same axis which is perpendicular to the grooves of the grating and specifically along the groove that is hit by the central ray. This is a simplification due to time constraints, but has minimal impact on both the induced polarisation by mirror reflections as well as implementation of the grating efficiencies. More accurate reflections are possibly implemented in future work.

The reflections direction vectors are based on m = -1 order and on the theory given in Section 3.4. Furthermore, the grating efficiencies, how efficiently each grating reflects differently polarised incident light, are manually imported from analyses performed in PCGrate, a software developed for diffraction grating modelling [15]. This was done because there seemed to be no theory available to create a function to compute the grating efficiencies in the ray tracer. The efficiencies are imported into the ray tracer to concentrate all the functions and perform complete analyses at once instead of in separate locations.

The efficiencies are defined in P- and S-polarisation efficiencies. Unpolarised light and light that is diagonally polarised between P- and S-direction are computed with the average efficiency. Circular polarisation is neglected in this report for two reasons: first, there is no option for this analysis in PCGrate and second, the circular polarisation component is relatively small with respect to the total degree of polarisation, which is already relatively small with respect to the total irradiance. As the ray tracer saves the polarisation state in the Stokes parameters instead of P- and S-polarised parts, a translation needs to be made. This is done for both the nominal science path and calibration path separately and shown in Figure 4.2 and Figure 4.3, respectively. In these figures, it is shown how the Stokes parameters of the incident beams relate to the geometry of the grating. The reason the Stokes parameters are positioned differently with respect to the grating for the two paths is because the two paths were designed in differently orientated OpticStudio files. In future work, this could be adjusted for by rotating the light beam starting position.

It should be noted that there is a small deviation for the nominal science path reference frame with the actual orientation, but it is neglected for this analysis. Due to time constraint, the exact orientation was not derived, but by performing multiple analyses around the precise orientation it was concluded that the difference in reflected ray irradiance is far below 1%. Future work could improve the model by taking this small misalignment into account.

The code for the reflection gratings can be found in Appendix D.

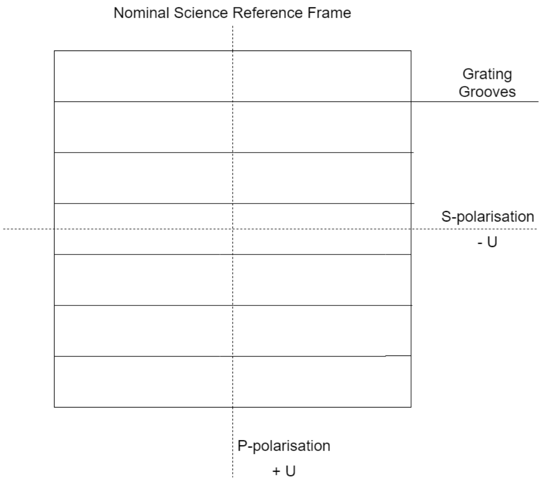

Figure 4.2: The reference frame to translate the Stokes parameters to P- and S-polarised orientation. For the nominal science configuration negative and positive U are in line with P- and S-polarised light, respectively.

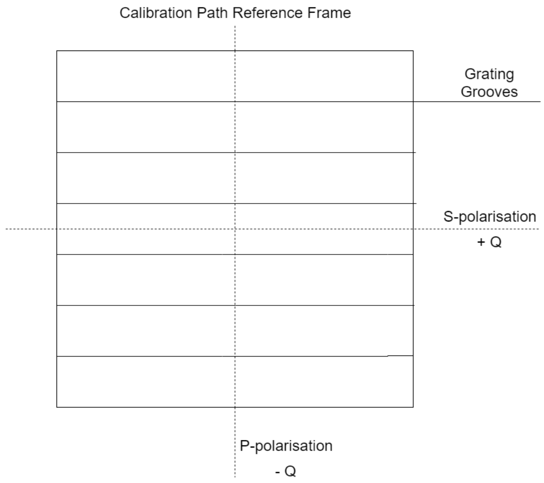

Figure 4.3: The reference frame to translate the Stokes parameters to P- and S-polarised orientation. For the nominal science configuration positive and negative Q are in line with P- and S-polarised light, respectively.

4.5. POLARISATION ELLIPSES

To directly compare the polarisation state of either different rays, it helps to visualise the Stokes parameter as a polarisation ellipse. This section details what it is and how it is made.

The Stokes parameters indicate both the magnitude as well as the direction of the polarisation. In these parameters, Q and U describe the magnitude and direction in which a ray is linearly polarised while V does the same for circularity of the polarisation. Because light generally has some degree of both linear and circular polarisation, the light is said to be elliptically polarised. The Q and U direction are defined in a reference frame at the start, as shown in Figure 4.1, and this means that a mostly positive Q-polarised ray would be a depicted as a horizontally lying polarisation ellipse, positive U-polarised light would result in a diagonally polarised ellipse from upper left to lower right, and negative Q-polarised light would be a vertically positioned ellipse.

The general equation of a two-dimensional tilted ellipse can be described as Equation (4.23) where θ is the in-plane tilt angle, and a (the major axis) and b (the minor axis) are elliptical constants that describe the shape. The elliptical constants can be derived from as shown in Equation (4.24) to Equation (4.26) and a visualisation is shown in Figure 4.4. In Equation (4.25), L represents the complex intensity of linear polarisation.

$$\frac{\left(x\cos(\theta)+y\sin(\theta)\right)^2}{a^2}+\frac{\left(x\sin(\theta)-y\cos(\theta)\right)^2}{b^2}=1 \tag{4.23}$$

$$I_p = Q^2+U^2+V^2 \tag{4.24}$$

$$L = Q+iU \rightarrow |L| = \sqrt{Q^2+U^2} \tag{4.25}$$

$$a=\sqrt{\frac{1}{2}(I_p+|L|)},\quad b=\sqrt{\frac{1}{2}(I_p-|L|)},\quad \theta=\frac{1}{2}\arg(L) \tag{4.26}$$

As an example, imagine a ray reflected by a mirror after which it will have a degree of elliptical polarisation represented by the blue ellipse in Figure 4.5. While continuously measuring, the mirror is gradually rotated, changing the incidence angle with respect to the ray and thus the polarisation state towards the red ellipse. This shift in demonstrates how polarisation ellipses can help visualise the change in polarisation state. From this figure it could be concluded that the direction of the linear polarisation is gradually shifted while the magnitude, and thus the degree of polarisation, remains approximately constant.

4.6. STEP SIZE ANALYSIS

As mentioned before, the number of points the mirror is computed with has an influence on the accuracy of determining the intersection points between an incident ray and mirror. As the mirrors are computed as

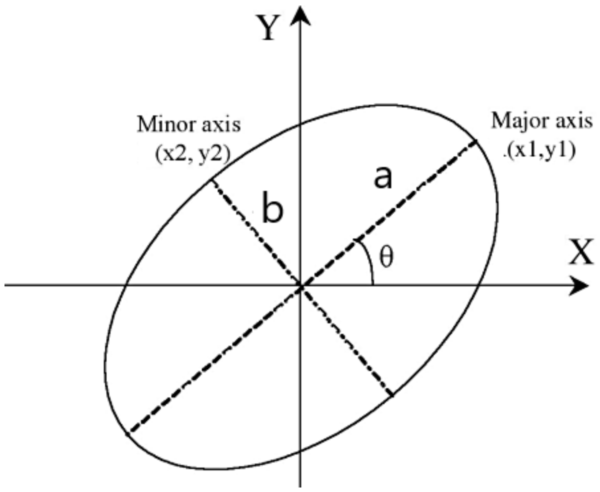

Figure 4.4: A two-dimensional tilted ellipse with major axis a, minor axis b, and tilt angle θ

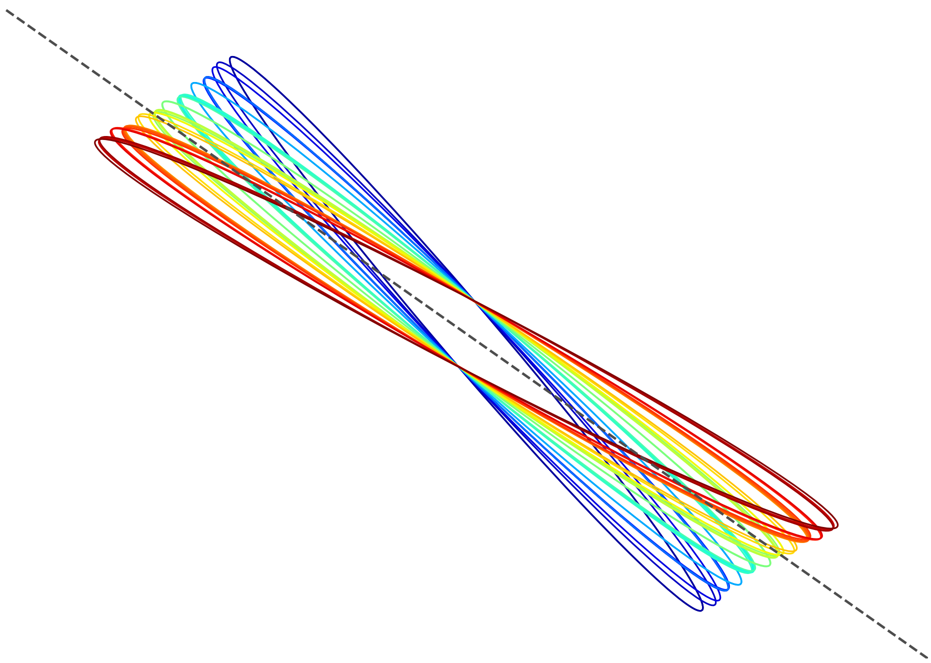

Figure 4.5: Example of how multiple polarisation ellipses can depict the change in polarisation state in a intuitive way. The polarisation state is changed over time from the red colour to the blue colour. Here it can be seen that the degree of polarisation stays approximately the same while the orientation shifts over the positive U-direction.

evenly distributed grids, a larger number of points means a smaller step size between each point of the mirror. This section discusses the effect of step size on both the incidence angle between a ray and mirror as well as the polarisation state.

To determine the influence of mirror step size on the polarisation state, a sensitivity analysis is performed in which the angles of incidence for nine rays is tracked with decreasing mirror step size. With decreasing step size, the angle of incidence should converge to a single value. First, an analysis is presented with a decreasing step size from 50 to 1.0 mm to show the macro trend, followed by a zoomed in analysis from 1.0 to 0.8 mm to determine the effects within 1 mm step size.

Figure 4.6 shows the change in incidence angle for all 16 optical elements for a decreasing step size from 50 to 1.0 mm for ray 0, a ray on the outer edges of the light beam. Ray 0 is chosen as depiction as it encounters the largest incidence angles, the other rays show a similar decrease in incidence angle difference with decreasing step size.

It can be seen that the angle of incidence does indeed seem to converge to a single value towards 1.0 mm step size. Furthermore, the relation between the mirrors can be seen, as they are placed sequentially and the angle of incidence on one mirror affects the angle on the following mirror. The mirrors therefore consistently follow a set of other mirrors depending on their orientation within the instrument. Finally, it can also be noted that the mirrors that are in the beginning of the sequence generally seem to have a lower deviation from the average than the latter mirrors, this is also due to the sequentially placed mirror effect that a higher incidence angle on the first mirror will result in even higher angles at following mirrors.

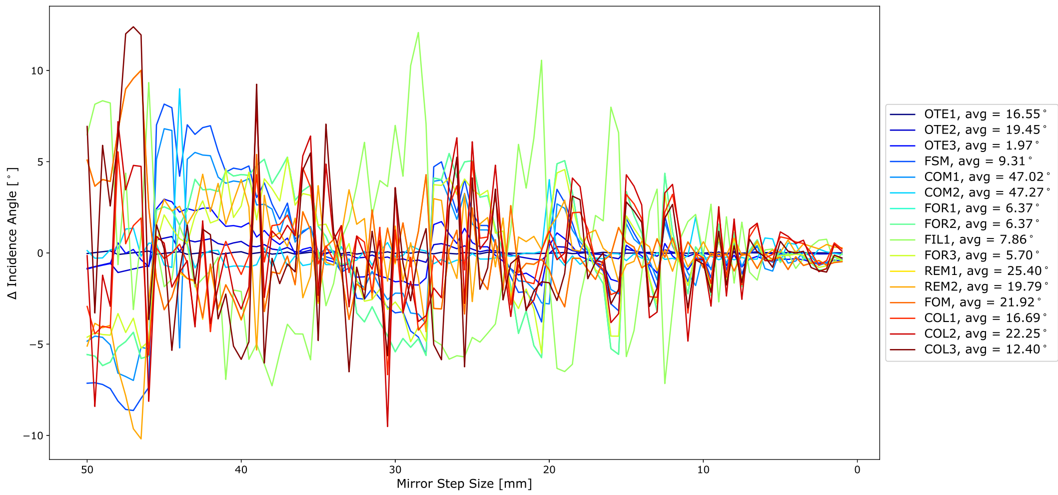

Figure 4.6: The difference in angle of incidence with respect to the average with decreasing step size from 50 to 1.0 mm for ray 0 for all 16 optical elements of NIRSpec described in Table 2.2. For every optical element, the average incidence angle with the ray with all step sizes is subtracted from the data set to visualise the deviation from that average. It can be seen that the angles converge to their average value towards the end as expected.

Similarly, the change in final degree of polarisation for 9 rays is analysed with the same step size range in Figure 4.7 in percentage points. It can be seen that the difference with the average converges towards 0 as expected. This degree of polarisation can be further examined in Stokes parameters to observe the change in orientation as well. The Stokes parameters can be visualised in a polarisation ellipse, Figure 4.8 shows how the polarisation ellipse of ray 0 changes with decreasing step size. Note that the polarisation ellipse is normalised over S_0 and the length of the major axis represents the degree of polarisation. Again, it can be seen that the polarisation ellipse converges to a single shape in both size and orientation.

The same analysis was performed for step sizes below 1.0 mm till 0.8 mm, but no significant increase in accuracy or additional convergence was found. For the remained of this report, a step size of 1.0 mm is therefore chosen to perform all following analyses.

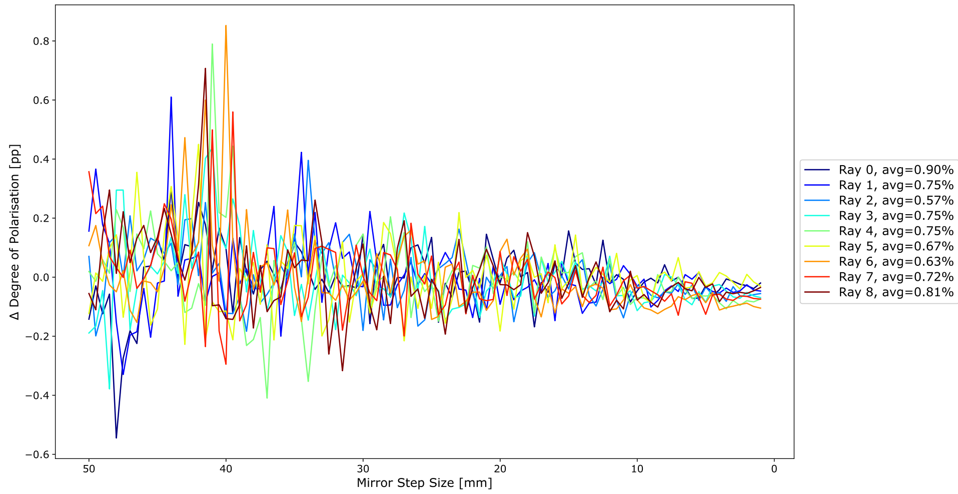

Figure 4.7: The change of degree of polarisation before the reflection grating with decreasing step size from 50 to 1.0 mm for all rays in percentage points. It can be seen that the degree of polarisation converges to the average similar to the local incidence angles, as expected.

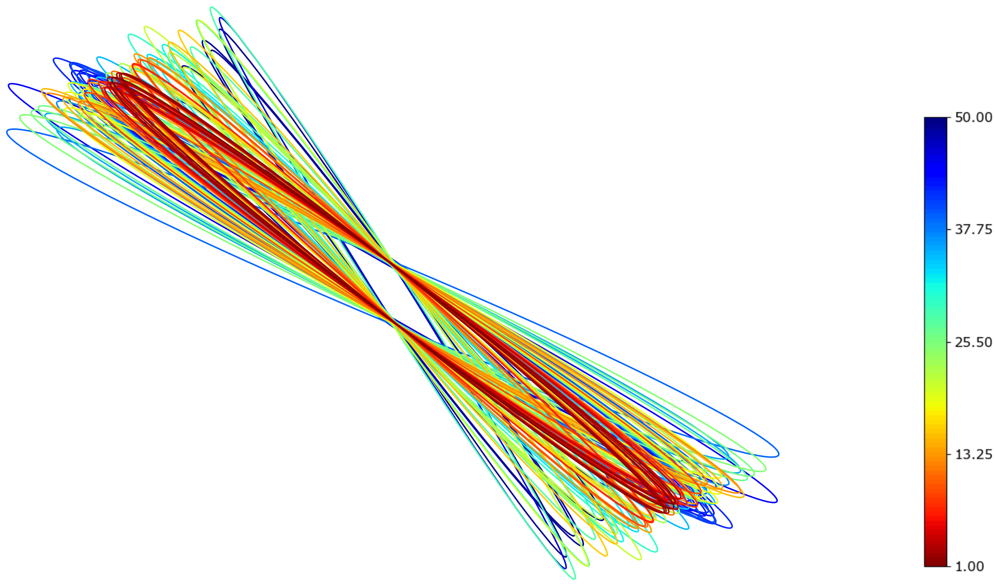

Figure 4.8: The polarisation ellipse of ray 0 with decreasing step size from 50 to 1.0 mm. It can be seen that the ellipse converges to a single shape in both magnitude as well as orientation indicating that the ellipse formed at 1.0 mm gives a representative polarisation state.

5

Induced Polarisation

The measured irradiance at the detector I can be described as shown in Equation (1.1) where I_{COL3} is the irradiance after COL3, the last mirror in the optical path before reaching the grating, G_{eff} is the effective grating efficiency, M_{eff} is the combined mirrors efficiency and D_{eff} is the detector efficiency which varies with incidence angle. G_{eff} is dependent on I_{COL3} described by Equation (1.2) in which NP, P, and S are the non-polarised, P-polarised, and S-polarised parts of I_{COL3}.

This chapter focuses on the polarisation state of I_{COL3}, specifically what the induced polarisation state is in Stokes parameters. These Stokes parameters are then translated to NP, P, and S in Section 6.1. Finally G_{eff}, M_{eff}, and D_{eff} are combined in Section 6.2.

$$I = I_{COL3}\, G_{eff}\, M_{eff}\, D_{eff} \tag{1.1}$$

$$G_{eff} = \frac{NP}{I_{COL3}} \frac{P_{eff}+S_{eff}}{2} + \frac{P}{I_{COL3}} P_{eff} + \frac{S}{I_{COL3}} S_{eff} \tag{1.2}$$

This chapter describes the analyses performed on the light in the instrument up to the reflection grating and provides a clear understanding of what degree of polarisation can be expected at the reflection grating. It focuses specifically on the reflection-induced polarisation on unpolarised light entering JWST and NIRSpec. This polarisation is induced through reflections with the mirrors throughout the optical path of NIRSpec. The degree of induced polarisation depends on two parameters; the wavelength and initial incidence angle. Chapter 6 discusses how this induced polarisation affects the reflection grating performances and overall polarisation sensitivity

5.1. Wavelength

The induced polarisation depends on wavelength because the complex refractive index of the coatings of the mirrors are wavelength dependent. Furthermore it is important to know whether rays with different wavelengths are polarised in different degrees to prevent erroneous interpretation of the data. The complex refractive index $\boldsymbol{n}$ consists of the real refractive index and extinction coefficient, see Equation (3.7). Note that the first four mirrors of JWST (OTE1. OTE2, OTE3, and FSM) are gold coated while from there onwards the mirrors of NIRSpec are silver coated.

The values for the complex refractive indices for both materials are taken from Palik [27] as those are commonly used in literature. It should be noted that different values can be found for the refractive indices in other literature as multiple variables affect these parameters. Ideally, the refractive indices and extinction coefficients of the coatings are measured, but there is no measurement data available.

Using the ray tracer, the computed induced degree of polarisation for initially unpolarised incident light following the nominal science path is plotted against the 1.0 to 5.2 μm wavelength range in Figure 5.1 for all 9 rays that describe the incident light beam. It can be seen that there is some variation per wavelength, but the degree of polarisation stays within the 0.5 and 1.5% range. Furthermore, there is a spread in values between rays, but the middle ray 4 seems representative for all rays as the absolute value in the spread is approximately 0.5 percentage point.

The noise between 1.0 and 2.0 μ is caused by the values of complex refractive index taken from Palik. The measurement of complex refractive index can be complicated and there are some differences between literature sources. A critical reassessment of the optical properties of silver and gold was performed by Babar

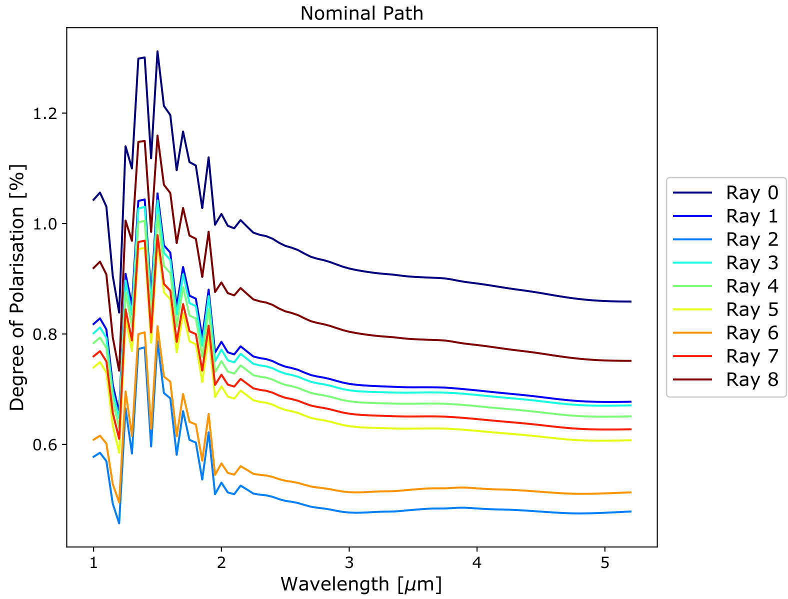

Figure 5.1: The degree of polarisation in percentage as a function of wavelength from 1.0 to 5.2 μm for 9 simulated rays over the nominal path till the grating. The degree of polarisation stays within 0.5 to 1.5%. It can be seen that there is a spread in degree of polarisation between rays, but ray 4 is in the middle as expected and can be seen as representative for the complete beam. The noise between 1 and 2 μm is caused by the noise in the data sets of extinction coefficient for both gold and silver from Palik.

and Weaver more recently and resulted in slightly different data [2]. To better visualise the effect of chosen source for refractive index values on the degree of polarisation, the effect of both refractive index and extinction coefficient on degree of polarisation is plotted in Figure 5.2 for the nominal path and ray 4. In this figure, both the refractive index and extinction coefficient are varied along the horizontal and vertical axes, respectively, for all mirrors. This means that, for this specific analysis only, the gold and silver coated mirrors are modelled with the same complex refractive index, and because most mirrors are silver, the silver complex refractive index is chosen. Furthermore, the complex refractive index of both gold and silver are plotted from two different sources from 1.0 to 5.2 μm. It can be seen that the assumption for all mirrors to have the same coating is still representative because the values for each source lie close enough for silver and gold to not change the degree of polarisation significantly. It can be seen that using Babar and Weaver 2015 [2] as source , the estimated degree of induced polarisation reduces to far below 1%. This is also slightly lower than using Palik, which resulted in degrees of polarisation close to 1%. Furthermore, only large values of refractive index compared to extinction coefficient would result in significant induced degrees of polarisation.

Another important take away from this figure is that the complex refractive index does not seem to change significantly in degree of polarisation with wavelength whichever source is chosen; the lines stay within the same degree of polarisation region. The refractive index and extinction coefficient are not independent and follow Kramers-Kronig relations [23] which translates to the curved lines in Figure 5.2. In other words, there would most likely not be a flat line with large refractive index compared to extinction coefficient that would result in significant differences in induced degree of polarisation between wavelengths.

Ideally, the complex refractive index of the coatings should be measured to accurately determine the induced degree of polarisation. If this is not possible due to practical reasons, the next best thing would be to search for literature that has measured this complex refractive index for comparable materials such as coatings of other space instrumentation. Even if the values of refractive indices are not known exactly, the induced degree of polarisation will likely not exceed 2% based on the used literature sources and Figure 5.2.

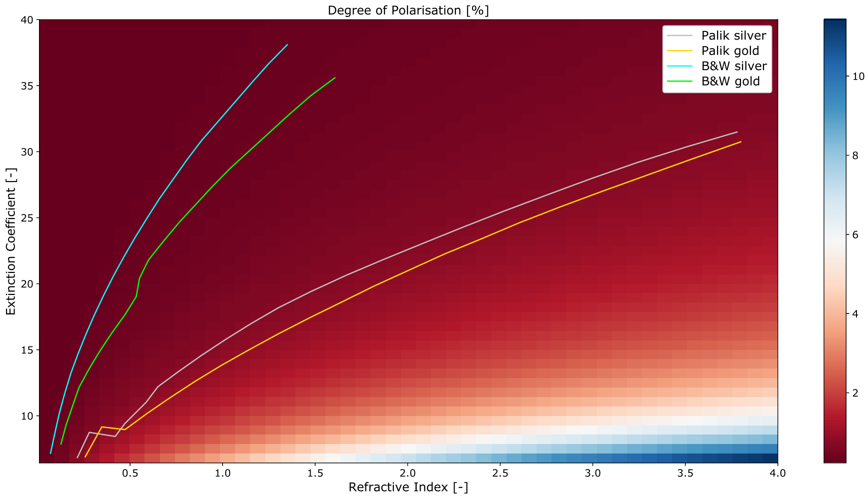

Figure 5.2: The degree of polarisation plotted against both refractive index and extinction coefficient for all mirrors in the nominal path for ray 4. The plotted lines represent the complex refractive index for silver and gold, both from two different sources from 1.0 to 5.2 μm wavelength. The difference in degree of polarisation can be up to approximately 2% depending on source used.

5.2. INITIAL INCIDENCE ANGLE

The initial angle of incidence is the angle with which the rays enter JWST and affects all sequential local angles of incidence for every mirror and thus influences the induced degree of polarisation. It is therefore necessary to understand the relation between the initial incidence angle and the induced degree of polarisation before every ray reaches the grating to ensure that different objects within the field of view are interpreted similarly.

The field of view of NIRSpec is 3.4’ x 3.4’ (arcminutes), the analyses will therefore be performed over a range from -1.7’ to 1.7’ over two perpendicular axes [22]. These axes will be parallel and perpendicular to the NIRSpec optical plane. Both the effect on total magnitude as well as the orientation of polarisation will be examined.

To visualise the change in initial angle over the two different axes, Figure 5.3 shows the path of the central ray 4, see Figure 4.1, over COL2 and COL3, the last two mirrors before reaching the grating, with varying incidence angle from -1.7’ to 1.7’ along the optical plane of NIRSpec, while Figure 5.4 shows the same process but perpendicular to the optical plane of NIRSpec.

The induced degree of polarisation for both the in-plane as well as perpendicular varying incidence angle are shown in Figure 5.5 for the middle ray 4 at 3.0 μm wavelength. Only ray 4 is shown because all other rays show similar trends and the middle ray is representative for the complete beam.

For the in-plane variation, the relevant angle which introduce the polarisation are linearly changed with initial incidence angle, it can be seen that the degree of polarisation follows this trend. Even though a linear increase can be found, the degree of polarisation stays within 0.3 percentage point from the centre of the field of view. To observe the orientation of polarisation, the polarisation ellipse of ray 4 is plotted in Figure 5.6. As the local incidence angles that induce the polarisation are not changed in direction, but only in magnitude, the polarisation orientation remains constant. The slight rotation appears to be due to the mirrors of JWST because they do not lie in the same optical plane as the mirrors of NIRSpec.

For the perpendicular variation, the variation in induced polarisation is even smaller because the varying initial angle introduces smaller changes in local incidence angles than the optical path itself. A trend can be found where the degree of polarisation is lowest at the field of view centre and changes orientation when moving away from this centre. This can be seen in Figure 5.7 where the magnitude of the ellipses stays approximately the same but polarisation in a different direction is added causing the ellipse to rotate over its neutral orientation.

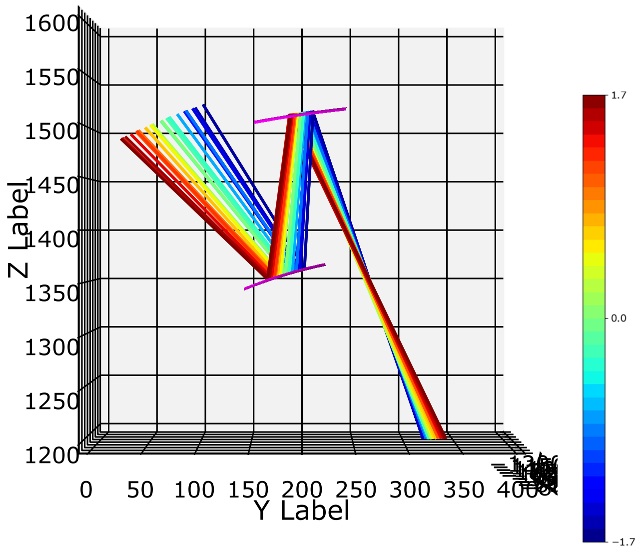

Figure 5.3: The central ray plotted over COL2 and COL3 before reaching the grating with varying initial incidence angle in the optical plane of NIRSpec from -1.7' to 1.7'. The lower fuchsia surface represents COL2 while the upper surface represents COL3. The ray propagates from the upper left to the lower right in this image.

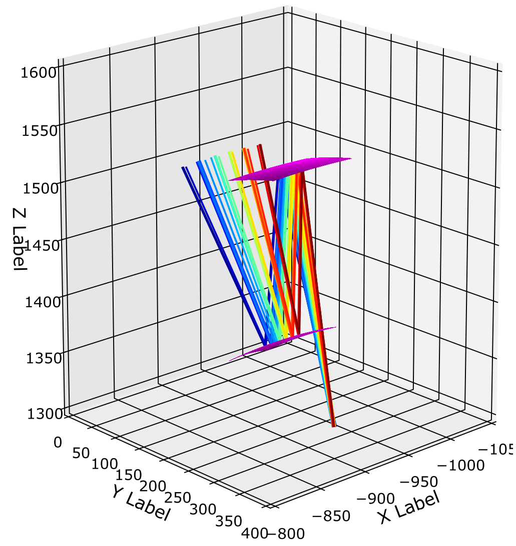

Figure 5.4: The central ray plotted over COL2 and COL3 before reaching the grating with varying initial incidence angle perpendicular to the optical plane of NIRSpec from -1.7' to 1.7'. Again, the lower and upper fuchsia surfaces represent COL2 and COL3, respectively, and the rays propagate from the upper left to lower right of the image.

Both in- and perpendicular initial incidence angle variation show expected change in magnitude and orientation of polarisation, but neither seem significant and will therefore not be taken into account for further analysis. It can be concluded that different objects in the field of view will reach the grating with the same induced degree of polarisation and therefore, no correction based on the object's field of view position is required to correct for any induced polarisation related matter.

It should be noted, however, that the angle with which the rays reach the grating changes over approximately 8° over the complete field of view range which could affect the reflection grating efficiencies. This is further examined in the grating efficiency analyses Section 6.1.

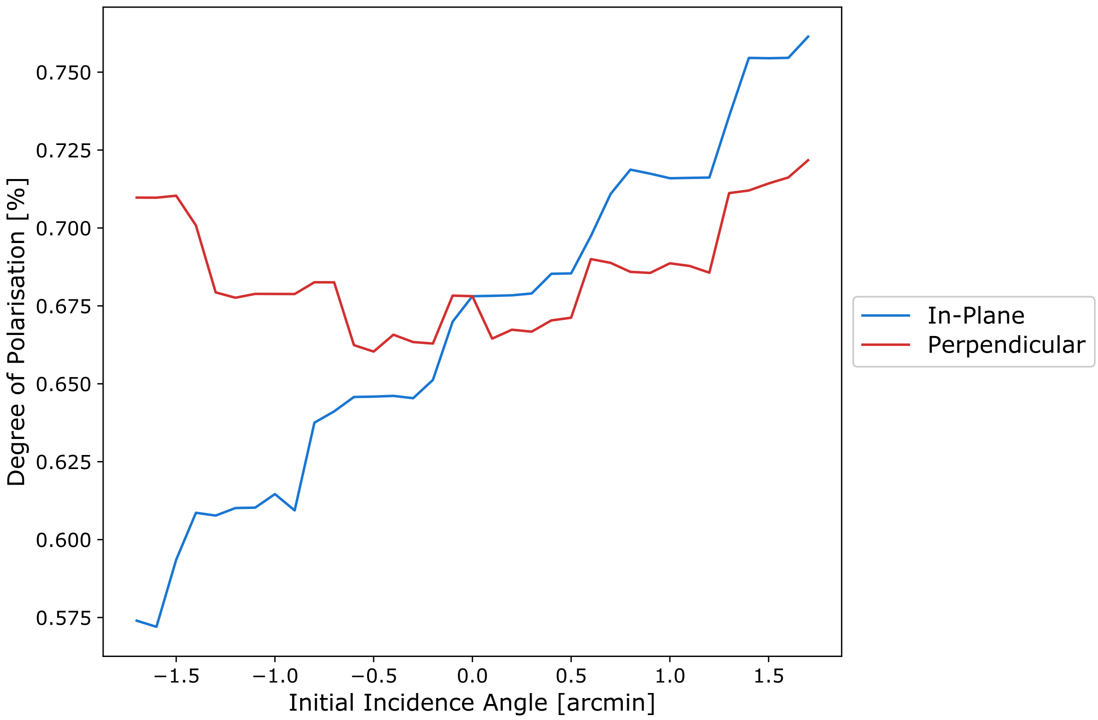

Figure 5.5: The degree of polarisation over varying initial incidence angle both in and perpendicular to NIRSPec's optical plane. It can be seen that for in-plane variation, the relevant angles that induce the polarisation are linearly increased with the initial incidence angle and the degree of polarisation follows. For the perpendicular variation, the change in degree of polarisation is smaller, but it increases when moving away from the field of view centre. For both variations, the change in degree of polarisation is smaller than 0.2 percentage points.

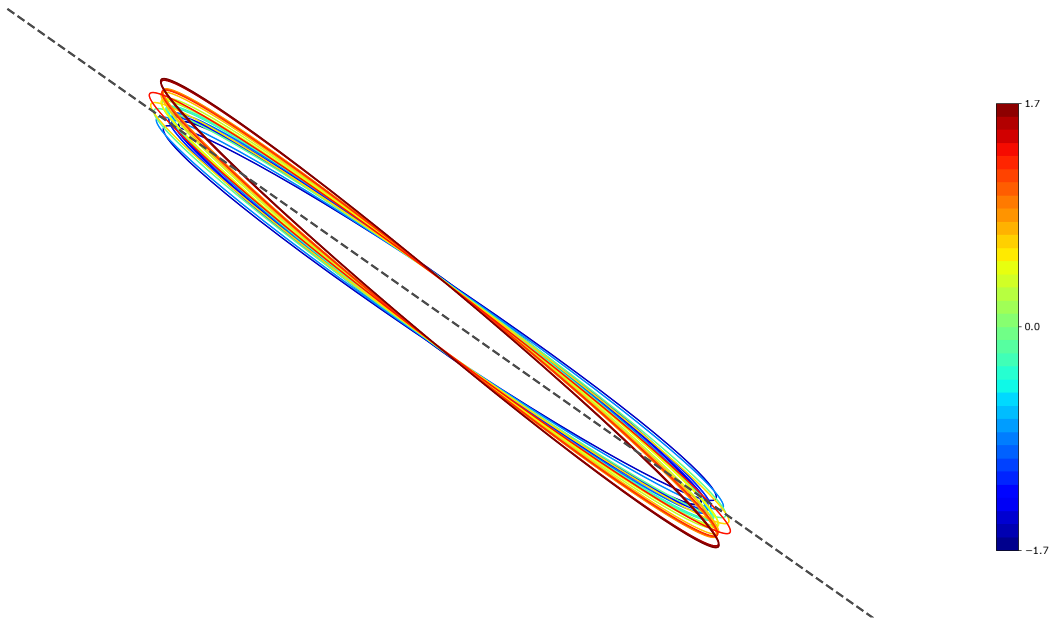

Figure 5.6: The normalised polarisation ellipse with various initial incidence angle in NIRSpec's optical plane for ray 4 from -1.7' to 1.7'. It can be seen that the orientation barely varies as can be expected, while a nearly linear growth is found in magnitude.

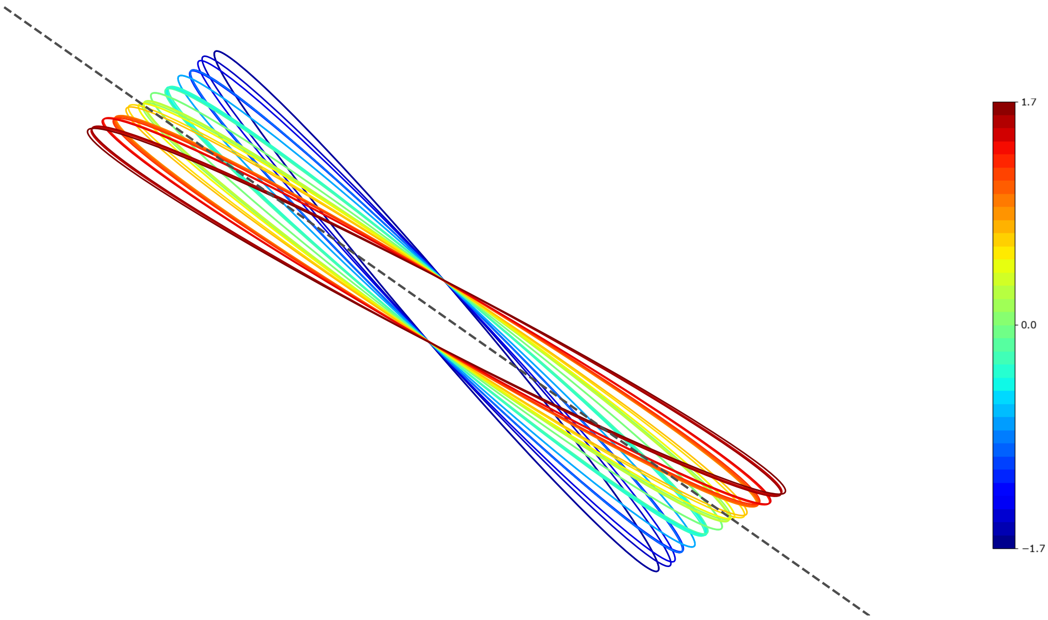

Figure 5.7: The polarisation ellipse change over varying initial incidence angle perpendicular to NIRSpec's optical plane. Here, a larger rotation in orientation can be found, but with a nearly constant magnitude.

6

Polarisation Sensitivity Analysis

In this chapter, first the reflection grating efficiencies are discussed separately before determining the overall polarisation sensitivity of NIRSpec in Section 6.1. This is because the gratings have different efficiencies for differently polarised light. Going back to the measured irradiance Equation (1.1) and overall grating efficiency Equation (1.2), first G_{eff} is discussed in detail in Section 6.1. This is followed by analysing overall irradiance throughput Section 6.2 in which M_{eff} and D_{eff} are included in the computations but not explicitly mentioned.

$$I = I_{COL3}\, G_{eff}\, M_{eff}\, D_{eff} \quad (1.1)$$

$$G_{eff} = \frac{NP}{I_{COL3}} \frac{P_{eff}+S_{eff}}{2} + \frac{P}{I_{COL3}} P_{eff} + \frac{S}{I_{COL3}} S_{eff} \quad (1.2)$$

The polarisation sensitivity of the gratings is analysed in detail via PCGrate [15]. The overall polarisation sensitivity of NIRSpec is put into perspective via uncertainty values for observing light with a 10% degree of polarisation. Note that this 10% degree of polarisation is from the source itself and not induced as discussed in the previous chapter. An initial degree of polarisation of light entering JWST can be added to the induced polarisation discussed in Chapter 5. The magnitude or orientation of induced polarisation by the reflections is not altered by this initial degree of polarisation.

6.1. Reflection Grating Efficiencies

Reflection gratings have a different efficiency for differently polarised incident light, this introduces a polarisation sensitivity of the instrument. The polarisation direction can be decomposed in two orientations, P-polarised light parallel to the plane of reflection and S-polarised light perpendicular to the plane of reflection of the grating. Keep in mind that the plane of reflection is perpendicular to the grooves of the grating, so P-polarised light is perpendicular to the grating grooves. Figure 4.2 shows how the Stokes parameters Q and U translate into these two decomposed polarisation directions for the nominal science path.

The reflection grating efficiencies in this report are described in two independent parameters, their efficiency to reflection of P-polarised light and S-polarised light, the so-called P-efficiency and S-efficiency, respectively. In equation form, the irradiance of light reflected by the grating, I, can be described as Equation (6.1) where I_0 denotes the irradiance of the incident light to the grating with subscripts NP, P, and S to denote the not polarised, P-, and S-polarised part of the incident light, respectively. Furthermore, G_{eff} represents the overall grating efficiency which can be decomposed in P_{eff} and S_{eff}, its P- and S-efficiency. It should be noted that unpolarised light is considered 50% P- and 50% S-polarised, as it can be evenly decomposed on those two components.

$$I = I_0 G_{eff} = I_{0,NP} \frac{P_{eff}+S_{eff}}{2} + I_{in,P}\, P_{eff} + I_{in,S}\, S_{eff} \quad (6.1)$$

From these two parameters, a third, dependent parameter is constructed: the P/S-ratio. This parameter is defined by ratio of P-efficiency over S-efficiency. Using these definitions, four possible combinations are elaborated on to provide context on how these parameters describe the grating.

1. P- and S-efficiency are 1 and independent of wavelength
2. Wavelength dependent P- and S-efficiencies, P/S-ratio remains 1
3. Wavelength dependent P- and S-efficiencies, P/S-ratio remains constant, but not 1
4. Both P- and S-efficiencies and P/S-ratio are wavelength dependent

1. In a perfect grating, both the efficiency for P- and S-polarised light would be 1 and there is no loss of information. This also means that there is no polarisation sensitivity.

2. In practice, the efficiencies are usually not equal to 1 and they depend on wavelength. When the P- and S-efficiencies change with wavelength, but their magnitude with respect to each other remains equal, the P/S-ratio remains 1 and there is no polarisation sensitivity.

3. Similarly to point 2, when the P- and S-efficiencies are wavelength dependent and the P/S-ratio remains constant, but not equal to 1, a polarisation sensitivity is present. This is because one polarisation orientation will be more present in the reflected ray than the other compared to before the grating. This means that differently polarised incident rays will be differently reflected, but incident rays with the same polarisation state undergo the same efficiencies at all wavelengths. Because the P/S-ratio is constant, the magnitude of sensitivity is constant for the whole wavelength range.

4. Finally, when the P/S-ratio is not constant over the wavelength range, the polarisation sensitivity is wavelength dependent. In this case, when incident rays at different wavelengths are reflected by the grating, they undergo different efficiencies even when they arrive at the grating with the exact same polarisation state.

Now that it is clear how the parameters describe the grating and its polarisation sensitivity, the gratings of NIRSpec can be analysed. The efficiencies for P- and S-polarised light for the medium and high resolution gratings are shown in Figure 6.1 and Figure 6.2, respectively. Immediately it can be seen that the P/S-ratio changes significantly over wavelength range for each grating; their maximum deviation from 1 is up to 20% for the medium resolution gratings and up to 40% for the high resolution gratings. This means that these gratings fall in the fourth category described above where a wavelength dependent polarisation sensitivity is present.

To give some context on what this means; consider two measurements using GRT2700-III at 5μm of a celestial object with 10% of inherent degree of polarisation and assume the light reaches the grating unaltered. At the first measurement it is effectively P-polarised and the second measurement is performed while rotated 90° with respect to the first measurement, which gives S-polarised light. The irradiance of the first and second measurement after the grating can be derived as a function of initial irradiance, I_0, as shown in Equation (6.2) and Equation (6.3), respectively. The values for P_{eff} and S_{eff} are taken from Figure 6.2. It can be seen that for reflected light by the grating, the irradiance of the measurement with P-polarised orientation will be approximately 4% higher than the S-polarised orientation even though the same object is observed.

$$I_1 = I_{0,NP}\frac{P_{eff}+S_{eff}}{2} + I_{0,P}\,P_{eff} = 0.9I_0 \cdot \frac{0.86+0.61}{2} + 0.1I_0 \cdot 0.86 \approx 0.75I_0 \tag{6.2}$$

$$I_2 = I_{0,NP}\frac{P_{eff}+S_{eff}}{2} + I_{0,S}\,S_{eff} = 0.9I_0 \cdot \frac{0.86+0.61}{2} + 0.1I_0 \cdot 0.61 \approx 0.72I_0 \tag{6.3}$$

The gratings with the same resolution show the same trends, so from here on out only the gratings in band III, GRT1000-III and GRT2700-III, will be analysed because they cover the largest wavelength range. The P/S-ratio for grating efficiencies effectively describes the polarisation sensitivity of the gratings. Before, it was concluded that the position in the field of view does not significantly change the local incidence angles to alter the induced degree of polarisation. It should also be tested whether position within the field of view has a significant effect on the P/S-ratio of the gratings. This effect is plotted in Figure 6.3. It can be seen that the P/S-ratio for different objects in the field of view changes slightly but considering the fact the the degree of polarisation is already likely a small percentage, the change in P/S-ratio does not seem significant. This is therefore not further taken into account in the remainder of this report.

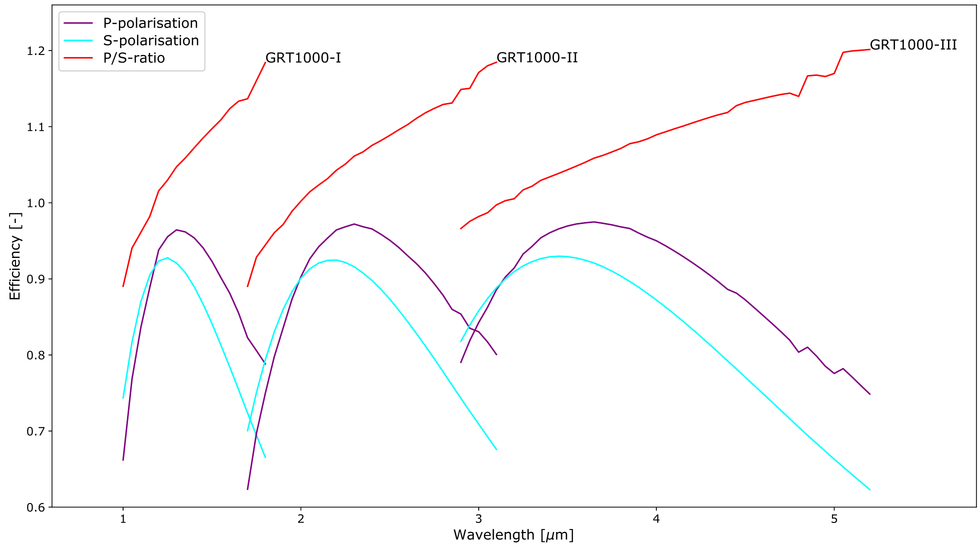

Figure 6.1: The P- and S-polarisation efficiencies and efficiency-ratios of the medium resolution gratings, GRT1000-I GRT1000-II and GRT1000-III, over their respective wavelength range. From the P/S-ratio, it can be seen that the polarisation sensitivity changes with wavelength and can be up to 20% for each grating at the end of their wavelength range.

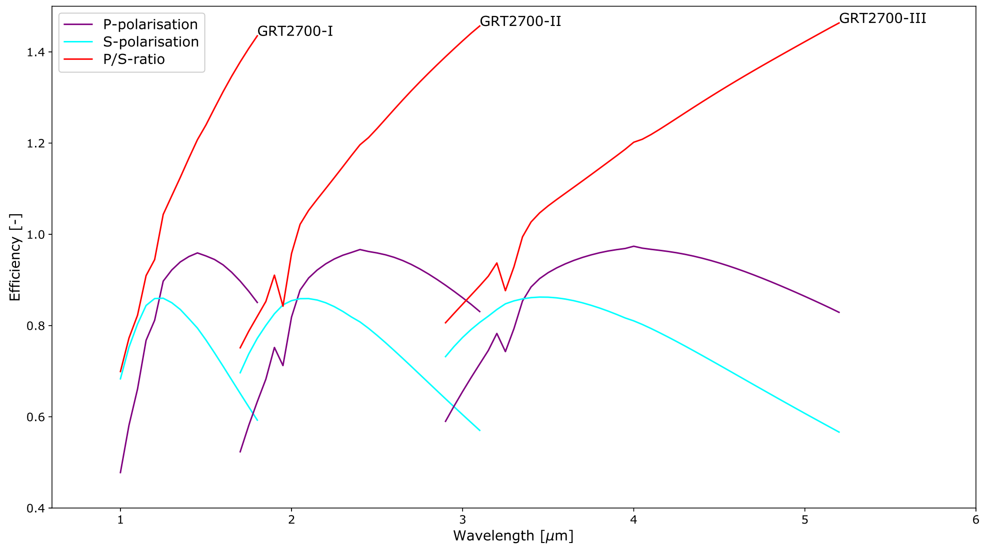

Figure 6.2: The P- and S-polarisation efficiencies and efficiency-ratios of the high resolution gratings, GRT2700-I GRT2700-II and GRT2700-III, over their respective wavelength range. More than the medium gratings, it can be seen that the polarisation sensitivity changes with wavelength and here, the difference can be up to 40% for each grating.

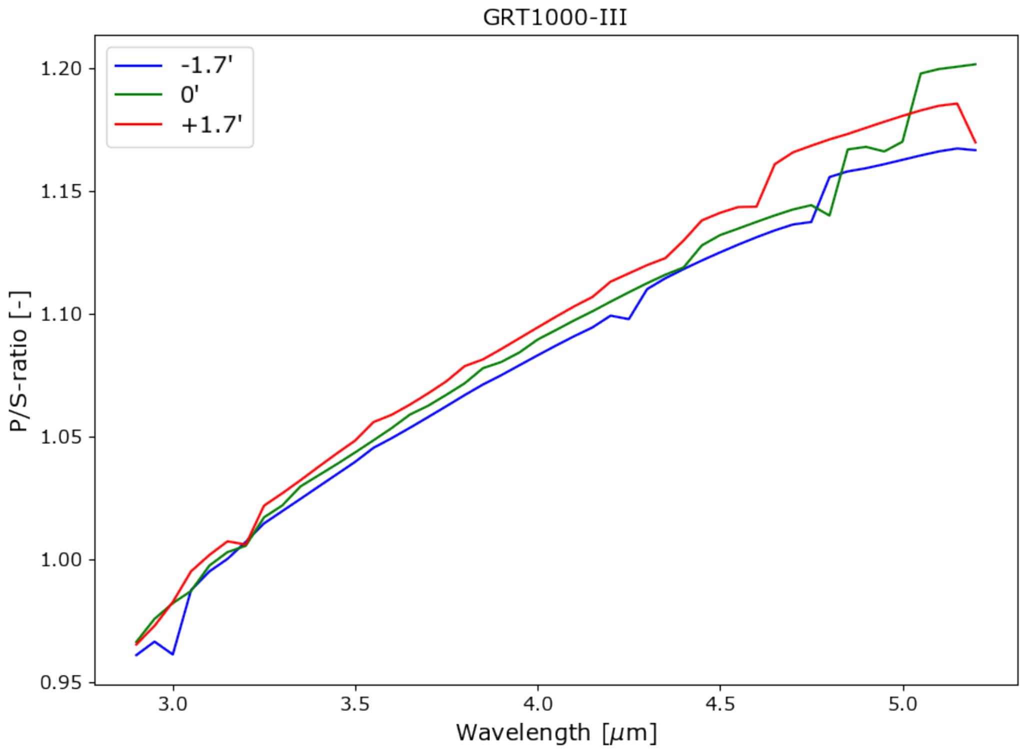

Figure 6.3: The P/S-ratio of GRT1000-III over its wavelength range for the objects at the centre (green) and outer edges (blue and red) within its field of view. It can be seen that the different incidence angle does not strongly change the P/S-ratio and thus does not influence the polarisation sensitivity of the grating. This is found to hold for all gratings.

6.2. Overall Sensitivity

Now that the grating efficiencies have been computed, the polarisation sensitivity of NIRSpec can be derived; by computing the throughput in normalised irradiance for light entering JWST (where the irradiance = 1) following the complete optical path to the detector. This computation s performed with the medium and high resolution grating in band III, GRT1000-III and GRT2700-III, as shown in Figure 6.4 and Figure 6.5, respectively.

It can be seen that the difference in output irradiance changes with wavelength due to the wavelength dependent grating efficiencies, and also changes with differently polarised light due to the wavelength dependent P/S-ratio as discussed before. It should again be noted that the detector is modelled as a basic Fresnel surface and further research should be performed to accurately determine the efficiency as a function of both wavelength and incidence angle.

To better examine the polarisation sensitivity, the computed irradiance at the detector for 10% P- and S-polarised light is normalised to the computed unpolarised irradiance at the detector in Figure 6.6 and Figure 6.7 for GRT1000-III and GRT2700-III, respectively. In these figures, the uncertainty is defined as the range in irradiance in which light incident on the grating could reflected depending on its degree of polarisation and polarisation orientation. The reason it is defined as uncertainty is because when the degree of polarisation is known, but not the orientation, the irradiance at the detector could be anywhere within that uncertainty range.

It can be seen how the uncertainty follows the deviation of the P/S-ratio's from 1 shown before in Figure 6.1 and Figure 6.2, but with a small adjustment coming from the induced polarisation in S-direction. This is because, regardless of initial polarisation state, a degree of polarisation in S-direction will be induced through reflections with the mirrors as discussed in Chapter 5. In the figures it can be seen that the uncertainty varies with wavelength and thus different wavelengths might undergo different efficiencies through the instrument and cause the data to be misinterpreted. Specifically for the high resolution gratings the uncertainty grows up to 4% in this example case.

Applying Equation (7.1) with the estimated induced degree of polarisation below 2% with Palik's data would result in a 0.2% mismatch at most. If additionally it is also taken into account that the orientation of the induced polarisation is known, S-polarised, that would further decrease the mismatch between actual irradiance and measured irradiance to a maximum of 0.1%. It can therefore be concluded that the induced polarisation will likely not influence the measurements significantly, but inherent polarisation of the incoming light could introduce a large uncertainty.

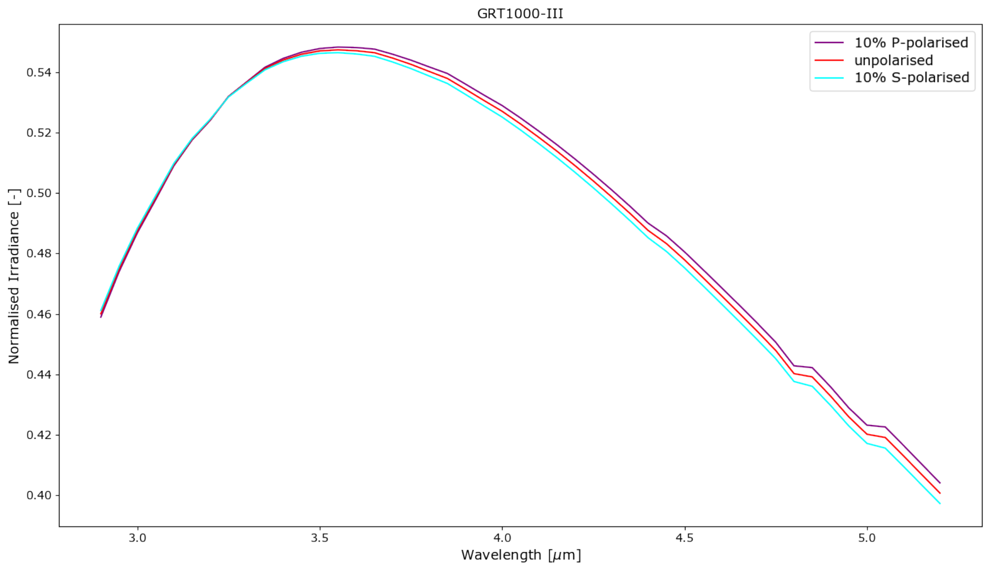

Figure 6.4: The throughput in irradiance for GRT1000-III for unpolarised and 10% polarised light, normalised with respect to the irradiance of the unpolarised incident light entering JWST. It can be seen that the degree of polarisation has a visible effect on the output, especially towards the end of the wavelength range.

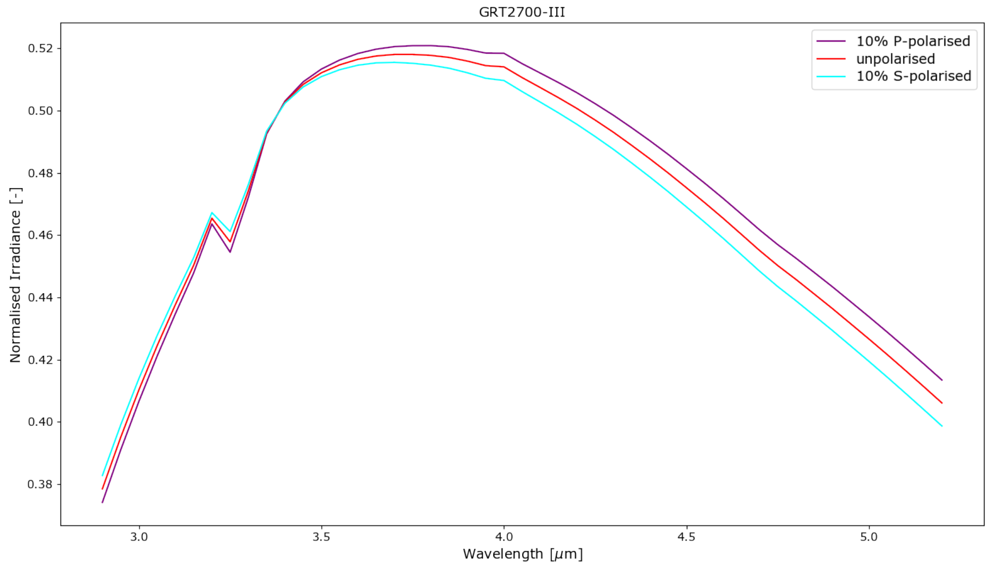

Figure 6.5: The throughput in irradiance for GRT2700-III for unpolarised and 10% polarised light, normalised with respect to the irradiance of the unpolarised incident light entering JWST. The effect in different throughput is even higher here due to the larger P/S-ratio of the grating.

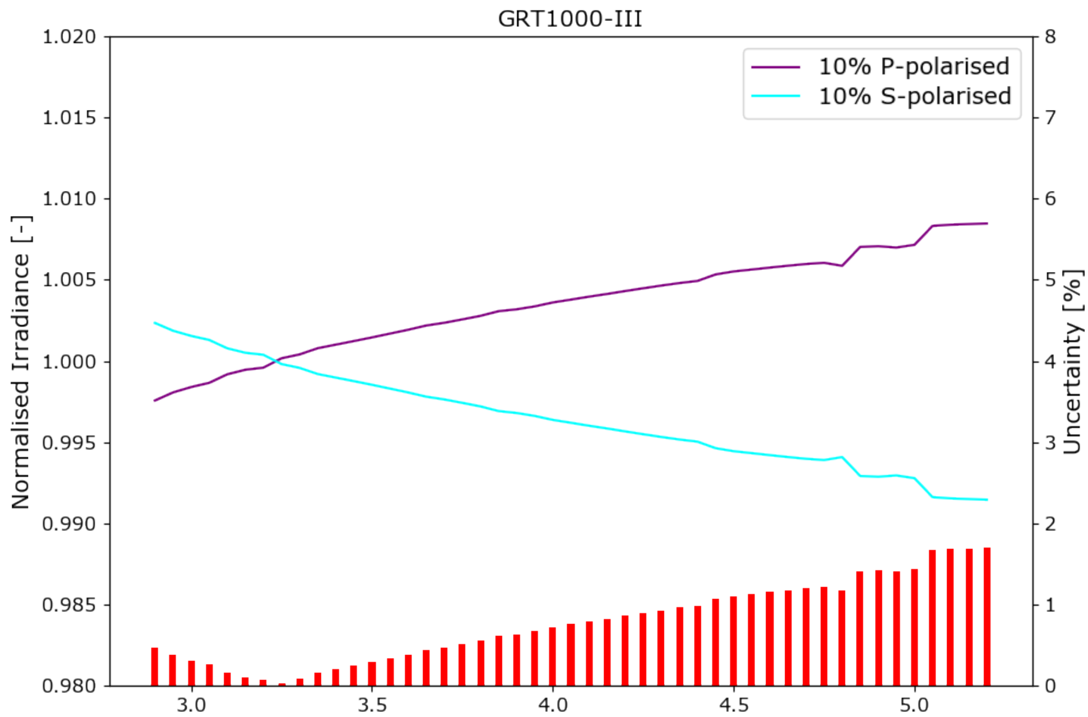

Figure 6.6: The normalised irradiance for 10% P- and S-polarised light in purple and cyan, respectively, projected on the left vertical axis using GRT1000-III for the nominal path. The uncertainty is projected on the right vertical axis and the red bars at the bottom. It can be seen that the uncertainty varies with wavelength and largely follows the difference between the P- and S-polarised lines, rising up to 2% at the end of the wavelength range.

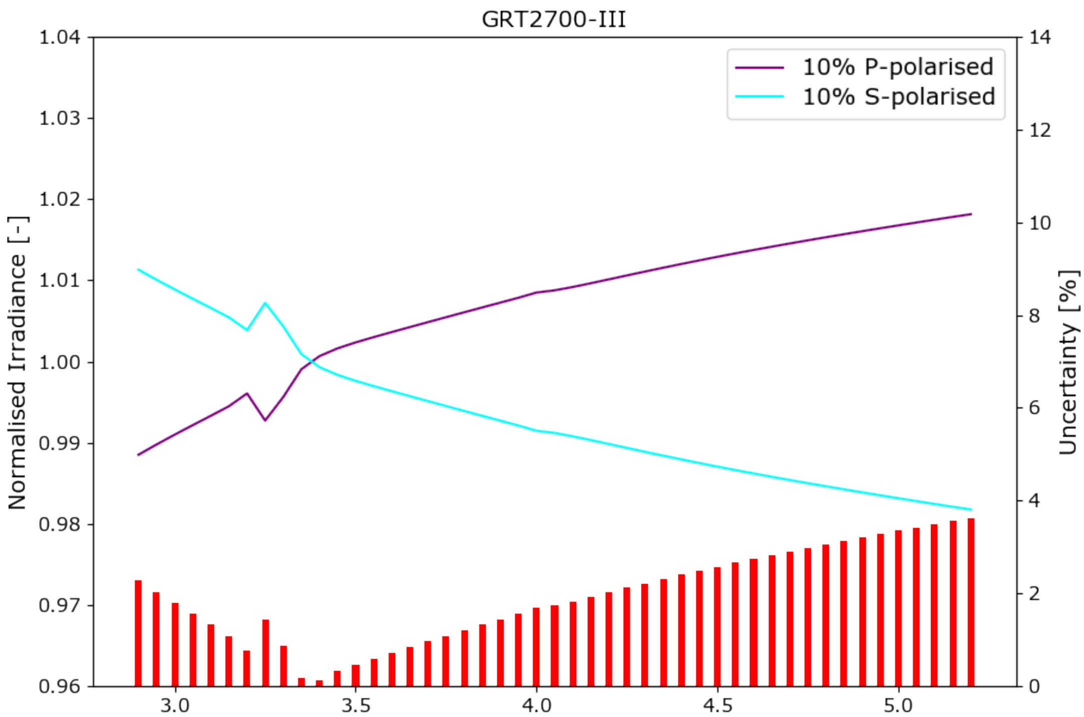

Figure 6.7: The same normalised irradiance for 10% P- and S-polarised light in purple and cyan, respectively, projected on the left vertical axis using GRT2700-III for the nominal path. The uncertainty is projected on the right vertical axis and the red bars at the bottom. . The uncertainty varies similarly with wavelength but reaches higher values up to almost 4% as the difference between the P- and S-polarised irradiance is greater than for GRT1000-III.

7

Calibration Assembly

In this chapter the calibration process is analysed in detail, depicted in Figure 7.1. First the induced polarisation is computed similar to the method used for the nominal science path. From here, conclusions are drawn on the effect on total throughput difference the polarisation makes. Second, a method for corrections is shown to verify assumptions that have been made for the analysis. Note that ray numbering for the calibration path is from 9 to 17 and they do not directly lie in the same orientation as ray 0 to 8. That is because they are, just like ray 0 to 8 in Figure 4.1, positioned with respect to the first mirror they encounter leaving the integrated sphere, which is CAL1 instead of the primary mirror of JWST, OTE1. This is shown in Figure 7.2. Because CAL1 and OTE1 are differently orientated, the position of the rays 9 to 17 do not align with 0 to 8 when they follow the nominal science path from CAL3 onwards. Because the central ray does have the same position and the outer rays still define the complete range of a light beam, it was considered acceptable. To change the orientation to a directly comparable orientation with the nominal science path, a rotation of the initial incident light from the integrated sphere of the calibration assembly could be applied in future work.

7.1. Analysis

Just like with the nominal science path, the induced polarisation via the calibration path is analysed before it reaches the grating to determine whether this will introduce efficiency differences between wavelengths. The degree of polarisation is plotted over the grating wavelength ranges for the calibration path in Figure 7.3. It can be seen that the calibration path rays follow the same shape as the nominal science path, but the rays reach a degree of polarisation that is approximately 1 to 2% higher values. This is specifically caused by the reflection between CAL2 and CAL3 as there is a large angle of incidence. Again, it can be seen that the middle ray gives a good indication of the expected polarisation for the complete beam, given that the spread in degree of polarisation is approximately 1 percentage point.

Again, the above results are obtained assuming the values for complex refractive index from Palik. To determine the effect of assumed complex refractive index on degree of polarisation, the same sensitivity analysis is performed as in Section 5.1 and the results are shown in Figure 7.4. The degree of polarisation follows the same shading as before, as expected, but in a larger range of values. Still, it can be seen that if the values of Babar and Weaver are assumed to be true, the computed induced polarisation would be approximately 1% over the complete wavelength.

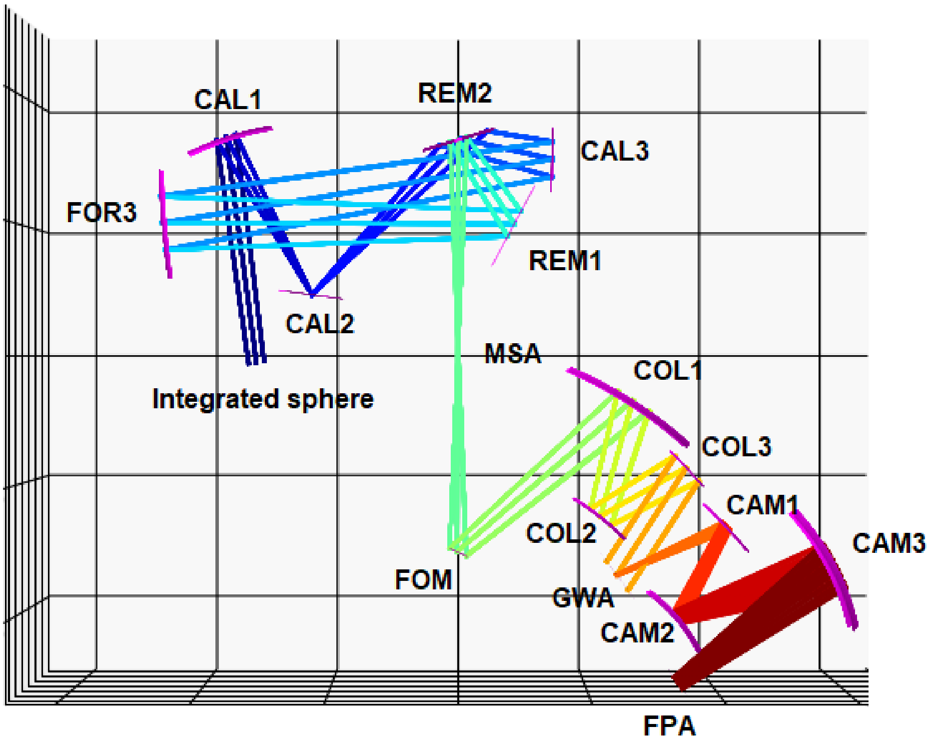

Figure 7.1: The calibration path from the integrated sphere towards the detector in the FPA. The colours indicate different polarisation states in between the optical elements. The beam consists of multiple wavelengths which are dispersed at the GWA

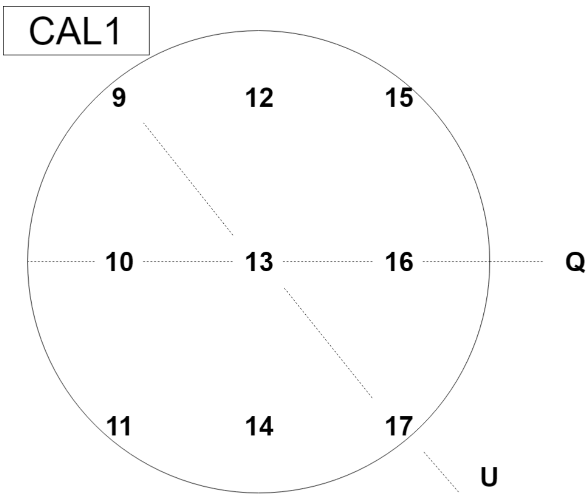

Figure 7.2: The position of the rays 9 to 17 with respect to the first mirror in the calibration path CAL1, looking into the direction of propagation into NIRSpec and the definitions of the positive Q and U Stokes parameters directions.

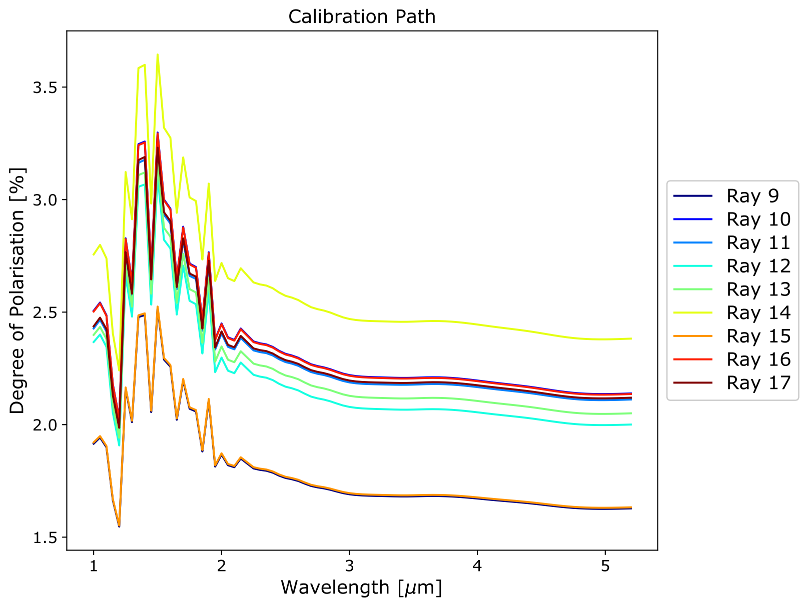

Figure 7.3: The degree of polarisation over wavelength but now for rays following the calibration path. The same shape can be found over wavelength and spread over rays, but at slightly higher values caused by a large angle of incidence between CAL2 and CAL3.

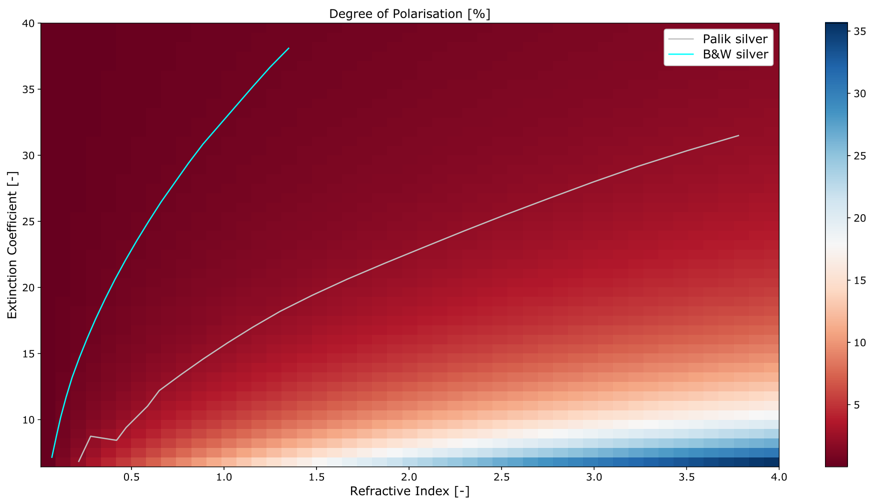

Figure 7.4: The degree of polarisation plotted against both refractive index and extinction coefficient for all mirrors in the nominal path for the ray in the centre of the beam, ray 13. The plotted lines represent the complex refractive index for silver from two different sources from 1.0 to 5.2 μm wavelength. The difference in degree of polarisation can be up to approximately 2% depending on source used.

7.2. CORRECTION

Multiple assumptions have been made during this analysis of the calibration path for induced polarisation, the grating efficiencies, and detector efficiencies. This section describes how they all relate and how one could find the needed correction for the induced polarisation in the calibration assembly if certain assumptions are validated through measurements.

Repeating Equation (1.1) for the measured irradiance at the detector. Assuming that all polarisation that is induced before it reaches the grating is S-polarised, the effective grating efficiency can be described by Equation (7.1). If two measurements are taken at the same wavelength, the ratio between the measured irradiances can be computed as Equation (7.2)

$$I = I_{COL3}\, G_{eff}\, M_{eff}\, D_{eff} \qquad (1.1) \qquad\qquad G_{eff} = \frac{NP}{I_{COL3}} \frac{P_{eff} + S_{eff}}{2} + \frac{S}{I_{COL3}} S_{eff} \qquad (7.1)$$

$$\frac{I_1}{I_2} = \frac{I_{COL3}\, G_{eff,1}\, M_{eff,1}\, D_{eff,1}}{I_{COL3}\, G_{eff,2}\, M_{eff,2}\, D_{eff,2}} \qquad (7.2)$$

As an example: one could compute the exact degree of induced polarisation before the grating as shown in Equation (7.3) if the grating and detector efficiencies are known. Specifically, the difference between P- and S-efficiencies are required for the gratings, while for the detector the efficiencies over incidence angle are required. This is also assuming that the mirror efficiencies do not change with the slightly different local incidence angles.

$$\frac{S}{NP} = \frac{\frac{P_{eff,1}+S_{eff,1}}{2} - \frac{P_{eff,2}+S_{eff,2}}{2} \frac{I_1}{I_2} \frac{D_{eff,2}}{D_{eff,1}}}{S_{eff,2} \frac{I_1}{I_2} \frac{D_{eff,2}}{D_{eff,1}} - S_{eff,1}} \rightarrow DOP = \frac{100}{1 + \frac{NP}{S}} \qquad (7.3)$$

8
Conclusion

The goal of this report was to determine the overall polarisation sensitivity of NIRSpec. Understanding the polarisation sensitivity is important to correctly interpret the output data and accurately calibrate the instrument during operational lifetime. Experimental research on this topic for NIRSpec was not practically viable as the instrument is already installed on the telescope and is waiting for launch in Kourou. Therefore, the choice has been made to make a software model that can simulate the light going through the instrument and perform the relevant analyses. A ray tracer was built that can be used for additional analyses or instruments thanks to its flexibility.

The analyses regarding the polarisation sensitivity were performed in three main categories: the induced polarisation, the grating efficiencies and overall throughput, and the effect on the calibration process.

The induced degree of polarisation for the nominal science path will likely remain below 2%. This degree of polarisation is slightly dependent on both wavelength and initial incidence angle. The wavelength influences the induced degree of polarisation because the optical constants of the mirror coatings are wavelength dependent. Because these optical constants, the refractive index and extinction coefficient, are complicated to measure, there is an uncertainty in their actual values. A sensitivity analysis has been performed which shows that optical constants data from different literature do not change the overall induced degree of polarisation significantly.

Similarly, a sensitivity analysis over the complete field of view of NIRSpec has been performed. Is has been shown that small variation in polarisation state may be found for differently positioned objects in the field of view; the induced degree of polarisation remains within a 0.2 percentage point range and the orientation of the induced polarisation could be rotated up to approximately 10° with respect to the induced polarisation state of rays at the centre of the field of view.

The analysis of the grating efficiencies clearly indicate a polarisation sensitivity up to 20% for the medium resolution gratings and up to 40% for the high resolution gratings. Due to the low estimated induced polarisation below 2%, the overall throughput is not altered significantly. Observing celestial objects with a inherent degree of polarisation, however, could introduce a significant uncertainty in the irradiances that are derived from the measurements. Incident light with a 10% degree of polarisation can introduce an uncertainty up to 4%.

The calibration process has been examined and it has been concluded that the overall polarisation sensitivity will most likely not affect the throughput significantly as the estimated difference will be below 1%. The induced polarisation for the calibration path is 1 to 2% higher than for the nominal science path, but considering the grating efficiencies this will not result in a large correction requirement. A method has been proposed to accurately determine what correction would be necessary if a higher accuracy is necessary.

9 Recommendations for Future Work

This master thesis research has provided insights in the polarisation sensitivity of NIRSpec divided into three main categories: the induced polarisation, the grating efficiencies and overall sensitivity, and the calibration assembly. Several assumptions have been made for the analyses presented in this report. In this chapter, potential improvements are listed as recommendations for future work divided into four categories: grating efficiencies, pass filters, additional NIRSpec configurations, and validation by measurement data.

- **Grating efficiencies** - A large part of the polarisation sensitivity of NIRSpec is introduced by the reflection gratings. The grating efficiencies were taken from PCGrate which has been used as a black box. Ideally, the theory of reflection efficiencies for different polarisation directions should be determined and implemented in an open software model and added to the ray tracer to better understand the uncertainty of the results. If that is done, it might also be possible to take into account the effects of circular polarisation which have been neglected in this report and is not supported by PCGrate.
- **Pass filters** - The filters, and specifically the detector, have been modelled as single layer Fresnel surfaces for transmission even though they consist of multiple layers of different materials. It is therefore uncertain what the accuracy of computed efficiency and how it varies with both wavelength and incidence angle of the incident rays.
- **Additional NIRSpec configurations** - Not all elements or functionalities of NIRSpec have been analysed. Only the operational configurations for the reflection gratings have been examined. Performing an analysis in the prism of the grating wheel assembly would also be interesting. Furthermore, only MOS mode has been analysed with the microshutter array as a perfect transmitter. Additional analyses for SLIT and IFU mode, which utilise long-slit spectroscopy and integral field spectroscopy, could provide valuable information on NIRSpec.
- **Validation by measurement data** - No validation of the ray tracer has been done with actual experimental measurements. During operational lifetime, NIRSpec will deliver output data which can be used to determine whether possible polarisation sensitivity effects can be found similar to the computed effects presented in this master thesis research. Alternatively, applying the ray tracer to a different instrument of which a lot of measurement data is available to check the ray tracer itself would also provide more insights in the accuracies of the presented results.

Bibliography

[1] European Space Agency. New launch date for james webb space telescope. https://www.esa.int, July 2019.

[2] S. Babar and J. H. Weaver. Optical constants of cu, ag, and au revisited. *Applied Optics*, 54(3):477–481, 2015.

[3] G. Bagnasco et al. Overview of the near infrared spectrograph (nirspec) instrument on-board the james webb space telescope (jwst). In *Proceedings of SPIE - The International Society for Optical Engineering*, volume 6692, 2007.

[4] G. Bagnasco et al. The on-ground calibration of the near infrared spectrograph (nirspec) instrument on-board the james webb space telescope (jwst). In *Proceedings of SPIE - The International Society for Optical Engineering*, volume 7010, 2008.

[5] J.M. Bennett. *Handbook of optics*. Mcgraw-Hill Inc., 1995.

[6] M. Clampin. Overview of the james webb space telescope observatory. In *Proceedings of SPIE - The International Society for Optical Engineering*, volume 8146, 2011.

[7] J. M. Cychosz. An introduction to ray tracing. edited by andrew s. glassner, published by academic press, new york, 1989, 327 pages. *Computers and Graphics*, 17(1), 1993.

[8] B. Dorner et al. A model-based approach to the spatial and spectral calibration of nirspec onboard jwst. *Astronomy and Astrophysics*, 592, 2016.

[9] M. M. Ellenrieder et al. The optical components of the nirspec wheel mechanisms. In *Proceedings of SPIE - The International Society for Optical Engineering*, volume 7018, 2008.

[10] R. Espinosa-Luna, D. Rodríguez-Carrera, E. Bernabeu, and S. Hinojosa-Ruíz. Transformation matrices for the mueller-jones formalism. *Optik*, 119(16):757–765, 2008.

[11] J. P. Gardner et al. The james webb space telescope. *Space Science Reviews*, 123(4):485–606, 2006.

[12] R. Geyl, E. Ruch, H. Vayssade, H. Leplan, and J. Rodolfo. Nirspec optics development: Final report. In *Proceedings of SPIE - The International Society for Optical Engineering*, 2017.

[13] D. H. Goldstein. *Polarized light*. CRC Press, 2010.

[14] M. Greenhouse. The james webb space telescope: Mission overview and status. In *IEEE Aerospace Conference Proceedings*, volume 2016-June, 2016.

[15] International Intellectual Group. https://www.pcgrate.com/index_html. Retrieved on August 28, 2019.

[16] J. B. Götte and M. R. Dennis. Generalized shifts and weak values for polarization components of reflected light beams. *New Journal of Physics*, 14, 2012.

[17] E Hecht. *Optics*. Pearson, 2016.

[18] Space Telescope Science Institute. https://jwst-docs.stsci.edu/near-infrared-spectrograph/nirspec-instrumentation/nirspec-dispersers-and-filters. Retrieved on August 28, 2019.

[19] A Kamp. Space instrumentation engineering. TU Delft, Faculty of Aerospace Engineering, 2007.

[20] R. A. Keski-Kuha, C. W. Bowers, M. A. Quijada, J. B. Heaney, B. Gallagher, A. McKay, and I. Stevenson. James webb space telescope optical telescope element mirror coatings. In *Proceedings of SPIE - The International Society for Optical Engineering*, volume 8442, 2012.

[21] D. B. Leviton, B. J. Frey, and T. J. Madison. Temperature-dependent refractive index of caf2 and infrasil 301. In *Proceedings of SPIE - The International Society for Optical Engineering*, volume 6692, 2007.

[22] M. J. Li et al. James webb space telescope microshutter arrays and beyond. *Journal of Micro/ Nanolithography, MEMS, and MOEMS*, 16(2), 2017.

[23] Valerio Lucarini, Jarkko J Saarinen, Kai-Erik Peiponen, and Erik M Vartiainen. *Kramers-Kronig relations in optical materials research*, volume 110. Springer Science & Business Media, 2005.

[24] A. Meurer et al. Sympy: symbolic computing in python. *PeerJ Computer Science*, 3:e103, 2017. ISSN 2376-5992. doi: 10.7717/peerj-cs.103. URL https://doi.org/10.7717/peerj-cs.103.

[25] NASA. https://www.nasa.gov. Retrieved on August 28, 2019.

[26] A. Novi, M. Taccola, J. Koehler, and M. Di Giampietro. The optical manufacturing of the refocusing mechanism of nirspec. In *Proceedings of SPIE - The International Society for Optical Engineering*, volume 7018, 2008.

[27] E. D. Palik. *Handbook of optical constants of solids*, volume 1, pages 1–804. Academic Press, 2012.

[28] B. J. Rauscher et al. New and better detectors for the jwst near-infrared spectrograph. *Publications of the Astronomical Society of the Pacific*, 126(942):739–749, 2014.

[29] Guido Rossum. Python reference manual. Technical report, 1995.

[30] M. Te Plate. Nirspec grating calculations with pc grate, 2018.

[31] M. Te Plate et al. Physical optics model for simulating the optical performance of the nirspec. In *Proceedings of SPIE - The International Society for Optical Engineering*, volume 6692, 2007.

[32] Geert Verhoeven. The reflection of two fields – electromagnetic radiation and its role in (aerial) imaging. *AARGNews*, 55:13–18, 2017.

[33] C. Wells and M. Coon. Opto-mechanical integration and alignment verification of the james webb space telescope (jwst) optical telescope element. In *Proceedings of SPIE - The International Society for Optical Engineering*, volume 7433, 2009.

[34] Zemax. https://www.zemax.com/products/opticstudio. Retrieved on August 28, 2019.

A

Light Beam

```python
import hcipy
import numpy as np

from General_Functions import compute_rotation_matrix

##############################################################################
# LIGHT SOURCE NEW
##############################################################################

def light_source(source_x, source_y, source_z, central_incidence_angle, rotation_axis_vector, f_number_beam, pupil_grid, plot=False):

    pupil_grid_polar = pupil_grid.as_('polar')
    r = hcipy.Field(pupil_grid_polar.r, pupil_grid)

    ray_start = np.zeros((3, len(r)))
    ray_start[:,0] = np.array([-3.3113888947E+03, -3.3126478721E+03, -5.5932625486E+03])
    ray_start[:,1] = np.array([-3.3113889153E+03, -1.0915872109E+01, -5.5932625486E+03])
    ray_start[:,2] = np.array([-3.3113888947E+03, 3.2908161279E+03, -5.5932625486E+03])
    ray_start[:,3] = np.array([-9.6568947093E+00, -3.3126478721E+03, -5.5932625486E+03])
    ray_start[:,4] = np.array([-9.6569153329E+00, -1.0915872109E+01, -5.5932625486E+03])
    ray_start[:,5] = np.array([-9.6568947092E+00, 3.2908161279E+03, -5.5932625486E+03])
    ray_start[:,6] = np.array([3.2920751053E+03, -3.3126478721E+03, -5.5932625486E+03])
    ray_start[:,7] = np.array([3.2920750847E+03, -1.0915872109E+01, -5.5932625486E+03])
    ray_start[:,8] = np.array([3.2920750847E+03, 3.2908161279E+03, -5.5932625486E+03])

    # Compute rotation matrix to simulate induced central incidence angle
    ray_direction_vector = np.array([[0.0018394014, 0.0020792057, 0.9999961467],]*len(r)).transpose()

    rotation_matrix = compute_rotation_matrix(rotation_axis_vector, central_incidence_angle)
    ray_direction_vector = np.dot(rotation_matrix, ray_direction_vector)

    return ray_start, ray_direction_vector, ray_start
```

B

Aspherical Mirrors

```python
import hcipy
import math
import numpy as np
from sympy import Symbol, sqrt, lambdify

from General_Functions import surface_plot_rotation, compute_rotation_matrix, \
                              normalise_vector, calculate_rotation_matrix, \
                              fresnel_reflection

##############################################################################
# ASPHERICAL MIRROR
##############################################################################

def aspherical_mirror(D, c, k, a4, a6, a8, x_position, y_position, z_position, decenter_x, decenter_y, \
                      tilt_x,  tilt_y, tilt_z, nt, kt, \
                      ray_origin, ray_direction_vector, Stokes, plot_colour, ax, pupil_grid, \
                      plot=True, normal=False, reflection=False, a10=0):

    if x_position == 0 and y_position == 0 and z_position ==0:
        OTE1_switch = 1
    else:
        OTE1_switch = 0

    number_of_rays = len(ray_origin[0,:])

    # Same intersection points for OTE1
    if OTE1_switch == 1:
        mirror_intersection = np.array([[-3.30189308e+03, -3.30189308e+03, -3.30189308e+03,
                                         -5.00059531e-01,  5.00059531e-01, -5.00059531e-01,
                                          3.30089296e+03,  3.30189308e+03,  3.30089296e+03],
                                        [-3.30289320e+03, -5.00059531e-01,  3.30089296e+03,
                                         -3.30189308e+03,  5.00059531e-01,  3.30189308e+03,
                                         -3.30289320e+03, -5.00059531e-01,  3.30089296e+03],
                                        [-6.86824894e+02, -3.43296052e+02, -6.86408922e+02,
                                         -3.43296052e+02, -1.57470977e-05, -3.43296052e+02,
                                         -6.86616940e+02, -3.43296052e+02, -6.86200967e+02]])

        mirror_domain_x = np.array([-D/2, D/2]) + decenter_x
        mirror_domain_y = np.array([-D/2, D/2]) + decenter_y
```

```
        mirror_steps = 10

        X_mirror = np.linspace(mirror_domain_x[0], mirror_domain_x[1], mirror_steps)
        Y_mirror = np.linspace(mirror_domain_y[0], mirror_domain_y[1], mirror_steps)
        X_mirror, Y_mirror = np.meshgrid(X_mirror, Y_mirror)
        R_eff = np.sqrt(X_mirror**2 + Y_mirror**2)

        Z_mirror = c * R_eff**2 / ( 1 + np.sqrt( 1 - (1+k) * c**2 * R_eff**2 ) ) + a4 * R_eff**4 + a6 * R_eff**6 + a8 * R_eff**8

        if plot == True:
            ax.plot_surface(X_mirror, Y_mirror, Z_mirror, color='fuchsia')

    else:
        ###########################################################################
        # Plot the 3D mirror

        mirror_index = number_of_rays * [0] # save the indeces at which intersections take place
        mirror_intersection = np.zeros((3, number_of_rays)) # save the intersection points

        # define the x-, y-, and z-rotation axes
        x_axis = [1, 0, 0]
        y_axis = [0, 1, 0]
        z_axis = [0, 0, 1]

        # first find where the ray hits approximately, then make detailed plot
        for ii in range(2):
            # define the mirror steps in the preliminary and final loop
            if ii == 0:
                mirror_domain_x = np.array([-D/2, D/2]) + decenter_x
                mirror_domain_y = np.array([-D/2, D/2]) + decenter_y
                mirror_steps = 10
            else:
                mirror_domain_x = np.array([min(X_local[mirror_index]) - D/mirror_steps, max(X_local[mirror_index]) + D/mirror_steps])
                mirror_domain_y = np.array([min(Y_local[mirror_index]) - D/mirror_steps, max(Y_local[mirror_index]) + D/mirror_steps])
                x_domain = mirror_domain_x[1] - mirror_domain_x[0]
                y_domain = mirror_domain_y[1] - mirror_domain_y[0]
                max_domain = max(x_domain, y_domain)
                mirror_step_size = 1
                mirror_steps = math.ceil(max_domain/mirror_step_size)

            X_mirror = np.linspace(mirror_domain_x[0], mirror_domain_x[1], mirror_steps)
            Y_mirror = np.linspace(mirror_domain_y[0], mirror_domain_y[1], mirror_steps)
            X_mirror, Y_mirror = np.meshgrid(X_mirror, Y_mirror)
            R_eff = np.sqrt(X_mirror**2 + Y_mirror**2)

            if c == np.inf: # for flat mirrors
                Z_mirror = 0*R_eff
            else: # general asphere equation
                Z_mirror = c * R_eff**2 / ( 1 + np.sqrt( 1 - (1+k) * c**2 * R_eff**2 ) ) + a4 * R_eff**4 + a6 * R_eff**6 + a8 * R_eff**8 + a10* R_eff**10

            # Save mirror in local coordinates
            X_local = X_mirror.ravel()
            Y_local = Y_mirror.ravel()
            Z_local = Z_mirror.ravel()
            local_mirror = np.array([X_local, Y_local, Z_local])

            # Transform to global coordinates
            if tilt_x != 0:
                X_mirror, Y_mirror, Z_mirror = surface_plot_rotation(x_axis, tilt_x, X_mirror, Y_mirror, Z_mirror)
                # redefine the new y- and z-rotation axes due to x-rotation
                y_axis = np.dot(compute_rotation_matrix(x_axis, tilt_x), y_axis)
                z_axis = np.dot(compute_rotation_matrix(x_axis, tilt_x), z_axis)
```

```
            if tilt_y != 0:
                X_mirror, Y_mirror, Z_mirror = surface_plot_rotation(y_axis, tilt_y, X_mirror, Y_mirror, Z_mirror)
                z_axis = np.dot(compute_rotation_matrix(y_axis, tilt_y), z_axis)
            if tilt_z != 0:
                X_mirror, Y_mirror, Z_mirror = surface_plot_rotation(z_axis, tilt_z, X_mirror, Y_mirror, Z_mirror)
            X_mirror = X_mirror + x_position
            Y_mirror = Y_mirror + y_position
            Z_mirror = Z_mirror + z_position

            # Save mirror in global coordinates
            X_intersection = X_mirror.ravel()
            Y_intersection = Y_mirror.ravel()
            Z_intersection = Z_mirror.ravel()
            global_mirror = np.array([X_intersection, Y_intersection, Z_intersection])

            if ii == 0 and plot == True:
                ax.plot_surface(X_mirror, Y_mirror, Z_mirror, color='fuchsia')

            ###########################################################################
            # Compute the intersection point of every individual ray with the mirror
            # This is done by comparing the ray_direction_vector with vectors to every point on the mirror

            for i in range(number_of_rays):
                mirror_direction = (global_mirror.transpose() - ray_origin[:,i]).transpose() # computes vectors from ray origin to mirror points
                mirror_direction = normalise_vector(mirror_direction).transpose()

                find_intersection = np.dot(mirror_direction, ray_direction_vector[:,i]) # dot product should be 1 if parallel
                find_intersection = np.fabs(find_intersection - 1)
                if min(find_intersection) > 0.1:
                    raise ValueError('Ray does not intersect with next mirror')

                mirror_index[i] = np.unravel_index(find_intersection.argmin(), find_intersection.shape)[0]

            # reset rotation axes
            x_axis = [1, 0, 0]
            y_axis = [0, 1, 0]
            z_axis = [0, 0, 1]

        mirror_intersection = global_mirror[:,mirror_index]

        ###########################################################################
        # Plot the incoming rays

        if plot == True:
            for i in range(number_of_rays):
                ax.plot((mirror_intersection[0,i], ray_origin[0][i]), (mirror_intersection[1,i], ray_origin[1][i]), (mirror_intersection[2,i], ray_origin[2][i]), color=plot_colour, zorder = 5)

    ###########################################################################
    # Define mirror function with r_mirror as symbol to compute the derivative function

    r_symbol = Symbol('r_symbol')   #this is the radial distance from the vertex of the mirror to a point
    mirror_symbol = c * r_symbol**2 / ( 1 + sqrt( 1 - (1+k) * c**2 * r_symbol**2 ) ) + a4 * r_symbol**4 + a6 * r_symbol**6 + a8 * r_symbol**8 + a10 * r_symbol**10
    mirror_derivative = mirror_symbol.diff(r_symbol)
    mirror_derivative_function = lambdify(r_symbol, mirror_derivative, 'numpy')

    ###########################################################################
    # Compute the reflection and incidence angle from the normal

    if OTE1_switch == 1:
        intersect_x = np.array([-3.30189308e+03, -3.30189308e+03, -3.30189308e+03, -5.00059531e-01,
```

```
                             5.00059531e-01, -5.00059531e-01,  3.30089296e+03, 3.30189308e+03,
                             3.30089296e+03])
    intersect_y = np.array([-3.30289320e+03, -5.00059531e-01,  3.30089296e+03, -3.30189308e+03,
                             5.00059531e-01,  3.30189308e+03, -3.30289320e+03, -5.00059531e-01,
                             3.30089296e+03])
    intersect_r = np.sqrt(intersect_x**2 + intersect_y**2)
    intersect_phi = np.arctan2(intersect_y, intersect_x)

    normal_vector = np.array([[ 1.99509489e-01,  2.03591196e-01,  1.99514284e-01,
                                3.08331358e-05, -3.14904461e-05,  3.08331358e-05,
                               -1.99451455e-01, -2.03591196e-01, -1.99456249e-01],
                              [ 1.99569919e-01,  3.08331358e-05, -1.99453852e-01,
                                2.03591196e-01, -3.14904461e-05, -2.03591196e-01,
                                1.99572316e-01,  3.08331358e-05, -1.99456249e-01],
                              [-9.59358020e-01, -9.79055986e-01, -9.59381161e-01,
                               -9.79055986e-01, -9.99999999e-01, -9.79055986e-01,
                               -9.59369589e-01, -9.79055986e-01, -9.59392730e-01]])
    OTE1_switch = 0

else:

    # Compute normal at intersection points
    intersect_x = local_mirror[0,mirror_index]
    intersect_y = local_mirror[1,mirror_index]
    intersect_r = np.sqrt(intersect_x**2 + intersect_y**2)
    intersect_phi = np.arctan2(intersect_y, intersect_x)

    if c == np.inf: # for flat mirror
        normal_vector = np.zeros((3, number_of_rays))
        normal_vector[2,:] = normal_vector[2,:] -1

    else:
        # find tangent at intersection point from derivative function in 2D
        tangent_vector_2d = np.array([np.ones(number_of_rays), mirror_derivative_function(intersect_r)])
        normal_vector_2d = np.array([tangent_vector_2d[1], -tangent_vector_2d[0]])

        # translate 2D normal to 3D using local phi
        normal_x = normal_vector_2d[0] * np.cos(intersect_phi)
        normal_y = normal_vector_2d[0] * np.sin(intersect_phi)
        normal_z = normal_vector_2d[1]
        normal_vector = normalise_vector([normal_x, normal_y, normal_z])

    # transform normal to global reference
    if tilt_x != 0:
        normal_vector = np.dot(compute_rotation_matrix(x_axis, tilt_x), normal_vector)
        y_axis = np.dot(compute_rotation_matrix(x_axis, tilt_x), y_axis)
        z_axis = np.dot(compute_rotation_matrix(x_axis, tilt_x), z_axis)
    if tilt_y != 0:
        normal_vector = np.dot(compute_rotation_matrix(y_axis, tilt_y), normal_vector)
        z_axis = np.dot(compute_rotation_matrix(y_axis, tilt_y), z_axis)
    if tilt_z != 0:
        normal_vector = np.dot(compute_rotation_matrix(z_axis, tilt_z), normal_vector)

# compute incidence angle from ray direction and normal
# https://stackoverflow.com/questions/2827393/angles-between-two-n-dimensional-vectors-in-python
incidence_angle = np.arccos(sum(ray_direction_vector * normal_vector))

# compute reflection direction from ray direction and normal
# https://math.stackexchange.com/questions/13261/how-to-get-a-reflection-vector
# https://stackoverflow.com/questions/17437817/python-how-to-get-diagonalab-without-having-to-perform-ab
A = ray_direction_vector
B = 2 * np.einsum('ij,ji->i', ray_direction_vector.transpose(), normal_vector)
```

```
    C = normal_vector

    reflection_direction_vector = A - B * C

    ###########################################################################
    # Computes Jones matrices

    e_s = np.zeros([3, 9])
    e_p = np.zeros([3, 9])
    P_s = np.zeros([2, 2, 9])
    P_p = np.zeros([2, 2, 9])

    for i in range(9):
        # rotate ray_direction_vector such that it is [0, 0, 1]
        R = calculate_rotation_matrix(ray_direction_vector[:,i], [0, 0, 1])

        # rotate normal_vector to ray_direction_vector reference frame
        normal_vector_rdv = np.dot(R, normal_vector[:,i])

        e_s[:,i] = normalise_vector(np.cross(normal_vector_rdv, [0, 0, 1]))
        e_p[:,i] = normalise_vector(np.cross(e_s[:,i], [0, 0, 1]))

        P_s[0,0,i] = e_s[0,i]*e_s[0,i]
        P_s[0,1,i] = e_s[0,i]*e_s[1,i]
        P_s[1,0,i] = e_s[1,i]*e_s[0,i]
        P_s[1,1,i] = e_s[1,i]*e_s[1,i]

        P_p[0,0,i] = e_p[0,i]*e_p[0,i]
        P_p[0,1,i] = e_p[0,i]*e_p[1,i]
        P_p[1,0,i] = e_p[1,i]*e_p[0,i]
        P_p[1,1,i] = e_p[1,i]*e_p[1,i]

    ni = 1
    r_p, r_s = fresnel_reflection(ni, nt, kt, incidence_angle)

    J_mirror = r_s*P_s - r_p*P_p

    Mueller = np.zeros((4, 4, number_of_rays))
    J_mirror_conj = np.conj(J_mirror)
    # looking in the propagation direction
    A = 1/np.sqrt(2) * np.matrix([[1, 0  , 0 , 1 ],
                                  [1, 0  , 0 , -1],
                                  [0, 1  , 1 , 0 ],
                                  [0, -1j, 1j, 0 ]])

    for i in range(number_of_rays):
        J_kron = np.matrix(np.kron(J_mirror[:,:,i], J_mirror_conj[:,:,i]))
        Mueller[:,:,i] = A * J_kron * A.conj().T

    Stokes_reflection = np.einsum('ijk,jk->ik', Mueller, Stokes)
    DOP = np.sqrt(Stokes_reflection[1,:]**2 + Stokes_reflection[2,:]**2 +
    Stokes_reflection[3,:]**2) / Stokes_reflection[0,:]

    return mirror_intersection, reflection_direction_vector, Stokes_reflection, DOP,
    incidence_angle
```

C

Pass Filters

```python
import math
import numpy as np

from General_Functions import surface_plot_rotation, compute_rotation_matrix, \
                              normalise_vector, calculate_rotation_matrix, \
                              fresnel_transmission

################################################################################
# PASS FILTER
################################################################################

def pass_filter(D, refractive_origin, refractive_new, \
                x_position, y_position, z_position, tilt_x, tilt_y, tilt_z, \
                ray_origin, ray_direction_vector, Stokes, plot_colour, ax, pupil_grid, \
                plot=True, normal=False, reflection=False):

    number_of_rays = len(ray_origin[0,:])

    ################################################################################
    # Plot the 3D mirror

    mirror_index = number_of_rays * [0] # save the indeces at which intersections take place
    mirror_intersection = np.zeros((3, number_of_rays)) # save the intersection points

    # define the x-, y-, and z-rotation axes
    x_axis = [1, 0, 0]
    y_axis = [0, 1, 0]
    z_axis = [0, 0, 1]

    # first find where the ray hits approximately, then make detailed plot
    for ii in range(2):
        # define the mirror steps in the preliminary and final loop
        if ii == 0:
            mirror_steps = 10
            mirror_domain_x = np.array([-D/2, D/2])
            mirror_domain_y = np.array([-D/2, D/2])
        else:
            mirror_domain_x = np.array([min(X_local[mirror_index]) - D/mirror_steps, max(X_local[mirror_index]) + D/mirror_steps])
            mirror_domain_y = np.array([min(Y_local[mirror_index]) - D/mirror_steps, max(Y_local[mirror_index]) + D/mirror_steps])
            x_domain = mirror_domain_x[1] - mirror_domain_x[0]
            y_domain = mirror_domain_y[1] - mirror_domain_y[0]
            max_domain = max(x_domain, y_domain)
            mirror_step_size = 1
            mirror_steps = math.ceil(max_domain/mirror_step_size)

        X_mirror = np.linspace(mirror_domain_x[0], mirror_domain_x[1], mirror_steps)
```

```
        Y_mirror = np.linspace(mirror_domain_y[0], mirror_domain_y[1], mirror_steps)
        X_mirror, Y_mirror = np.meshgrid(X_mirror, Y_mirror)
        R_eff = np.sqrt(X_mirror**2 + Y_mirror**2)

        Z_mirror = 0*R_eff

        # Save mirror in local coordinates
        X_local = X_mirror.ravel()
        Y_local = Y_mirror.ravel()
        Z_local = Z_mirror.ravel()

        # Transform to global coordinates
        if tilt_x != 0:
            X_mirror, Y_mirror, Z_mirror = surface_plot_rotation(x_axis, tilt_x, X_mirror, Y_mirror, Z_mirror)
            # redefine the new y- and z-rotation axes due to x-rotation
            y_axis = np.dot(compute_rotation_matrix(x_axis, tilt_x), y_axis)
            z_axis = np.dot(compute_rotation_matrix(x_axis, tilt_x), z_axis)
        if tilt_y != 0:
            X_mirror, Y_mirror, Z_mirror = surface_plot_rotation(y_axis, tilt_y, X_mirror, Y_mirror, Z_mirror)
            z_axis = np.dot(compute_rotation_matrix(y_axis, tilt_y), z_axis)
        if tilt_z != 0:
            X_mirror, Y_mirror, Z_mirror = surface_plot_rotation(z_axis, tilt_z, X_mirror, Y_mirror, Z_mirror)
        X_mirror = X_mirror + x_position
        Y_mirror = Y_mirror + y_position
        Z_mirror = Z_mirror + z_position

        # Save mirror in global coordinates
        X_intersection = X_mirror.ravel()
        Y_intersection = Y_mirror.ravel()
        Z_intersection = Z_mirror.ravel()
        global_mirror = np.array([X_intersection, Y_intersection, Z_intersection])

        if ii == 0 and plot == True:
            ax.plot_surface(X_mirror, Y_mirror, Z_mirror, color='fuchsia')

        ###########################################################################
        # Compute the intersection point of every individual ray with the mirror
        # This is done by comparing the ray_direction_vector with vectors to every point on the mirror

        for i in range(number_of_rays):
            mirror_direction = (global_mirror.transpose() - ray_origin[:,i]).transpose() # computes vectors from ray origin to mirror points
            mirror_direction = normalise_vector(mirror_direction).transpose()

            find_intersection = np.dot(mirror_direction, ray_direction_vector[:,i]) # dot product should be 1 if parallel
            find_intersection = np.fabs(find_intersection - 1)

            mirror_index[i] = np.unravel_index(find_intersection.argmin(), find_intersection.shape)[0]

        # reset rotation axes
        x_axis = [1, 0, 0]
        y_axis = [0, 1, 0]
        z_axis = [0, 0, 1]

    mirror_intersection = global_mirror[:,mirror_index]

    ###########################################################################
    # Plot the incoming rays

    if plot == True:
        for i in range(number_of_rays):
            ax.plot((mirror_intersection[0,i], ray_origin[0][i]), (mirror_intersection[1,i], ray_origin[1][i]), (mirror_intersection[2,i], ray_origin[2][i]), color=plot_colour, zorder = 5)

```

```
    # Compute incidence angle and reflection
    normal_vector = np.zeros((3, number_of_rays))
    normal_vector[2,:] = normal_vector[2,:] -1


    # transform normal to global reference
    if tilt_x != 0:
        normal_vector = np.dot(compute_rotation_matrix(x_axis, tilt_x), normal_vector)
        y_axis = np.dot(compute_rotation_matrix(x_axis, tilt_x), y_axis)
        z_axis = np.dot(compute_rotation_matrix(x_axis, tilt_x), z_axis)
    if tilt_y != 0:
        normal_vector = np.dot(compute_rotation_matrix(y_axis, tilt_y), normal_vector)
        z_axis = np.dot(compute_rotation_matrix(y_axis, tilt_y), z_axis)
    if tilt_z != 0:
        normal_vector = np.dot(compute_rotation_matrix(z_axis, tilt_z), normal_vector)

    # compute incidence angle from ray direction and normal
    # https://stackoverflow.com/questions/2827393/angles-between-two-n-dimensional-vectors-in-python
    incidence_angle = np.arccos(sum(ray_direction_vector * -normal_vector))

    n_ratio = refractive_origin/refractive_new

    #https://en.wikipedia.org/wiki/Snell%27s_law#Vector_form
    A = np.einsum('ij,ji->i', -normal_vector.transpose(), ray_direction_vector)
    reflection_direction_vector = n_ratio * ray_direction_vector + (n_ratio * A - np.sqrt(1-n_ratio**2*(1-A**2)))*normal_vector

    ##########################################################################
    # Computes Jones matrices

    e_s = np.zeros([3, 9])
    e_p = np.zeros([3, 9])
    P_s = np.zeros([2, 2, 9])
    P_p = np.zeros([2, 2, 9])

    for i in range(9):
        # rotate ray_direction_vector such that it is [0, 0, 1]
        R = calculate_rotation_matrix(ray_direction_vector[:,i], [0, 0, 1])

        # rotate normal_vector to ray_direction_vector reference frame
        normal_vector_rdv = np.dot(R, normal_vector[:,i])

        e_s[:,i] = normalise_vector(np.cross(normal_vector_rdv, [0, 0, 1]))
        e_p[:,i] = normalise_vector(np.cross(e_s[:,i], [0, 0, 1]))

        P_s[0,0,i] = e_s[0,i]*e_s[0,i]
        P_s[0,1,i] = e_s[0,i]*e_s[1,i]
        P_s[1,0,i] = e_s[1,i]*e_s[0,i]
        P_s[1,1,i] = e_s[1,i]*e_s[1,i]

        P_p[0,0,i] = e_p[0,i]*e_p[0,i]
        P_p[0,1,i] = e_p[0,i]*e_p[1,i]
        P_p[1,0,i] = e_p[1,i]*e_p[0,i]
        P_p[1,1,i] = e_p[1,i]*e_p[1,i]

    t_p, t_s = fresnel_transmission(refractive_origin, refractive_new, incidence_angle)

    J_mirror = t_s*P_s + t_p*P_p

    Mueller = np.zeros((4, 4, number_of_rays))
    J_mirror_conj = np.conj(J_mirror)
    # looking to the propagation direction
    A = 1/np.sqrt(2) * np.matrix([[1, 0  , 0 , 1 ],
                                  [1, 0  , 0 , -1],
                                  [0, 1  , 1 , 0 ],
                                  [0, -1j, 1j, 0 ]])

    for i in range(number_of_rays):
        J_kron = np.matrix(np.kron(J_mirror[:,:,i], J_mirror_conj[:,:,i]))
        Mueller[:,:,i] = A * J_kron * A.conj().T
```

```
    Stokes_reflection = np.einsum('ijk,jk->ik', Mueller, Stokes)
    DOP = np.sqrt(Stokes_reflection[1,:]**2 + Stokes_reflection[2,:]**2 +
    Stokes_reflection[3,:]**2) / Stokes_reflection[0,:]

    efficiency = Stokes_reflection[0] / Stokes[0]

    return mirror_intersection, reflection_direction_vector, Stokes_reflection, DOP,
    incidence_angle, efficiency, t_p, t_s, J_mirror, Mueller
```

D

Reflection Gratings

```python
import math
import numpy as np

from General_Functions import compute_rotation_matrix, normalise_vector, \
                               surface_plot_rotation2

from PCGrate_Data import GRT1000I_P, GRT1000I_S,                        \
                         GRT1000II_P, GRT1000II_S,                      \
                         GRT1000III_P, GRT1000III_S,                    \
                         GRT2700I_P, GRT2700I_S,                        \
                         GRT2700II_P, GRT2700II_S,                      \
                         GRT2700III_P, GRT2700III_S

##############################################################################
# GRATING
##############################################################################

def grating(D, groove_density, x_position, y_position, z_position, tilt_x, tilt_y, tilt_z, \
                wavelength, grating_resolution, grating_band, \
                ray_origin, ray_direction_vector, Stokes, plot_colour, ax, pupil_grid, \
                plot=True, normal=False, reflection=False):

    number_of_rays = len(ray_origin[0,:])
    rotation_matrix = np.array([tilt_x, tilt_y, tilt_z])

    ##########################################################################
    # Plot the 3D mirror

    mirror_index = number_of_rays * [0] # save the indeces at which intersections take place
    mirror_intersection = np.zeros((3, number_of_rays)) # save the intersection points

    # define the x-, y-, and z-rotation axes
    x_axis = [1, 0, 0]
    y_axis = [0, 1, 0]
    z_axis = [0, 0, 1]

    # first find where the ray hits approximately, then make detailed plot
    for ii in range(2):
        # define the mirror steps in the preliminary and final loop
        if ii == 0:
            mirror_steps = 10
            mirror_domain_x = np.array([-D/2, D/2])
            mirror_domain_y = np.array([-D/2, D/2])
        else:
            mirror_domain_x = np.array([min(X_local[mirror_index]) - D/mirror_steps, max(X_local[mirror_index]) + D/mirror_steps])
```

```
            mirror_domain_y = np.array([min(Y_local[mirror_index]) - D/mirror_steps, max(Y_local[mirror_index]) + D/mirror_steps])
            x_domain = mirror_domain_x[1] - mirror_domain_x[0]
            y_domain = mirror_domain_y[1] - mirror_domain_y[0]
            max_domain = max(x_domain, y_domain)
            mirror_step_size = 1
            mirror_steps = math.ceil(max_domain/mirror_step_size)

        X_mirror = np.linspace(mirror_domain_x[0], mirror_domain_x[1], mirror_steps)
        Y_mirror = np.linspace(mirror_domain_y[0], mirror_domain_y[1], mirror_steps)
        X_mirror, Y_mirror = np.meshgrid(X_mirror, Y_mirror)
        R_eff = np.sqrt(X_mirror**2 + Y_mirror**2)

        Z_mirror = 0*R_eff

        # Save mirror in local coordinates
        X_local = X_mirror.ravel()
        Y_local = Y_mirror.ravel()
        Z_local = Z_mirror.ravel()
        local_mirror = np.array([X_local, Y_local, Z_local])

        # Transform to global coordinates
        X_mirror, Y_mirror, Z_mirror = surface_plot_rotation2(rotation_matrix, X_mirror, Y_mirror, Z_mirror)

        X_mirror = X_mirror + x_position
        Y_mirror = Y_mirror + y_position
        Z_mirror = Z_mirror + z_position

        # Save mirror in global coordinates
        X_intersection = X_mirror.ravel()
        Y_intersection = Y_mirror.ravel()
        Z_intersection = Z_mirror.ravel()
        global_mirror = np.array([X_intersection, Y_intersection, Z_intersection])

        if ii == 0 and plot == True:
            ax.plot_surface(X_mirror, Y_mirror, Z_mirror, color='fuchsia')

        ###########################################################################
        # Compute the intersection point of every individual ray with the mirror
        # This is done by comparing the ray_direction_vector with vectors to every point on the mirror

        for i in range(number_of_rays):
            mirror_direction = (global_mirror.transpose() - ray_origin[:,i]).transpose() # computes vectors from ray origin to mirror points
            mirror_direction = normalise_vector(mirror_direction).transpose()

            find_intersection = np.dot(mirror_direction, ray_direction_vector[:,i]) # dot product should be 1 if parallel
            find_intersection = np.fabs(find_intersection - 1)
#            if min(find_intersection) > 0.01:
#                raise ValueError('Ray does not intersect with next mirror')

            mirror_index[i] = np.unravel_index(find_intersection.argmin(), find_intersection.shape)[0]

        # reset rotation axes
        x_axis = [1, 0, 0]
        y_axis = [0, 1, 0]
        z_axis = [0, 0, 1]

    mirror_intersection = global_mirror[:,mirror_index]

    ###########################################################################
    # Plot the incoming rays

    if plot == True:
        for i in range(number_of_rays):
            ax.plot((mirror_intersection[0,i], ray_origin[0][i]), (mirror_intersection[1,i], ray_origin[1][i]), (mirror_intersection[2,i], ray_origin[2][i]), color=
```

```
    plot_colour, zorder = 5)

    ##########################################################################
    # CREATE GRATING REFLECTION LINE

    X_mirror = np.linspace(mirror_domain_x[0], mirror_domain_x[1], mirror_steps)
    Y_mirror = np.ones(mirror_steps) * Y_local[mirror_index[4]]
    #Y_mirror = np.linspace(Y_local[mirror_index[4]]-10, Y_local[mirror_index[4]]+10, mirror_steps)
    X_mirror, Y_mirror = np.meshgrid(X_mirror, Y_mirror)
    R_eff = np.sqrt(X_mirror**2 + Y_mirror**2)

    Z_mirror = 0*R_eff

    # Save mirror in local coordinates
    X_local = X_mirror.ravel()
    Y_local = Y_mirror.ravel()
    Z_local = Z_mirror.ravel()
    local_mirror = np.array([X_local, Y_local, Z_local])

    # Transform to global coordinates
    X_mirror, Y_mirror, Z_mirror = surface_plot_rotation2(rotation_matrix, X_mirror, Y_mirror, Z_mirror)

    X_mirror = X_mirror + x_position
    Y_mirror = Y_mirror + y_position
    Z_mirror = Z_mirror + z_position

    # Save mirror in global coordinates
    X_intersection = X_mirror.ravel()
    Y_intersection = Y_mirror.ravel()
    Z_intersection = Z_mirror.ravel()
    global_mirror = np.array([X_intersection, Y_intersection, Z_intersection])

    if plot == True:
        ax.plot_surface(X_mirror, Y_mirror, Z_mirror, color='black')

        ##########################################################################
    # Compute the intersection point of every individual ray with the mirror
    # This is done by comparing the ray_direction_vector with vectors to every point on the mirror

    for i in range(number_of_rays):
        mirror_direction = (global_mirror.transpose() - ray_origin[:,i]).transpose() # computes vectors from ray origin to mirror points
        mirror_direction = normalise_vector(mirror_direction).transpose()

        find_intersection = np.dot(mirror_direction, ray_direction_vector[:,i]) # dot product should be 1 if parallel
        find_intersection = np.fabs(find_intersection - 1)
#           if min(find_intersection) > 0.01:
#               raise ValueError('Ray does not intersect with next mirror')

        mirror_index[i] = np.unravel_index(find_intersection.argmin(), find_intersection.shape)[0]

    x_axis = np.dot([1, 0, 0], rotation_matrix)

    # This is as from where all beams will effectively be reflected from
    mirror_intersection = global_mirror[:,mirror_index]

    normal_vector = np.zeros((3, number_of_rays))
    normal_vector[2,:] = normal_vector[2,:] -1

    # Transform to global coordinates
    normal_vector = np.dot(normal_vector.transpose(), rotation_matrix).transpose()

    # compute incidence angle from ray direction and normal
    # https://stackoverflow.com/questions/2827393/angles-between-two-n-dimensional-vectors-in-python
    incidence_angle = np.arccos(sum(ray_direction_vector * normal_vector))
```

```
    incidence_angle = np.ones(number_of_rays) * incidence_angle[4]

    m = -1
    a = groove_density
    theta_m = np.arcsin(m*wavelength/a + np.sin(incidence_angle[4]))
    reflection_direction_vector = np.dot(compute_rotation_matrix(x_axis, -theta_m), -
    normal_vector)

    # select P and S efficiency based on grating
    if grating_resolution == 1000:
        if grating_band == 1:
            P_eff = GRT1000I_P
            S_eff = GRT1000I_S
        elif grating_band == 2:
            P_eff = GRT1000II_P
            S_eff = GRT1000II_S
        elif grating_band == 3:
            P_eff = GRT1000III_P
            S_eff = GRT1000III_S
    elif grating_resolution == 2700:
        if grating_band == 1:
            P_eff = GRT2700I_P
            S_eff = GRT2700I_S
        elif grating_band == 2:
            P_eff = GRT2700II_P
            S_eff = GRT2700II_S
        elif grating_band == 3:
            P_eff = GRT2700III_P
            S_eff = GRT2700III_S

    # implement efficiencies on Stokes parameters for nominal path
    Stokes_reflection = np.array(Stokes)

#     NP = Stokes[0] - np.sqrt(Stokes[1]**2 + Stokes[2]**2 + Stokes[3]**2)
#     NP_new = NP * (P_eff(wavelength) + S_eff(wavelength))/2
#     Q = Stokes[1] * (P_eff(wavelength) + S_eff(wavelength))/2
#     U = np.zeros(number_of_rays)
#     for i in range(number_of_rays):
#         if Stokes[2][i] < 0:
#             U[i] = Stokes[2][i] * S_eff(wavelength)
#         else:
#             U[i] = Stokes[2][i] * P_eff(wavelength)
#     V = Stokes[3]

    # For calibration path
    NP = Stokes[0] - np.sqrt(Stokes[1]**2 + Stokes[2]**2 + Stokes[3]**2)
    NP_new = NP * (P_eff(wavelength) + S_eff(wavelength))/2
    U = Stokes[2] * (P_eff(wavelength) + S_eff(wavelength))/2
    Q = np.zeros(number_of_rays)
    for i in range(number_of_rays):
        if Stokes[1][i] > 0:
            Q[i] = Stokes[1][i] * S_eff(wavelength)
        else:
            Q[i] = Stokes[1][i] * P_eff(wavelength)
    V = Stokes[3]

    Stokes_reflection[0] = NP_new + np.sqrt(Q**2 + U**2 + V**2)
    Stokes_reflection[1] = Q
    Stokes_reflection[2] = U
    DOP = np.sqrt(Stokes_reflection[1,:]**2 + Stokes_reflection[2,:]**2 +
    Stokes_reflection[3,:]**2) / Stokes_reflection[0,:]

    return mirror_intersection, reflection_direction_vector, Stokes_reflection, DOP,
    incidence_angle, P_eff(wavelength), S_eff(wavelength)
```